POLITECNICO

MILANO 1863

School of Civil, Environmental and Land Management Engineering

M.Sc. programme in Civil Engineering for Risk Mitigation

Geo-Engineering Techniques for Unstable Slopes

Supervised by:

Professor Laura Longoni

Professor Marco Scaioni

Professor Azadeh Hojat

Presented by:

Ahmed Gamal Mahmoud Ebrahim Salem (988499)

Mehdi Hatami Goloujeh   **(993376)**

Quynh Le Thi Nhu   **(992648)**

Ke Zhengyun   **(991299)**

Selin Korucu   **(992503)**

Shabnam Neisani   **(995120)**

Contents

1. Introduction

"A mass of rock and earth moving suddenly and quickly down a steep slope" is the definition of the term "landslide" in the Cambridge dictionary *[1]*. However, in the technical context, the term "landslide" is designated to a variety of processes resulting in the downward, mass movement of materials such as soil, rock, or a combination of them, due to gravity. Landslides are one of the major devastating geohazards and claim thousands of lives and create acute economic losses related to property damage every year *[2]*. As catastrophic events, landslides can cause human injury, loss of life and economic devastation, and destroy construction works and cultural and natural heritage *[3]*. Having said that, the quantification of the death toll and the monetary loss due to landslides is said to be poorly quantified *[4]*.
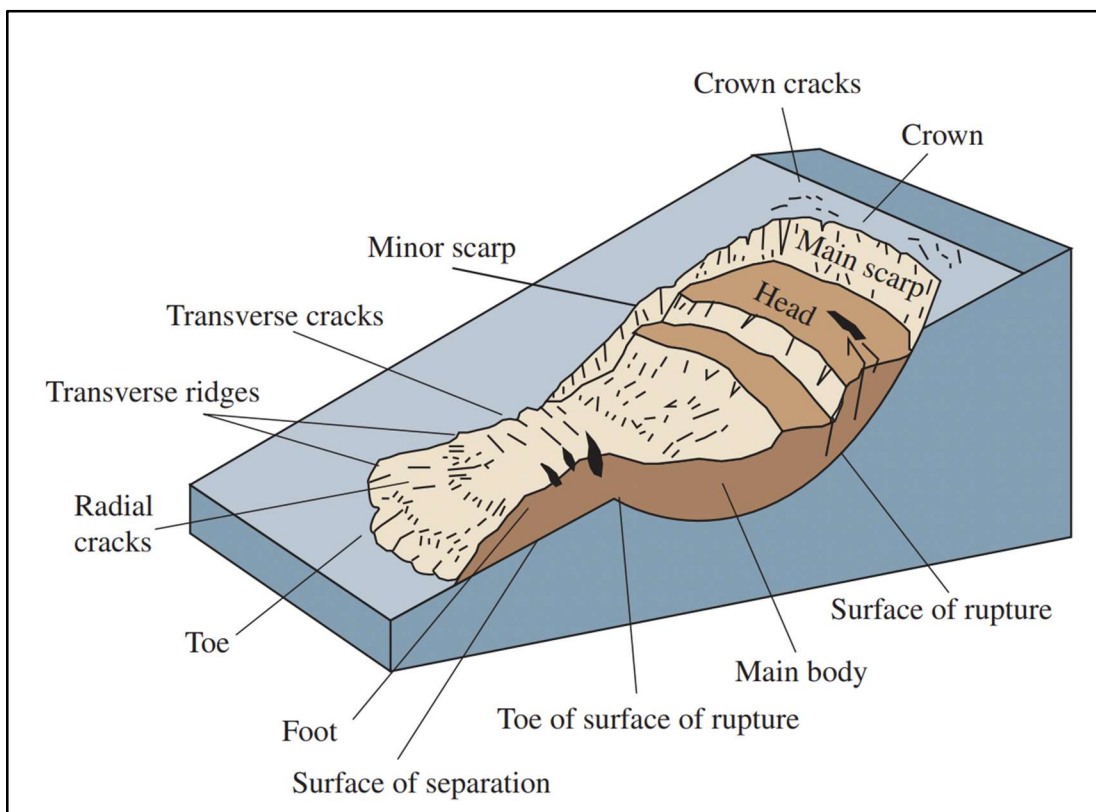
Fig. 1. An Idealized Landslide Used for Labelling Different Parts of a Landslide

One of the most recent classifications of landslides is found in *[5]* which categorizes landslides into 6 different types: 1. Falls, 2. Topples, 3. Slides, 4. Lateral spreads, 5. Flows, and 6. Complex, which refers to any combination of the previously mentioned landslide types. According to Science for disaster risk management 2017 *[6]*, this hazardous phenomenon can be triggered by different natural and anthropogenic factors such as: heavy rainfalls, large earthquakes, volcanic activities, and human-induced causes such as deforestation, irrigation, mining activities, and the construction of hydroelectric stations. Shallow landslides induced by rainfall events are one of the most common geological hazards around the globe which can pose serious threats to people and their assets in mountainous regions. To analyze the stability of the slopes

toward this dangerous phenomenon, we used a laboratory-scaled physical model, as well as a numerical model called Shallow Landslide Instability Prediction (SLIP model).

In this report we are presenting and comparing the results of two separate experiments performed in the laboratory to simulate a rainfall-induced shallow landslide, both of which were monitored and evaluated with three different geo-engineering techniques including geological, photogrammetry and geophysical techniques. And the results obtained through all mentioned techniques were combined and compared to confirm the analysis done on the experiments. Also, the SLIP model was used to obtain a rough estimation of the safety factor variation with respect to time during the rainfall event. To go one step further, we have investigated the SLIP model in depth, and discussed limitations of that such as not considering the run-off water or considering the whole slope as a single layer. In addition, we have proposed some modifications to tackle the mentioned limitations, after which, the SLIP model gave the crack time accurately.

2. Experiment Description

To compare the different conditions affecting a rainfall-induced landslide, two experiments with different physical situations were conducted *[Tab.1]*.

Table 1. Characteristics of Slope on Landslide Simulator

Slope Dimension		
Length	2	m
Width	0.8	m
Height	0.15	m
Area	1.6	m^2

Experiment 0: This experiment was shared by all groups on 20th of October, and it consisted of 3 layers of compacted soil, 5 cm each, and 35 degrees inclination of the landslide simulator, simulating a rainfall event with the intensity of 57.5 mm/h with 4 sprinklers.

Experiment 1: This experiment which was shared between groups 2 and 4 on 28th of October, consisted of 2 different layers. The bottom layer was 7.5 cm of compacted soil, and the top layer's height was the same, 7.5 cm, but without compacting the soil. The configuration of the landslide simulator was like an experiment 0, 35 degrees of inclination and a rainfall with an intensity of 57.5 mm/h.

2.1. Landslide simulator

In the experiments, we used a landslide simulator created by transparent plastics attached together with metal bars and mounted on a hydraulic jack which enabled us to change the inclination of the set-up up to 45°. There are also 6 sprinklers attached to the bars on the top of the simulator to create the artificial rain event for us. The hydraulic jack itself has 4 wheels which make it easier to move around when needed *[Fig.2]*.
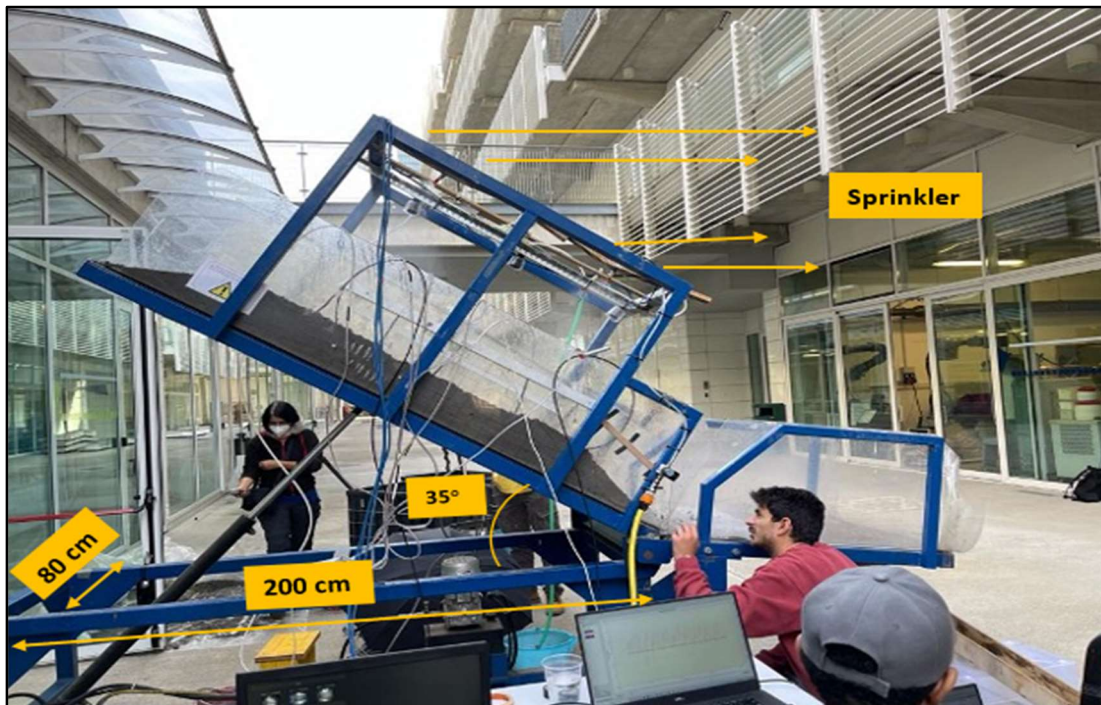
Fig. 2.. Landslide Fume Test dimensions

2.2. Schematic representation of experiments

2.2.1 Experiment 0

As said before, in this experiment we used 3 layers of uniformly compacted soil which made a 15 cm layer of compacted soil at the end. The geometry of the soil configuration is shown *[Fig.3]*.
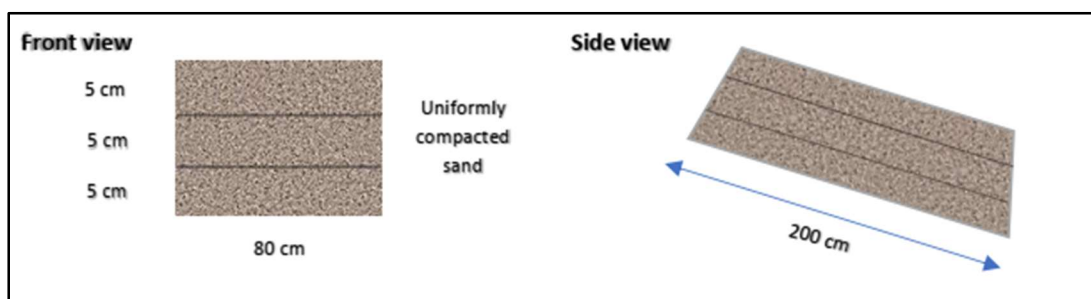
Fig.3. Schematic Representation of the Soil in Exp.0

2.2.2. Experiment 1

In this experiment, the model has been built up using a 15-centimeter sand layer and it has been performed through two 7.5-centimeter layers in which the first layer was fully compacted, and the second layer didn't go through any compaction process *[Fig.4]*.
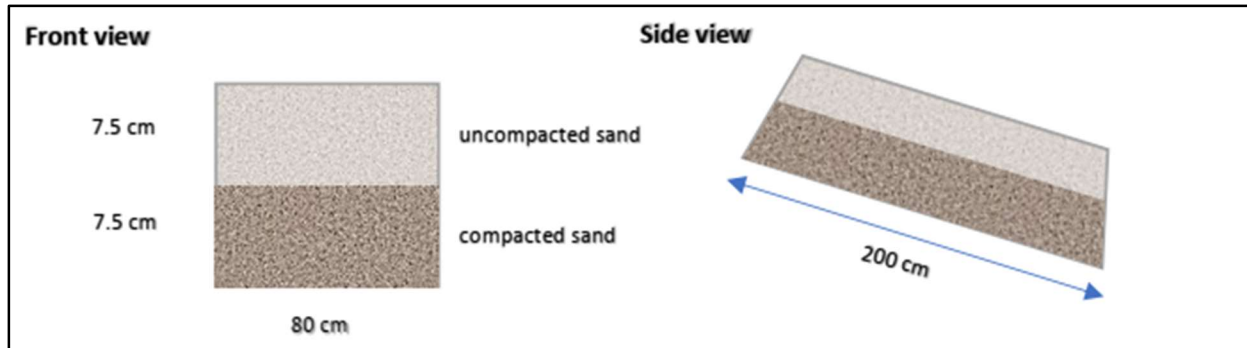
Fig.4. Schematic Representation of the Soil in Exp.1

2.3. Geological Monitoring Instruments

2.3.1. Time Domain Reflectometry (TDR)

It is a device measuring the soil water content indirectly based on the travel time of a high frequency electromagnetic pulse through the soil. This travel time is used to calculate the permittivity (dielectric constant) of the material. The TDR probes are inserted directly into the soil for in situ measurement. The measurement takes only seconds, and the instrument can be attached to a data logger for ongoing measurements. The Volumetric Water Content (VWC) of each bucket of soil used to create the landslide was measured and used to find the mean value as the initial VWC before the start of the rainfall *[Fig.5]*.

Fig.5. TDR Sensor Measuring VWC of Each Soil Bucket

2.3.2. Tensiometer

It is one of the commonly used devices to measure negative pressure(suction). This device typically consists of a glass or plastic tube with a porous ceramic cup filled with water. With the implementation of electronic sensors, it defines changes of pressure between the water contained in the ceramic cup and the water present in the soil around. We use two probes during our experiment. When the water pressure in the ceramic cup is larger than the water pressure in the soil, it gives us a negative value, and sometime after the rainfall event, when the saturation of the soil increases, the water pressure difference between them becomes zero *[Fig.6]*.

Fig.6. Tensiometer Instrument and Installation

2.3.3. Arduino

The aim of these sensors is to measure soil moisture during the experiment. The Arduino sensor consists of two probes that are used to measure the volumetric content of water. The two probes allow the current to pass through the soil, which gives the resistance value to measure the moisture value. The presence of water will increase the conductivity of the soil; therefore, the soil layer would be less resistant in presence of water. Dry soil on the other hand, does not allow the current to pass as easily, indicating the lower conductivity (higher resistivity) of the soil layer. In both experiments we used 6 Arduino probes, but the 6th probe was not functioning, so we removed its results from the data before making the analysis. They were buried in the soil at equispaced distances of 25 cm each *[Fig.7]*.

Fig.7. Installation of Arduino Sensors

2.3.4. Sprinklers

The sprinklers are devices used to spray water. These elements simulate natural rainfall in laboratory-scale configuration. The intensity of the simulated rainfall created by the sprinklers can be set by a gauge connected to the simulator which shows the pressure. In both experiments, this pressure was set to 1.5 atm *[Fig.8]*.
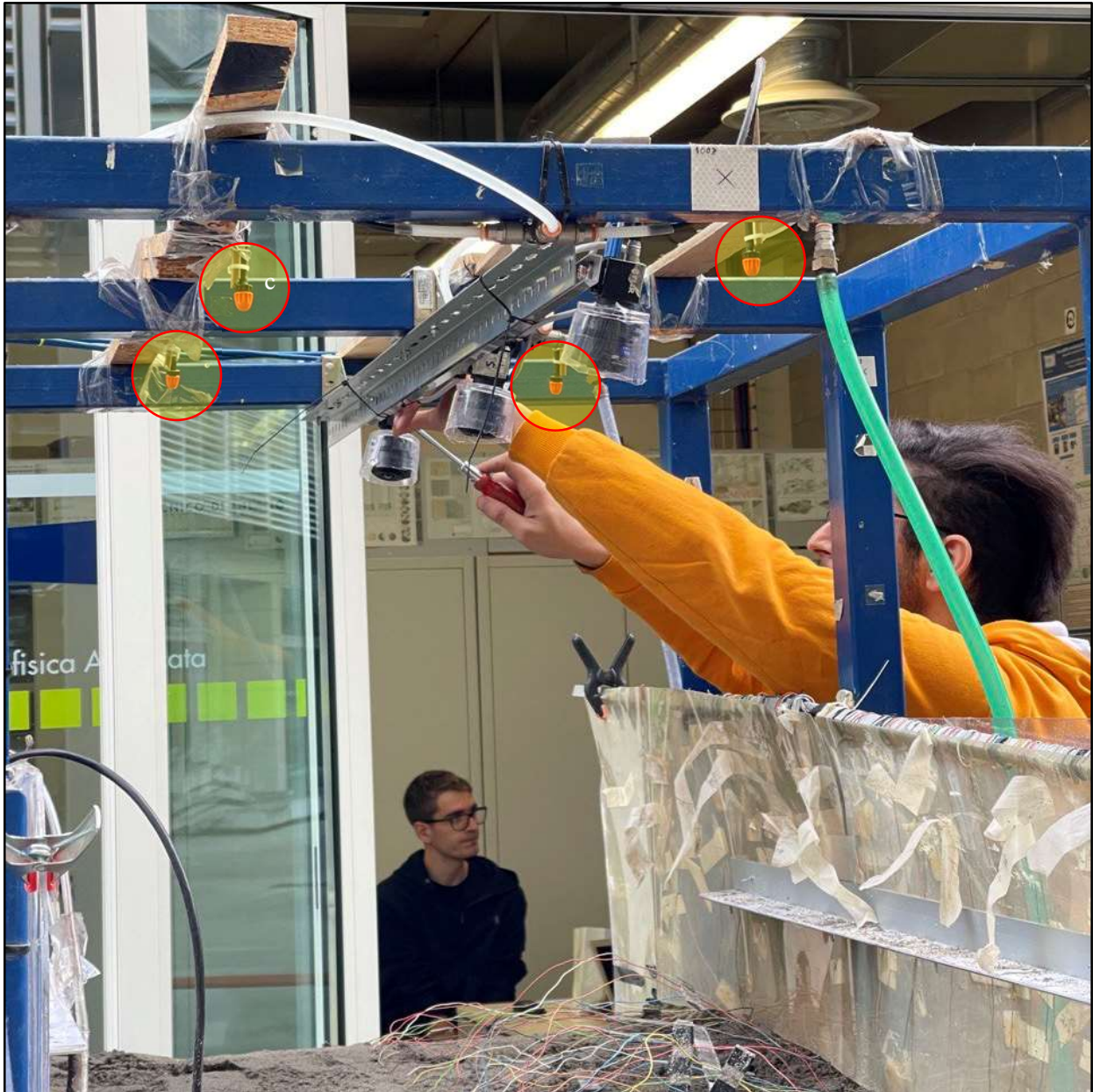
Fig.8. Sprinklers Simulating the Rainfall Event

2.4. Physical Characteristics of Sand

In addition to the characteristics of the geometry and soil layers, it is necessary to characterize the slope in terms of additional parameters such as porosity, volumetric water content, and specific gravity before starting the simulation. These parameters were calculated based on the data collected from the instruments implemented in the initial state, the geometry of each experiment, and the intrinsic properties of each material. This data will be exploited in the following steps of the analysis.

Table 2.Physical Characteristics of Sand

	Experiment 1	Experiment 2
Height [m]	0.15	0.15
Weight [kg]	278.30	307.30
Water Volume[l]	58.27	64.40
Sand Volume [l]	0.235	0.235
Mean VWC [%]	15	15

2.5. Artificial Rainfall Intensity Calibration

In both experiments we needed to create an artificial rainfall event, so we used a rainfall simulator which was constructed from 4 separate sprinklers attached to the top bars of the landslide simulator and connected all together to a source of tap water after going through a gauge through which we could set the pressure. The intensity of the rainfall was calculated with the SLIP model spreadsheet, which is a function of the number of sprinklers, and the area with the formula below.

$$RainfallIntensity[mm/h] = N * \left(\left(SprinklerDischarge \left[^l/_{(min)} \right] * 60 \right) \right) / (Area[m^2]) \textit{Equation 1}$$

The rainfall event could have been simulated with both 4 and 6 sprinklers. The comparison between the intensity and pressure of each event is shown in *[Fig.9]*.

Fig. 9. Comparison of Pressure vs. Rainfall Intensity for 6 and 4 Sprinklers

Also, since the discharge of each sprinkler is of great importance to our experiments, another comparison between different water pressure of the sprinklers, and the discharge of each of them has been made and presented in *[Fig.10]*.
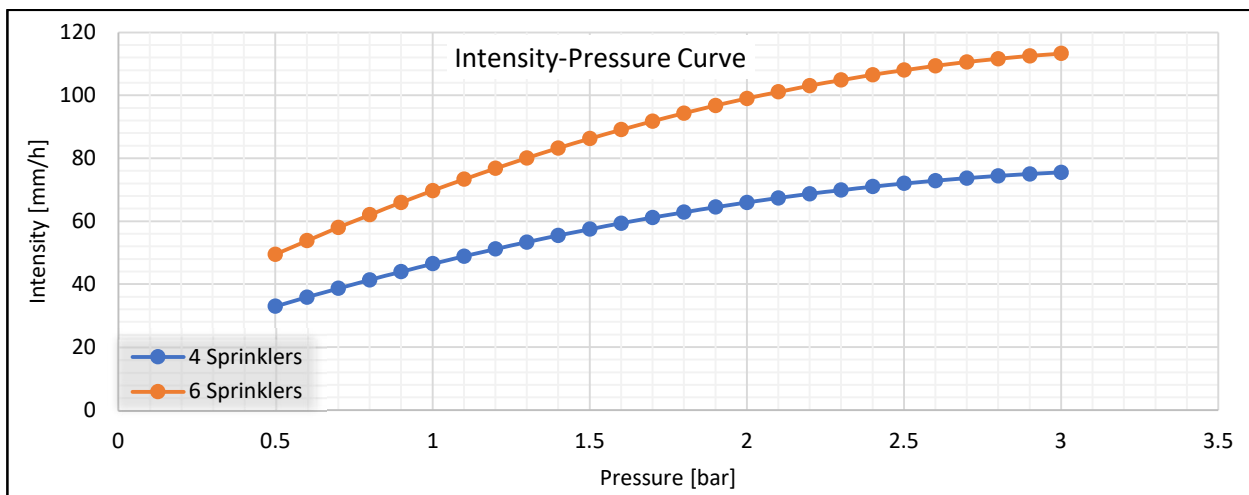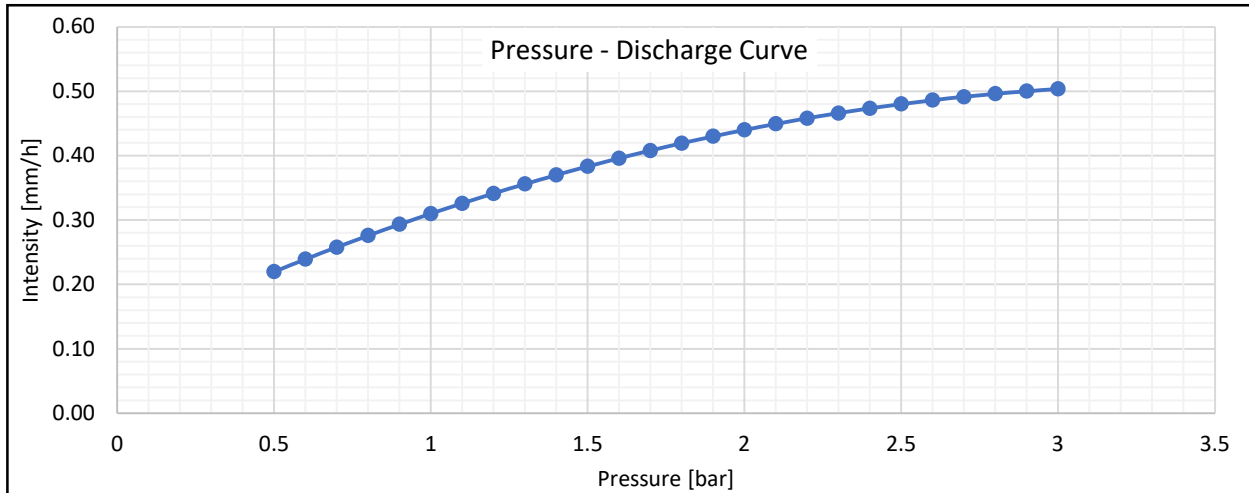

Fig.10. Comparison of Pressure vs. Discharge Values for Sprinklers

3. Representation and Comparison of Acquired Data

In this section, the data obtained through application of the geological tools and the measurements during the experiment are represented first, the anomalies are highlighted, numbered, and explained, and in the following sections, those explanations are confirmed by the data coming from Photogrammetry and Geophysics.

3.1. TDR Sensor Results

3. 1.1. Experiment 1

Volumetric Water Content

$y = \mathbf{0.3745x} + 20.476$

$y = \mathbf{1.193x} + 10.88$
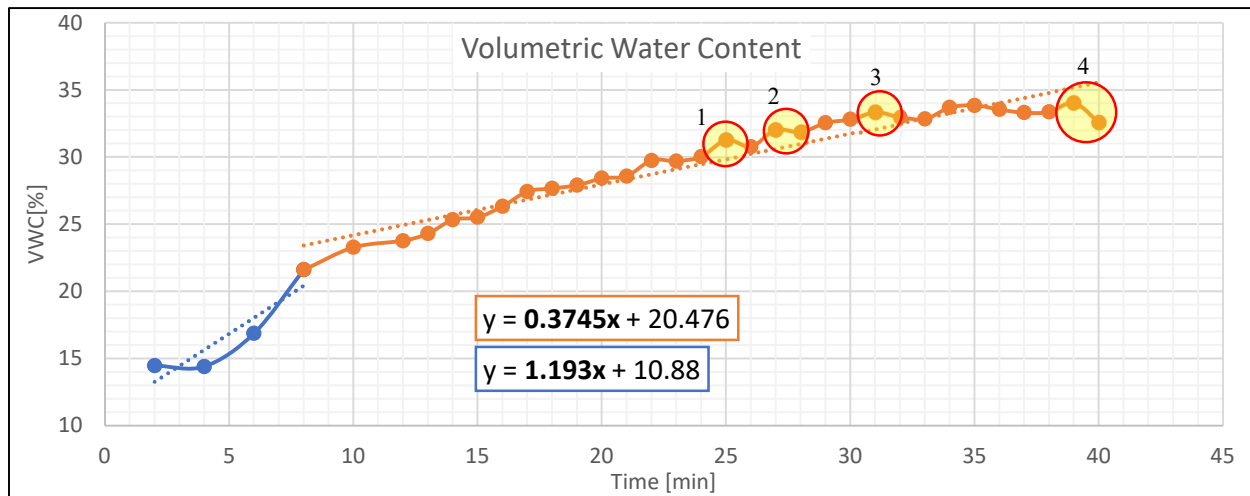
Fig.11. TDR Results for Experiment 1

The figure above *[Fig.11]* shows the data acquired through the geological instruments. According to the procedure followed in the experiment (starting with low VWC and increasing the saturation of the soil during the experiment), it was expected to see an increasing trend in the values of Tensiometer and VWC profiles. This experiment started at 14:44 P.M., and right after that, as the figures suggest, the value of VWC shows a sharp increase in the first 8 minutes of the experiment, followed by a smoother, and stable increase for the rest of the time. Since there is constant artificial rainfall occurring during the experiment, it is expected for the VWC values to keep increasing, but there are some anomalies occurring at the highlighted areas in which the VWC trend shows a decrease. The highlighted anomalies can be representatives of formation of cracks in this case, however, the validation of this hypothesis will be checked with the data from Photogrammetry in the following sections.

3.1.2. Experiment 0
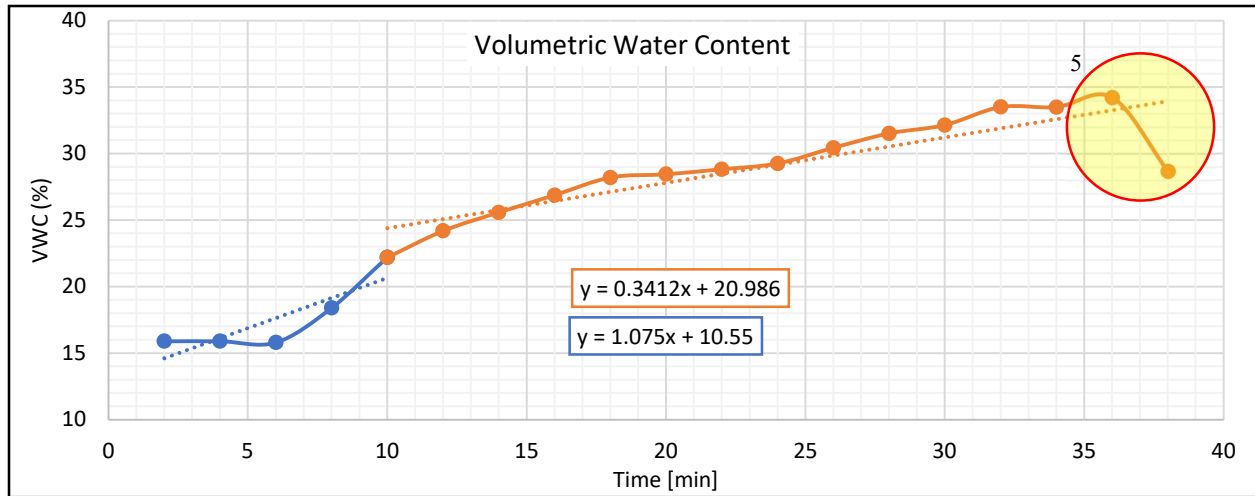
Fig.12. TDR Results for Experiment 0

[Fig.12] represent the obtained data through the same geological instruments that we explained for Experiment 1. This experiment started at 15:40 P.M., and right after that there was a somewhat stable increase in the Volumetric Water Content value measured by TDR and this value continued increasing, with a smaller slope later, until 16:14 when the results show an unexpected decrease at around 36 minutes after the beginning of the project. Since the slope of this decreasing line is very large, we can say that at that time, a collapse might have happened, we will confirm this hypothesis in the following chapters.

3.1.3. Comparing the Results

TDR instrument shows the Volumetric Water Content (VWC) of the soil, and in our experiment, with artificial rainfall, we are trying to increase the saturation of the soil to investigate its possible failures. So, it is expected the VWC value increases during the experiment. Considering the results of both experiments, they followed the same general increasing trends which affirms the theory. In both experiments we had a sharper increase in the beginning, followed by a smoother increase. There are two points two to elaborate on:

1. Similar in both experiments, the VWC increase in the first 8-10 minutes has a larger slope compared with the rest of the experiment. It can be explained by the saturation of the sand getting increased with the pass of time. The more saturated the sand is, the less water it absorbs in a certain amount of time
2. The only noticeable "difference" in these charts is the changes of the slope between the first and second part of them, shown by the trendlines (blue & orange). The difference between the first and second part of the TDR charts in experiment 1 is larger than that of experiment 2. This might be explained by the configuration of the sand layers. In experiment 1, the water has infiltrated the top layer easily, but when it reaches to the compacted bottom layer, it gets harder

for that to infiltrate, so there is a more significant drop in the rate of the water absorption of the sand. So, after the first 10 minutes, the sand gets more saturated, and water also reaches the compacted soil, and both factors contribute to this drop in the rate of VWC increase. However, in experiment 0, where the difference in the rate of the water absorption is less significant, the only differentiating factor is the sand getting saturated and it gets harder for more water to get in; therefore, the difference between the first 10 minutes and the rest of the experiment is less evident.

3.2. Tensiometer Sensor Results

For the data obtained from the tensiometers we have developed 2 graphs, in the first graph we have used the exact values which were exported from the tensiometer, and in the second one, we have averaged the exported data in 2-minute periods. This was done to remove the effect of any inaccuracies in the process of installing the instruments. We used 2 separate tensiometers in the landslide to measure the negative pressure. Tensiometer 1 was in the depth of around 4 cm in the top part of the landslide, and Tensiometer 2, was in the depth of around 12 cm in the toe of the landslide. *[Fig.13 & Fig.14]*
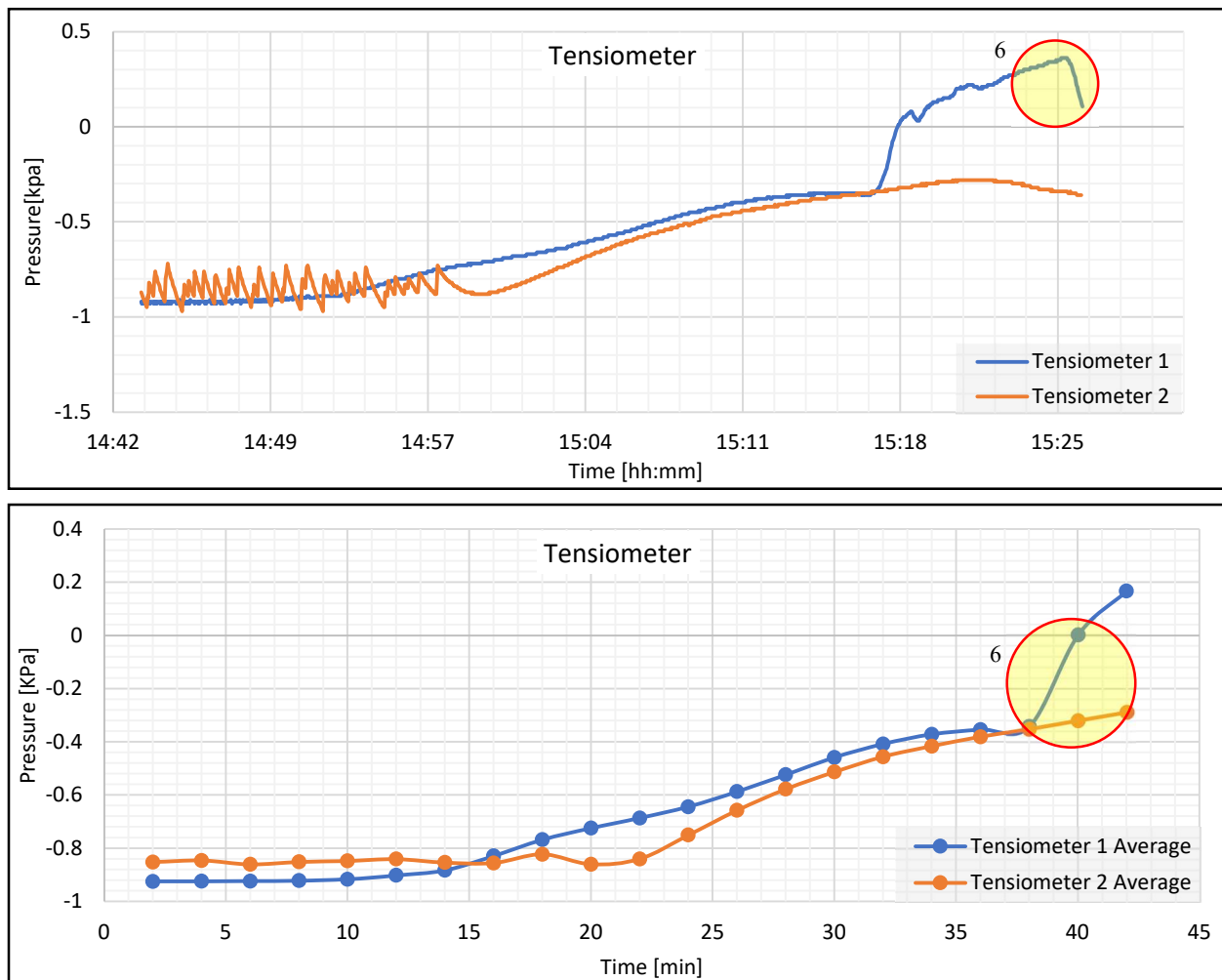
3.2.1. Experiment 1

Fig. 13 & 14. Tensiometer Original/Averaged Results for Experiment 1

16

In the first glance at the real-valued graph, we can see that there is a noticeable volatility in the values of Tensiometer 2 in the beginning of the experiment. One possible explanation for this could be that the ceramic head not getting full of water. By averaging the values, we tried to tackle this problem. It was expected to have the very same similar values in the beginning of the experiment for both tensiometers, but as figures indicate, Tensiometer 2 shows a slightly larger value, and the reason for that can be the uneven distribution of the more saturated sand. Simply put, the buckets of sand which surrounds Tensiometer 2 were more saturated than those of Tensiometer 1. Moreover, the increasing trend of the tensiometer (which shows the soil getting more saturated due to the rainfall), starts at around 14:55 P.M., approximately 10 minutes after the start of the experiment. This 10-minute delay can be explained due to the placement of the tensiometers, which are buried in the soil, it takes some time for the rainfall to penetrate the soil and reach the area around tensiometers. Tensiometer 1, which was placed in the depth of 5 cm in the toe of the landslide reaches to 0, and even gets positive, which shows the saturation of soil around the device. However, the Tensiometer 2, which was in 12 cm depth and at the crown of the landslide didn't reach to 0, so the sand around that didn't get fully saturated.

A noticeable feature of this figure is the jump in the tensiometer 1 at the time of around 15:20. Considering that this jump is seen only in Tensiometer 1, and since this Tensiometer was placed near the toe of the landslide, it can be because of the translation of the landslide in the middle which happened around that time. Having said that, this hypothesis will also be validated with information from other domains.

3.2.2. Experiment 0
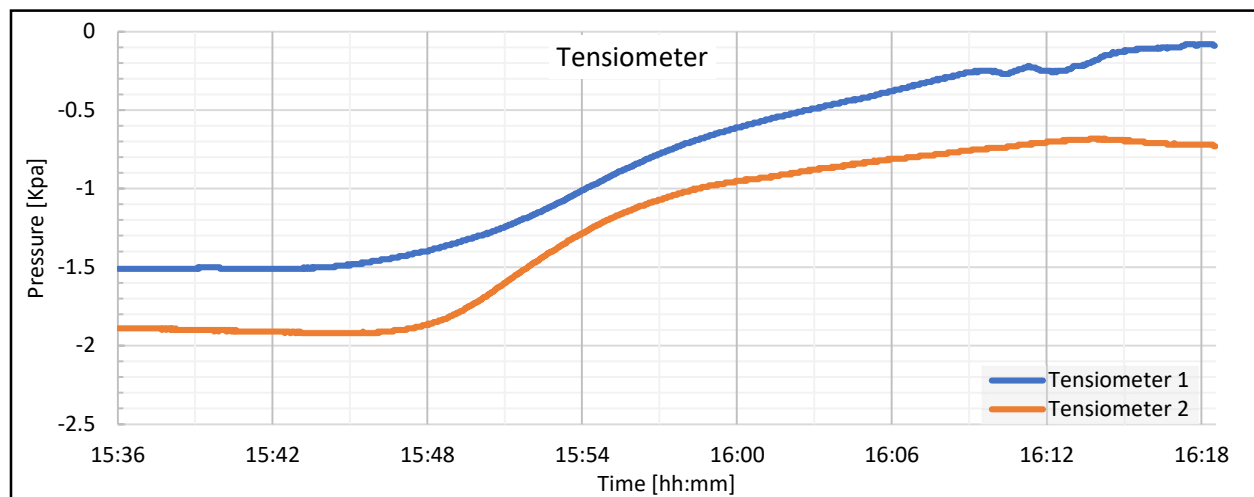
Fig. 15. Tensiometer Results for Experiment 0

Like the procedure of experiment 1, we used 2 separate tensiometers in the same locations that we had in experiment 1, to measure the negative pressure. However, the depth at which we have put these tensiometers was different compared to experiment 1, which can be understood from the figures as well. Concerning the general trend of this figure, as it was expected, since we have the rainfall in the experiment, by the passage of time the amount of water inside the landslide increases and the sand gets more saturated. This negative pressure kept increasing during the experiment. Although the general trend in the tensiometers is the same in both experiments, there are also some noticeable differences which will be discussed in the following sections.

3.2.3. Comparing the Results

1. In terms of the similarities, both show an increasing trend throughout the experiment time, which is totally in accordance with the theory and use of the instruments.
2. Another similarity between the Tensiometer sensor results in experiments 0 and 1 is the delay time in the beginning of the experiments before the increasing trends start. Since the sensors were buried inside the sand, it takes some time (between 10-15 minutes in both cases) for the water to infiltrates and makes the soil around the instruments more saturated
3. A noticeable difference between results of these experiments is that in Experiment 1, the tensiometer 1 ends up showing a positive value, however, in experiment 0, at the end of the experiments, that hardly reaches 0. This difference can be explained through the placement of the devices. In experiment 1, the tensiometer 1 was buried in a depth of around 4 cm, which is very close to the surface, so the sand around it gets fully saturated easily, but in experiment 0, both of them are buried in a depth of around 8 cm, so none of them are close to the surface to get fully saturated.

3.3. Arduino Sensor Results

Concerning the Arduino sensors, 6 of them were placed along a straight line in the middle of the landslide in depth of around 8 centimeters, but since Arduino 6 was not functioning properly, we removed it from the analysis to keep the results consistent.

3.3.1. Experiment 1
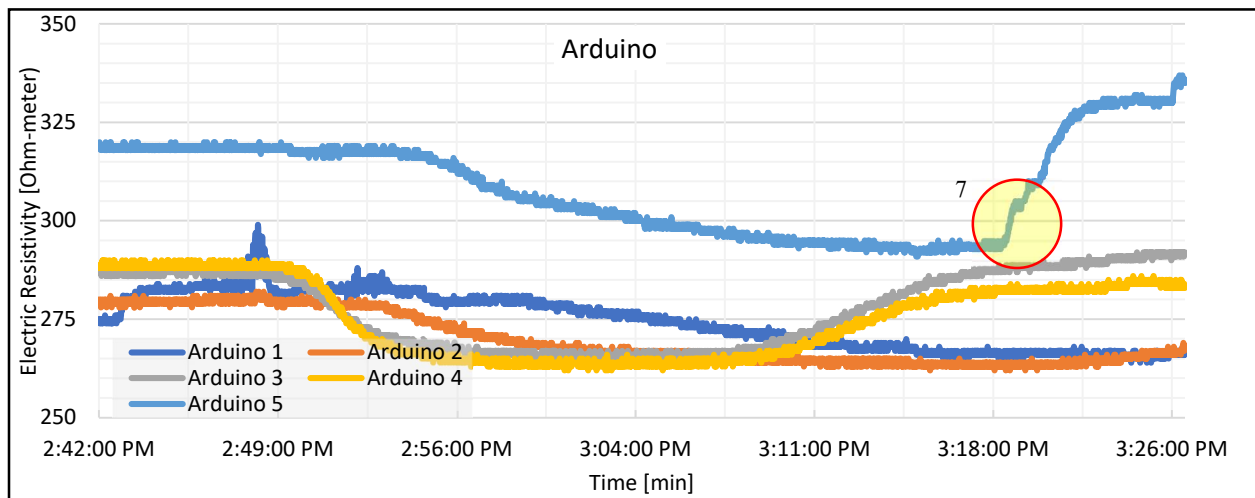
Fig.16. Arduino Results for Experiment 1

The general trend in the Arduino sensors shows a decrease which is expected due to the increase in the saturation value. But as the figure indicates, after a general decrease in the electric resistivity values, concerning Arduino 1, and 2, they kept the decreasing trend until almost the end of the experiment. *This is* simply because of their location, which is in the upper part of the landslide, far from the cracks and failures. Arduino 3, and 4, followed a very similar trend in the second part when they started increasing, and this

increase started at around 15:10, which is probably the time of the first crack opening (highlight 7). Moreover, Arduino 5 Also shows a similar trend, a decrease in the beginning followed by an increase around the end of the experiment, but the difference is that its increase is much sharper than the increase of the Arduino 3, and 4. Also its time was around 15:20, which is probably the translational movement of the landslide (highlight 7) *[Fig.16]*.
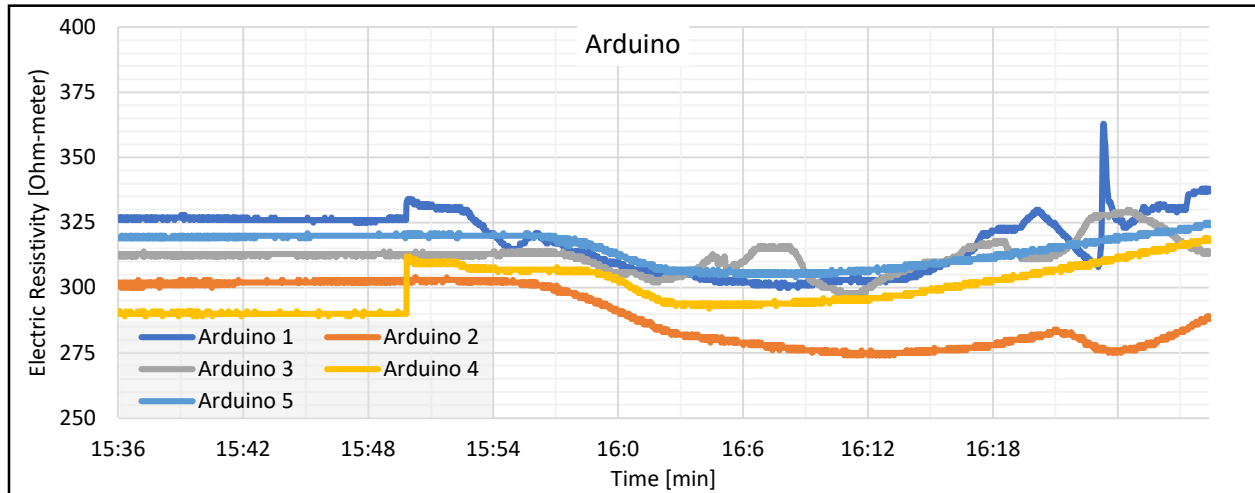
3.3.2. Experiment 0

Fig.17. Arduino Results for Experiment 0

These results here also suggest the expected decrease in the value of resistivity for the initial part of the graph before the cracks happen, and after the creation of the cracks, the value of resistivity increases which shows the presence of voids. At around 15:50 there is a sudden unexpected jump in the values of Arduino 1, and 2 witnessed in the results. This is simply the effect of the start of the geophysical sections, the current passing by geophysical instruments is intervening with Arduino results. Also, another anomaly in this figure is what happens to Arduino 1 around the end of the experiment, there is a peak created there, which similarly shows the end of the geophysical experiments.

3.3.3. Comparing the Results

In both experiments, the Arduino sensors were placed in the depth of around 7 cm from the top of landslides and the general trend of the figures show similarities. In both experiments, Arduino 1 & 2, which are placed in the top of the slope show the same decreasing results, and the other 3 sensors show an increasing trend in the second half of the experiment, which is due to the creation of the cracks.
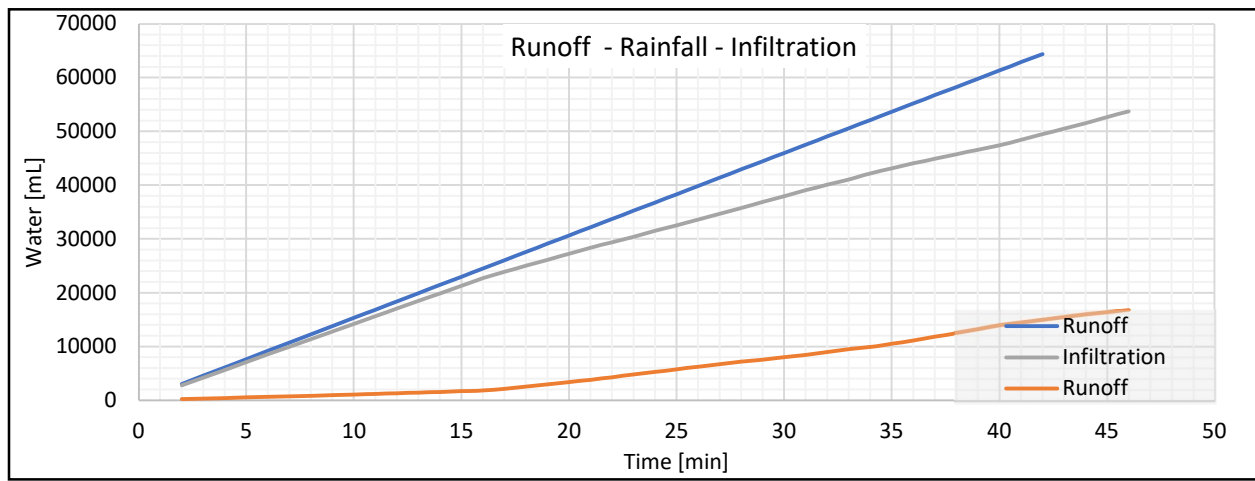
3.3.3.4 Rainfall Comparison

Fig.18. Comparison Between Accumulated Rainfall, Runoff, and Infiltration

The artificial rainfall event used in both experiments 0, and 1 was the same in terms of the intensity and the number of sprinklers, which makes it easier to compare the response of the landslide to different soil configurations. Assuming that the precipitation on the whole area of the simulated landslide was uniform, we have calculated the accumulated rainfall for the model area to find the total amount of rainfall. Also because, except for TDR, there is no other instrument to measure the value of soil saturation to evaluate the volume of infiltrated water, we have tried to measure infiltration by subtracting the measured runoff water from the accumulated rainfall. In *[Fig.18]*, we have shown the value of accumulated values of rainfall, runoff, and infiltration. Also, to compare the effect of the intensity of the rainfall, the sensitivity analysis to the rainfall intensity has been done by the slip model, the result of which will be represented in the following sections.

3.4. Experiments Configuration Comparison

In two experiments done, we tried to keep most of the conditions similar except for one condition and check how that difference will affect the results of our experiment. In experiments 0, and 1, we tried to simulate the same rainfall event by using the same number of sprinklers, and the same water pressure, so the amount of rainfall the landslide got was almost the same. We used the same landslide simulator, so the dimensions of our landslides in both experiments were the same. Also, the same instruments were used in both experiments with the same setting, except for a few changes such as the depth in which we had put Tensiometers, which will be discussed in each instrument. The factor which we tried to make different in order to investigate its effects was the soil layer configuration. In experiment 0, we used 3 layers of 5 cm compacted sand, however, in experiment 1, we built the landslide in 2 layers of 7.5 cm, and only the bottom layer was compacted. We tried to not to give any compaction to the second top layer and we tried to only make its surface smooth for the sake of the experiment.

3.5. Geological Vs. Photogrammetry Vs. Geophysics

Table 3. List of Anomalies and Related Information

Geophysical Assessment			Photogrammetry Assessment		Geophysical Assessment	
Anomaly No.	Exp. Equipment	Time	Fracture ID	Time	Measurement ID	Time
1	TDR Exp.1	24-26	Fracture 2	24:10	T5 T6	22 27
2	TDR Exp.1	27-29	Fracture 3 Fracture 4 Fracture 5	27:09 27:50 28:20	T6	27
3	TDR Exp.1	31-33	Fracture 7 Fracture 8 Fracture 9	31:00 30:50 38:10	T7	33
4	TDR Exp.1	38-40	Fracture 10 Fracture 11 Fracture 12 Fracture 13 Fracture 14	37:00 37:30 38:00 39:30 30:45	T9 T10	37 39
5	TDR Exp.0	35			T6	33
6	Tensiometer Exp. 1	0.235	Same anomaly as No.4			
7	Arduino Exp. 1	15	Same anomaly as No. 4			

In the previous sections, the data obtained from geological instruments has been presented, the theory behind them as well as the expected results have been elaborated on, and some anomalies were highlighted and the reason behind those anomalies were tried to be found. Now in this section, we will try to confirm those reasoning by the data coming from the Geophysical Assessment, and Photogrammetric sections. In the table below, we have provided a list of the anomalies detected by the analysis of the results of the geological instruments, and in the following, the explanation and data mentioned in the table will be provided.

3.5.1. Anomaly 1

This anomaly was found in the results of the TDR sensor of experiment 1. At around 24 minutes after the beginning of the experiment, the VWC showed a drop, where it was supposed to be increasing, according to the theory explained in the TDR sensor section. The initial guess for this anomaly was said to be the creation of a crack.

3.5.1.1. Geology vs. Photogrammetry

The initial guess for this anomaly was the formation of a crack. To validate this initial guess, we checked data coming from the Photogrammetry domain. We had a picture around that time and that picture confirmed the formation of a crack then. Here are the characteristics of the crack which caused anomaly No.1. As mentioned in the table at the beginning of this section, there was one fractures happening around this time (Fracture 2), whose information and images could be found in photogrammetry section in following figures.

3.5.1.2. Geology vs. Geophysics

Checking the data coming from Geophysical Assessment, the time of this anomaly is between T5, and T6 measurements. By comparing the resistivity models coming from Res2Dinv software, we can see that the light orange parts of the figures are extending and enlarging, which indicates the decrease of resistivity in those parts, most probably due to the movement of the water from crown toward the toe. In the resistivity model at T6, on the top left of the model we can see the appearance of the blue color, which indicates resistivity decreasing. It is in compliance with the increase of the resistivity in the crown part because water has moved toward downslope, so the soil gets more saturated, therefore, the resistivity decreases around that area.
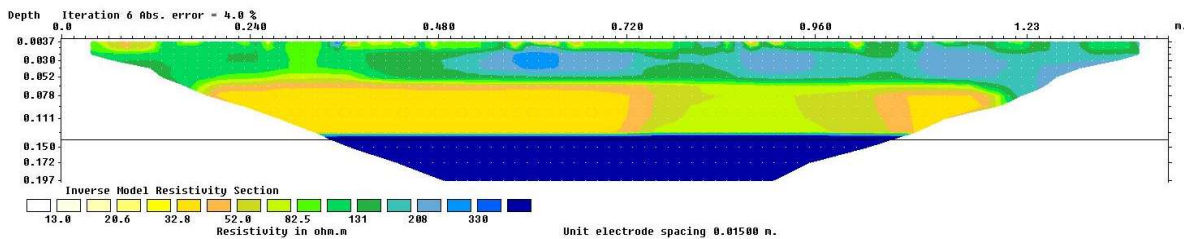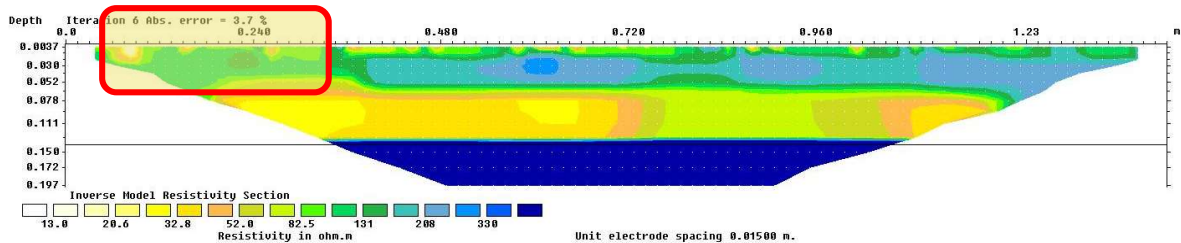

Fig.19

Fig.20

3.5.2. Anomaly 2

Similar to anomaly 1, this also was recognized in the TDR sensor results of experiment 1, and where the VWC value was supposed to be increasing, it went through a slight decrease at around 28 minutes after the beginning of the experiment. According to the similar characteristics of anomalies 1, and 2, the initial hypothesis causing this anomaly was the creation of a crack as well.

3.5.2.1. Geology vs. Photogrammetry

To see if the reason behind this anomaly formation of a crack was or not, we revisit the photogrammetry data. There is another crack opened at around 28 minutes after the beginning of the experiment, which confirms the hypothesis again. The characteristics of the crack are as below.
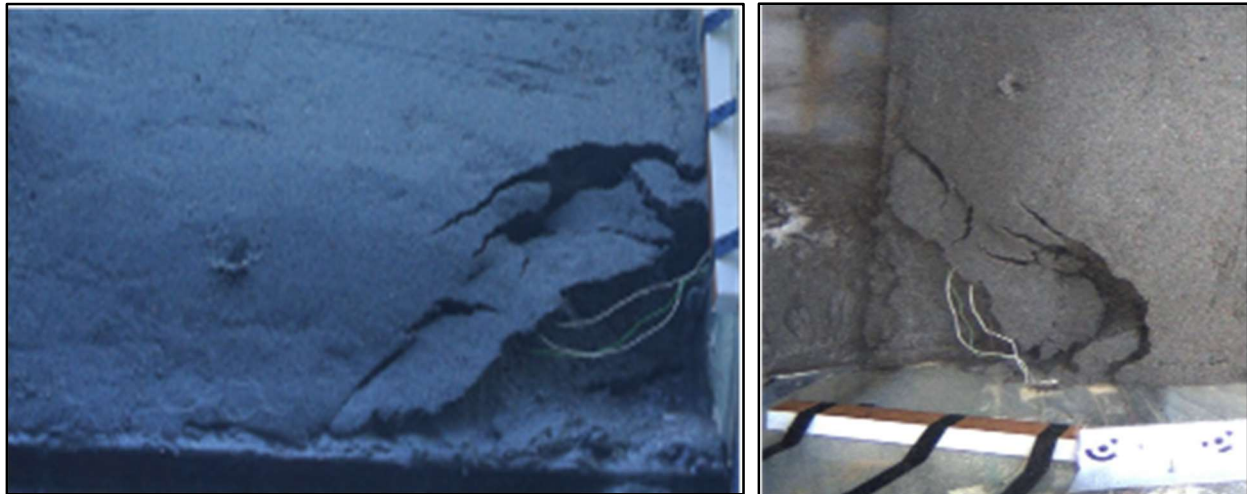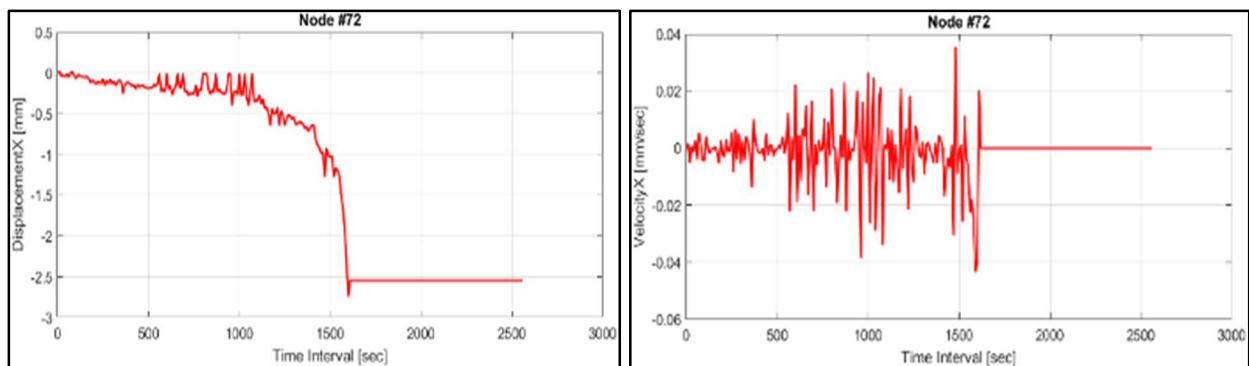

Fig.21.

Fig.22.

3.5.2.2. Photogrammetry vs. Geophysics

Looking at the resistivity model at T6, measured at approximately 27 minutes after the beginning of the experiment, we can see that the light orange part (highlighted in the image below) is extended along the slope to some extent. Comparing it with the previous time model, the change is not significant, and we cannot see the cracks happening in the slope that much. The reason behind that is the fact that the

placement of the electrodes were finished almost before reaching the downslope, so those cracks do not affect either the electric nor the magnetic field that much.
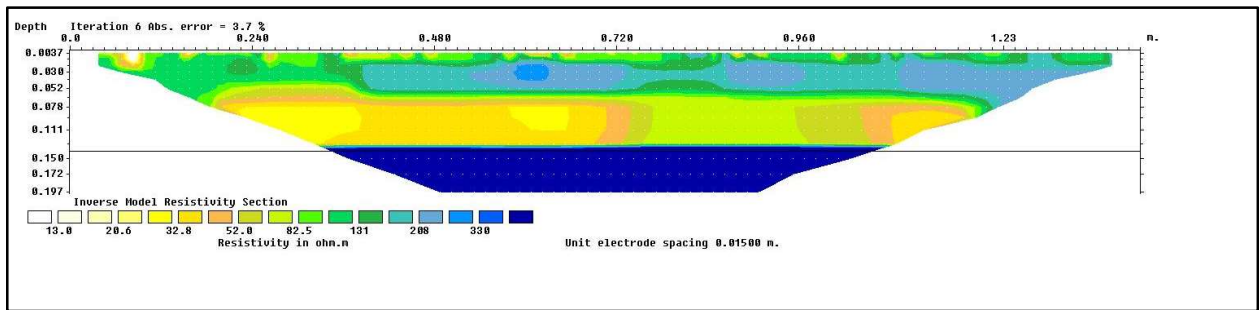

Fig. 23

3.5.3. Anomaly 3

According to the TDR data for experiment 1, there is another anomaly happening at 31-33 minutes after beginning of the experiment. Since the duration of this anomaly is longer than two previous anomalies, it is expected to be more significant, which will be confirmed by the data from Photogrammetry as well.

3.5.3.1. Geology vs. Photogrammetry

As mentioned in the table at the beginning of this section, fractures No. 7, and 8, has happened around this time According to the data coming from photogrammetry Fracture 7 is one of the most significant cracks during the whole experiment with 14 mm of displacement, which confirms the hypothesis presented in the geology section that this anomaly is more important than the previous ones. Here we only present the more important fracture (No. 7), the other one could be found in the photogrammetry section.
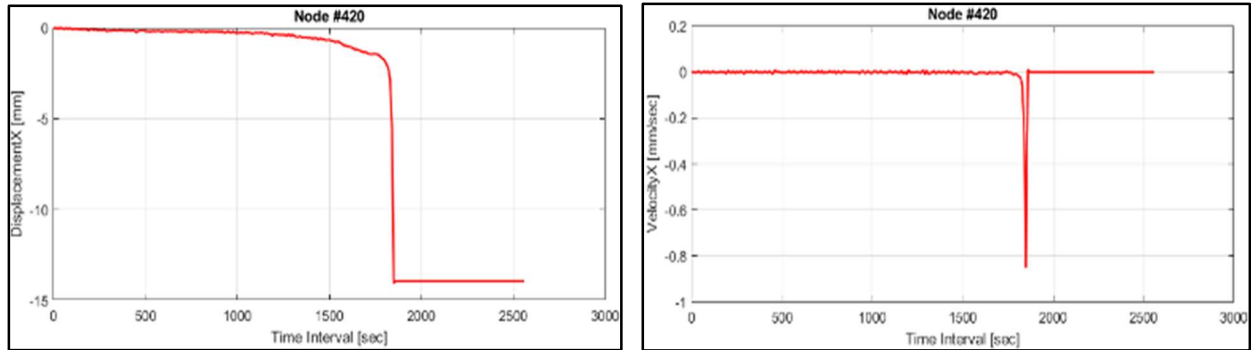

Fig.24.

Fig. 25.

3.5.3.2. Geology vs. Geophysics

Comparing the resistivity models acquired at T6, and T7, we can see that all the green areas are wiped out, and all the slope is showing a relatively high resistivity indicated by yellow and dark orange colors. This can show the formation of micro cracks inside the soil which are invisible to unarmed eyes, and photogrammetry devices. These cracks will be merged thereafter, and will lead to the larger collapses and transnational movements of the slope.
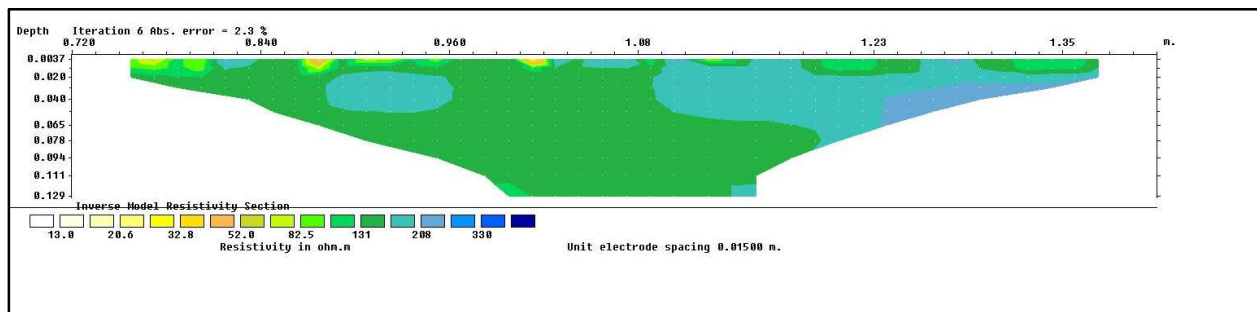

Fig.26.

3.5.4. Anomaly 4

This anomaly was both larger in size, and longer in time, compared with the first 3 anomalies, so it might indicate the collapse of the slope. This idea will be validated by data coming from other domains.

3.5.4.1. Geology vs. Photogrammetry

According to the data presented in the table, there are 6 different cracks happening at somewhat different parts of the slope around this time of the experiment. Also, the size of some of these cracks are very significant. For example, Fracture 4 caused a displacement of 12 mm, or fracture 13 led to an 11-mm displacement. So we can confirm that this is the failure and collapse of the slope. Among the 6 named fractures in the table, only fractures 9, and 11 are presented below; pictures and information about the other ones could be found in the photogrammetry part.
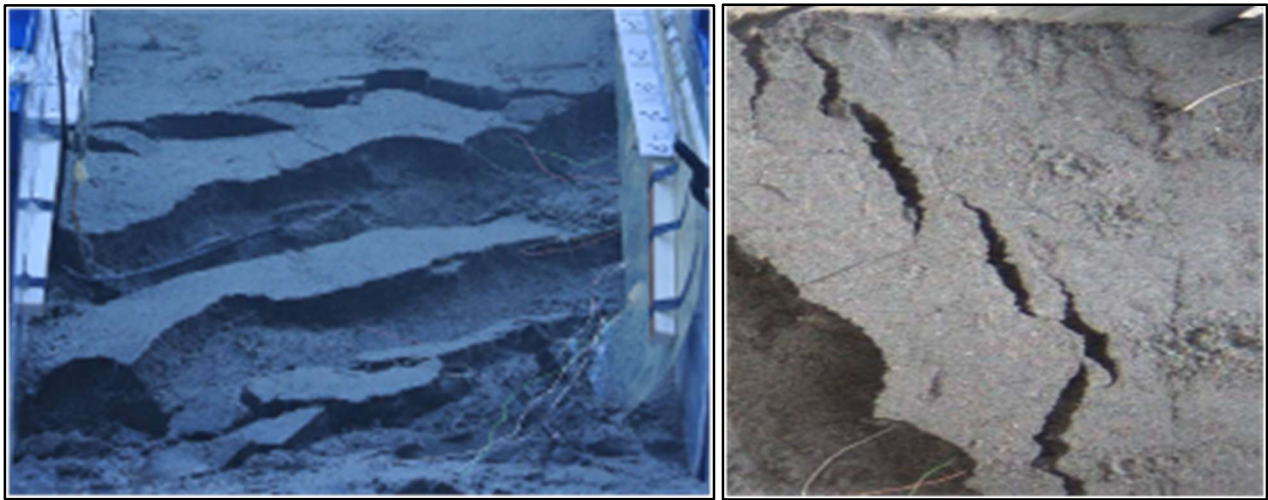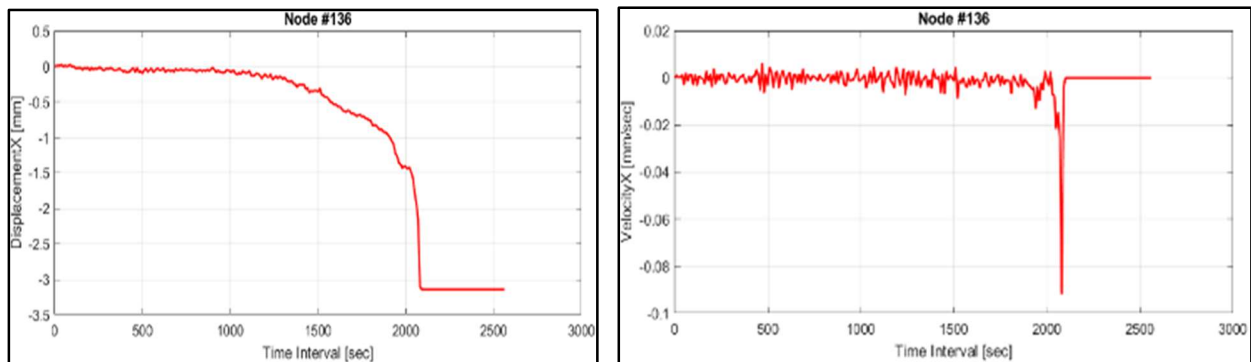
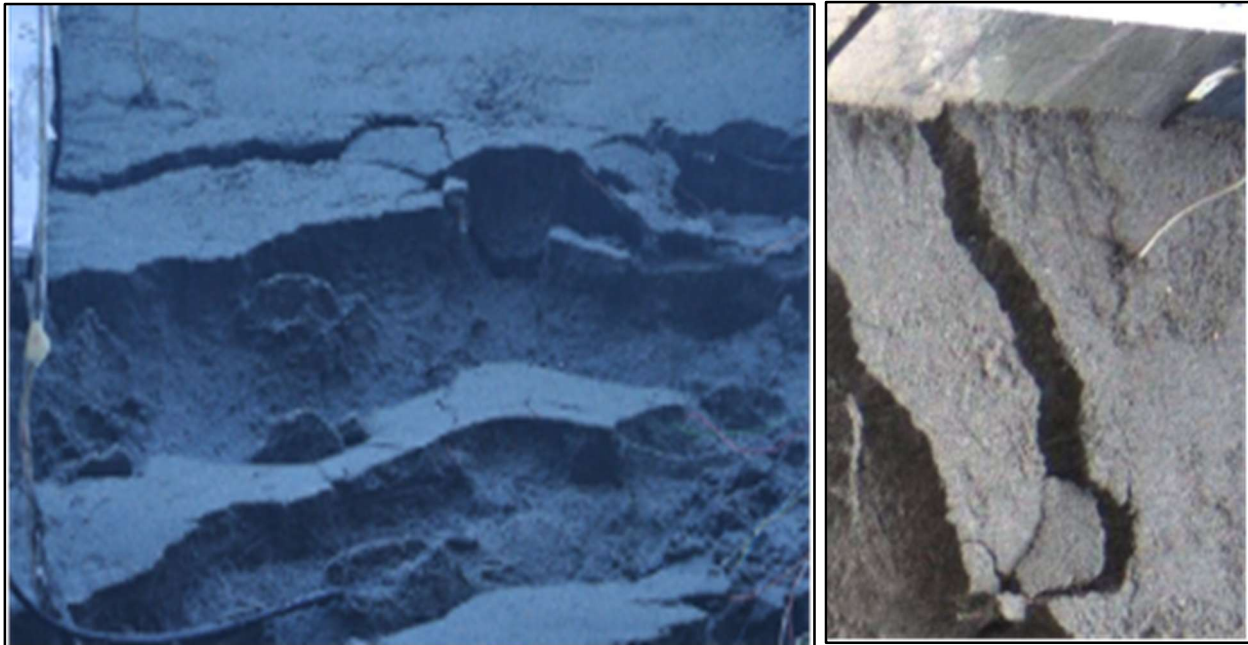Fracture 9:

Fig.27.

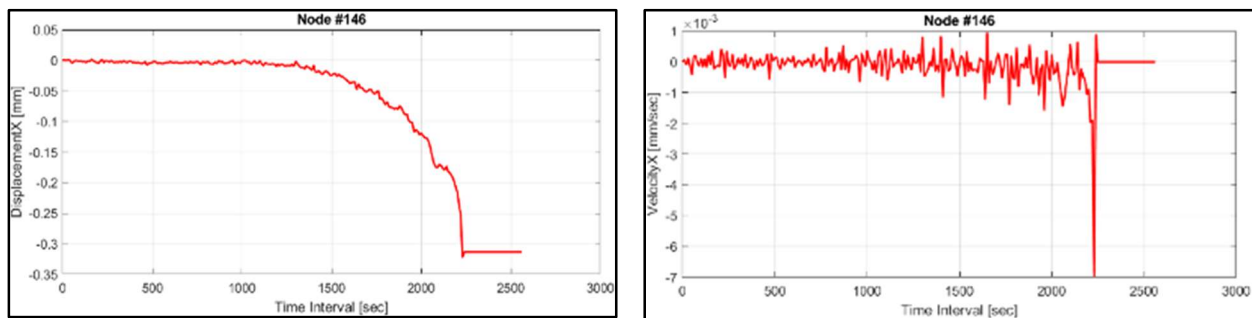*Fig. 28.*

Fracture 11:

Fig.29.

Fig. 30.

3.5.4.2. Geophysics vs. Geology vs. Photogrammetry

For this anomaly, according to the data from geology, we hypothesized that the collapse of the slope has happened, and this was validated through the information coming from the photogrammetry domain. According to the data from geophysics we can validate them as well. Comparing the resistivity models T9, and T10, shown below, there is a strange change in the toe of the slope, while in previous resistivity measurements, this part of the figure hasn't shown any special changes. In this part, all of a sudden, it shows a strange increase in the resistivity. As we said before, previous cracks happening at the downslope did not affect the geophysical instrument since they were far from each other. Having said that, this failure, which was a major crack with a translational movement as well, did affect the geophysical instrument. Due to this translational movement we lost some of the electrodes, and this is exactly visible in

the toe part of the T10. The red and dark purple colors indicate creation of the crack and losing the electrodes
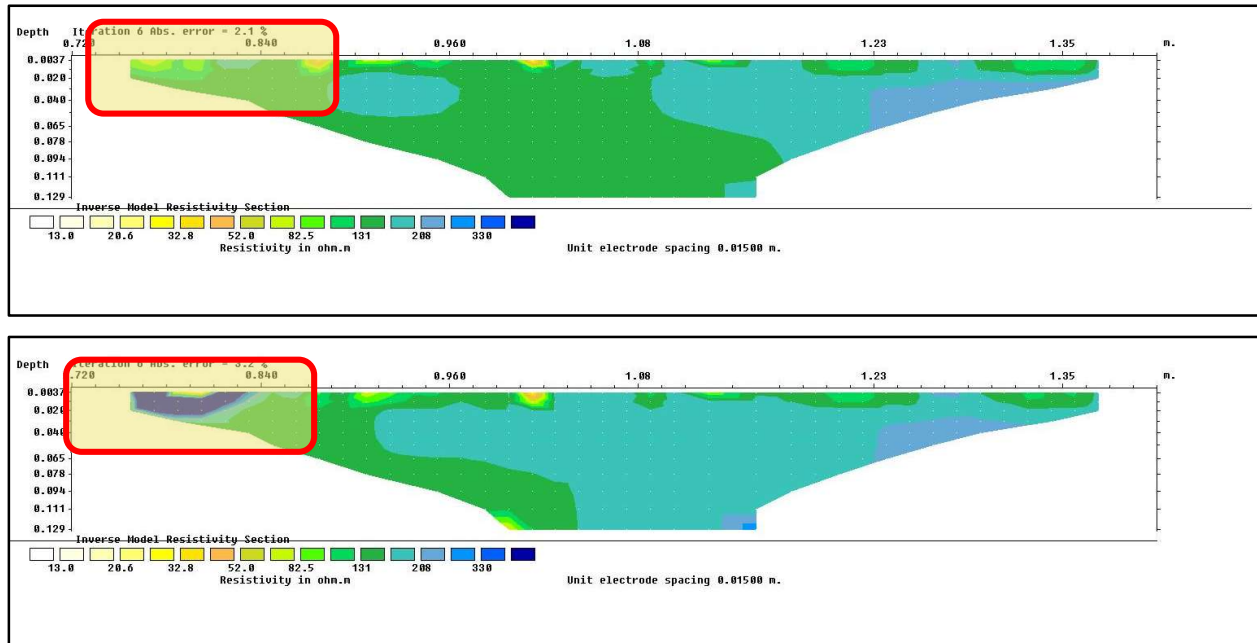
can be confirmed from here.

Fig.31.

3.5.5. Anomaly 5

This anomaly happened around 35 minutes after the beginning of the experiment in the TDR sensor results. As discussed in previous anomalies, given the constant rainfall, the value VWC is supposed to increase all through the experiment. In this anomaly, the value of VWC shows a sharp decrease, and since it is near the end of the experiment, it can be because of the last collapse.

3.5.5.2. Geology vs. Geophysics

As confirmed with the photogrammetry part, this anomaly is showing the collapse of the slope, which includes large movements of the sand, as the result of which, we should have lost some electrodes. According to the resistivity model, at around this time we have the T6 model. In this model, as it is highlighted in the figure below, there is dark purple color in the toe of the slope. This shows very high values of the resistivity which confirms the idea of losing the electrodes around that area.
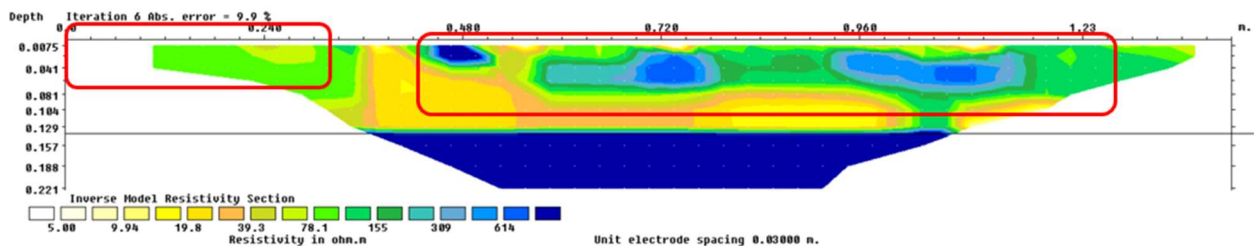

Fig. 32.

4. Numerical Modeling: SLIP Model

Scientists have developed a handful of models to be used in the management of emergency plans and to find the best planning for the purpose of mitigation measures. The most used models are statistical models with the implementation of the AI, and Machine Learning algorithms such as the Neural Network (NN), Random Forest (RF), Gradient Boosted Regression Tree (GBRT). However, the fact that these statistical models use only the rainfall data as their input to predict the shallow landslide, and do not take into account the geological, geotechnical, and geomorphological characteristics of the studied site, thus, they are assumed to be extremely simplified. Some scientists, on the other hand, have tried to apply physically based slope stability models such as SHALSTAB, SINMAP, TRIGRS, GEOtop-FS. These models have tried to take into account the physical characteristics of the studied sites, and with integrating those data with geographical information systems (GIS), they have been able to determine the timing as well as the localization of the possible landslides induced by rainfalls in the regional scale. The problem with those models is that they are computationally very expensive, therefore, can be used on small areas and for a short period of time. Therefore, scientists have developed another model, which needs much less computational effort, to apply it on larger scales.

SLIP (Shallow Landslides Instability Prediction) is a mathematical model developed to foresee the triggering of rainfall-induced shallow landslides (soil slips) and the unstable condition of slopes affected by these phenomena. This physically based model gives the factor of safety in function of the principal variables influencing the trigger of soil slips: rainfall, geometry, soil state, mechanical and hydraulic characteristics of soil. In this section, we are going to use the SLIP model for experiment 1 and compare the results with what we observed in the laboratory experiment.

4.1. Assumptions behind the SLIP model

1. *Soil slip happens only in thin superficial covers for a thickness of around 1-1.5 meters. This type of soil contains numerous pores, and openings created by small animals, shrinkage-drying cycles, and other factors. These processes create two types of pathways for water to infiltrate into the soil, the macro-porosity, and the pores in the soil matrix.*

2. *In the SLIP model, the water infiltrating into macro-porosities plays a vital role in the instability of the landslides. What happens in this case is the water in macro-porosity creates saturated zones, and the volume of these zones tends to increase by increasing the saturation of soil by rainfall events. The dimensions of these saturated zones increase till it makes the slope unstable.*

3. *Slopes can be considered to be infinite for the purpose of stability analyses.*

4.2. Theoretical Background and General Procedure

The SLIP model tries to give us the safety factor (Fs) by the application of the <u>limit equilibrium</u> <u>method</u>, to an equivalent infinite slope, and this slope is assumed to be composed of two separate soil parts. One part is supposed to be partially saturated, and another part, which consists of the saturated zones, is considered fully saturated. For the sake of simplicity, this separation is applied to the SLIP model by

considering the sub-layer fully saturated, as if all the saturated zones came together in the bottom half of the slope, and the partially saturated soil stays on the top of that. The bottom layer (saturated sub-layer) is assumed to have a thickness of mH (0<m<1) where H is the thickness of the soil which can be involved in the soil slip. In this formula, h is the rainfall depth, given by the pluviometric diagrams as a function of time, beta * is the proportion of the rain infiltrating into the soil, n is the porosity and Sr is the saturation degree.

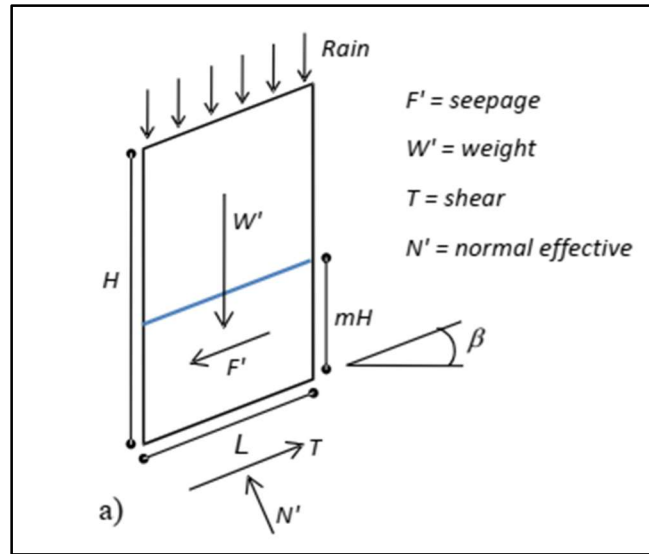$$mH = \frac{\beta^* h}{n(1 - S_r})$$ *(Equation 2)*

Fig.33. Representation of Stabilizing and destabilizing forces in SLIP model

According to [*Fig.19*]. There are a couple of formulas to implement the equilibrium equation and calculate the safety factor from it. The most important ones are listed below:

$$F_s = \frac{T_s}{T_d}$$ *Equation 3*

$$T_s = N' + tan\varphi' + C'$$ *Equation 4*

$$T_d = W' Sin\beta + F'$$ *Equation 5*

4.3. Using Slip Models

We have tried to modify the parameters such as the porosity, the slope, and the specific gravity, as well as the rainfall intensity and discharge data to apply the SLIP model for both experiments 0, and 1. The results of the SLIP model for experiment 1 were much more coherent with the laboratory experiment, compared with those of experiment 0. This difference in the accuracy of the SLIP model for two experiments can be explained by the configuration of the slope, on which we will elaborate in the upcoming section after presenting the results of each experiment. *[Fig.20]*.

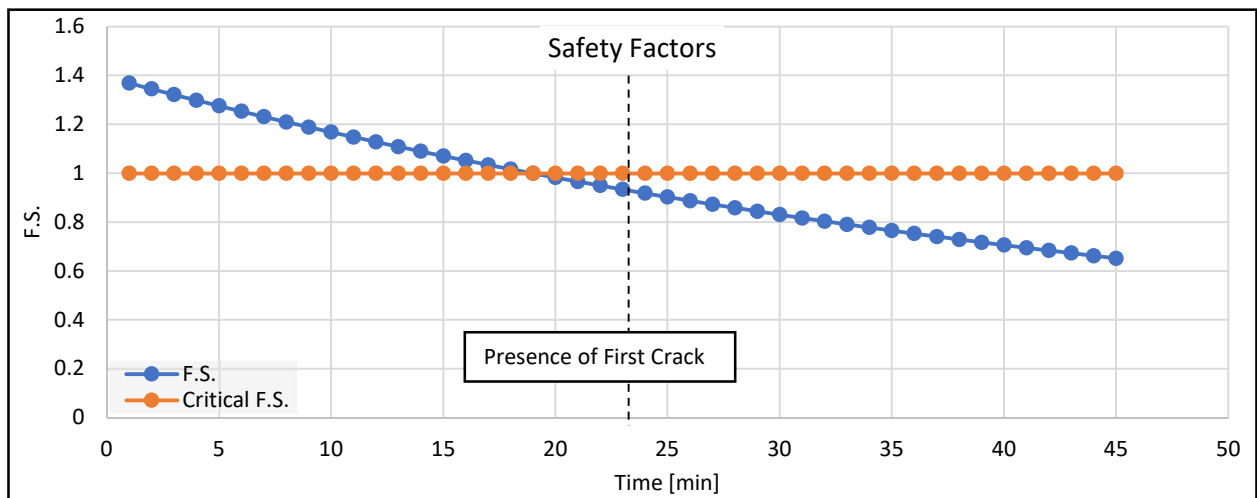### 4.3.1. Slip Model for Experiment 1

Fig.34. Safety Factors calculation due in Exp. 1

As the above figure presents, the SLIP model application for experiment 1 shows the time of the appearance of the first crack almost accurately, with only 2-3 minutes inaccuracy. According to the SLIP model, 19 minutes after the beginning of the experiment, the resisting forces become equal to the destabilizing forces, therefore, the Safety Factor (the blue curve) touches the Critical Fs, which is equal to 1.
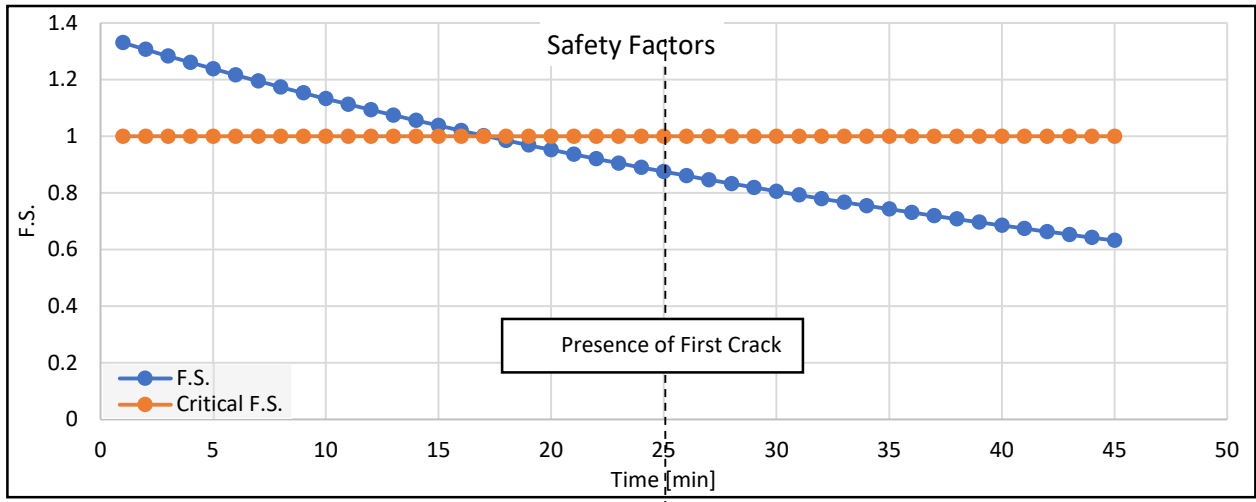
31

4.3.2. Slip Model for Experiment 0

Fig.35. Factor of Safety obtained from SLIP Model for Exp.0

As we mentioned before, the application of the SLIP model for experiment 0, failed to give a good approximation of the slope stability. In this case, the difference between the occurrence of the first crack in the laboratory test had 8 minutes delay, with respect to the results of the SLIP model. We will discuss the possible reasons behind this in the next section.

4.3.3. Analysis of the SLIP model for two experiments

As we discussed in the previous sections, the SLIP model worked well for experiment 1, however, it poorly approximated the crack time for experiment 0. Let's discuss the similarities and dissimilarities between the results of the SLIP model for both experiments.

4.3.3.1. Similarities

In both experiments, the time of the presence of the first crack is sooner than what happened in the laboratory experiment. This is due to one of the one of the most important weaknesses of the SLIP model, which is the fact that it doesn't consider run-off water. So, all the rainfall is assumed to infiltrate. So according to the SLIP model, more water flows into the pores of the slope, than in the real case scenario (the laboratory experiment); therefore, the destabilizing forces grow faster, and it gives an earlier crack time compared to what happens.

4.3.3.2. Dissimilarities

The level of inaccuracy of the SLIP model in two experiments was different. In experiment 0, the SLIP model time was 8 minutes earlier than the laboratory experiment, however, in experiment 1, this was only around 2 minutes. The reason behind this root in the theoretical mathematics of the SLIP model. As we explained in the section related to the theoretical background of the SLIP model, to develop this model, scientists have used a limit equilibrium method, in which soil is assumed to have two parts. A saturated sub-layer, and a partially saturated layer on the top of that. This is done for the sake of simplicity, and

32

therefore, can be a source of inaccuracy. But in the case of experiment 1, the slope configuration was exactly like this. In experiment 1, we built the slope. So, this fact, which is a source of inaccuracy for other experiments, works in favor of experiment 1, and increases its accuracy.

4.4. Sensitivity Analysis for SLIP Model

After comparing the results of the two experiments with the results obtained from the SLIP model, and finding the inaccuracies of the SLIP model, the next step is doing sensitivity analysis for the slip model, to understand how sensitive its results is, to the change of the different parameters such as the slope, the porosity, the friction angle, and the rainfall intensity. Since the two experiments were almost similar, except for the soil configuration, which cannot be considered in the SLIP model, we will present the sensitivity analysis of the SLIP model only for experiment 1.
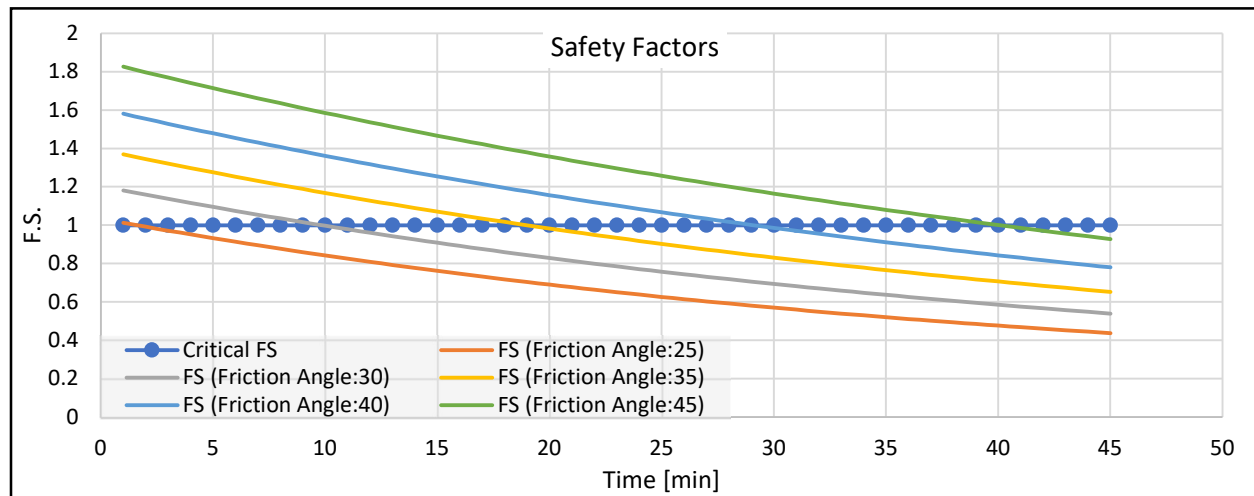
4.4.1. Sensitivity of Model to Friction Angle

Fig.36. Sensitivity of SLIP Model to Friction Angle

Soil friction angle is a shear strength parameter of soils. Its definition is derived from the Mohr-Coulomb failure criterion, and it is used to describe the friction shear resistance of soils together with the normal effective stress. Friction angle is one of the parameters that we must define in the SLIP model, and in order to see to what extent it affects the SLIP model, we did a sensitivity analysis on the variations of the friction angle, with keeping all other factors constant, to see how the variation of the friction angle changes the safety factor. According to *[Fig.22]*, we can see that the SLIP model is very sensitive to the changes of the friction angle, so it is very important to use a very accurate value for friction angle in the real case uses of the SLIP model.

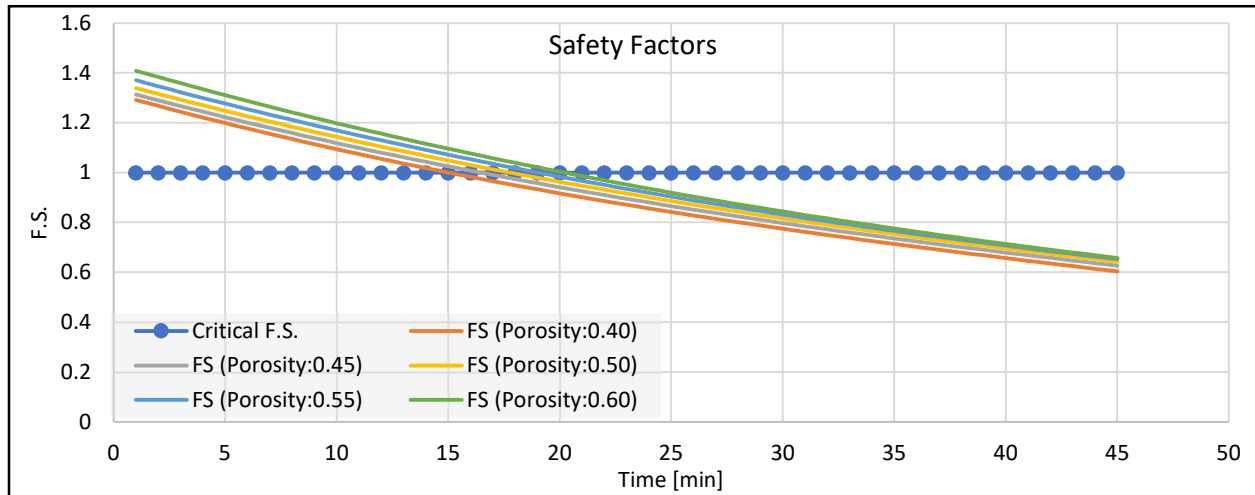## 4.4.2. Sensitivity of Model to Porosity

Fig.37. Sensitivity of the SLIP Model to Porosity

Porosity or void fraction is a measure of the void spaces in a material and is a fraction of the volume of voids over the total volume, between 0 and 1, or as a percentage between 0% and 100%. We performed another sensitivity analysis on the values of porosity, however, as the results suggest, the SLIP model is not very sensitive to the porosity values *[Fig.23]*.

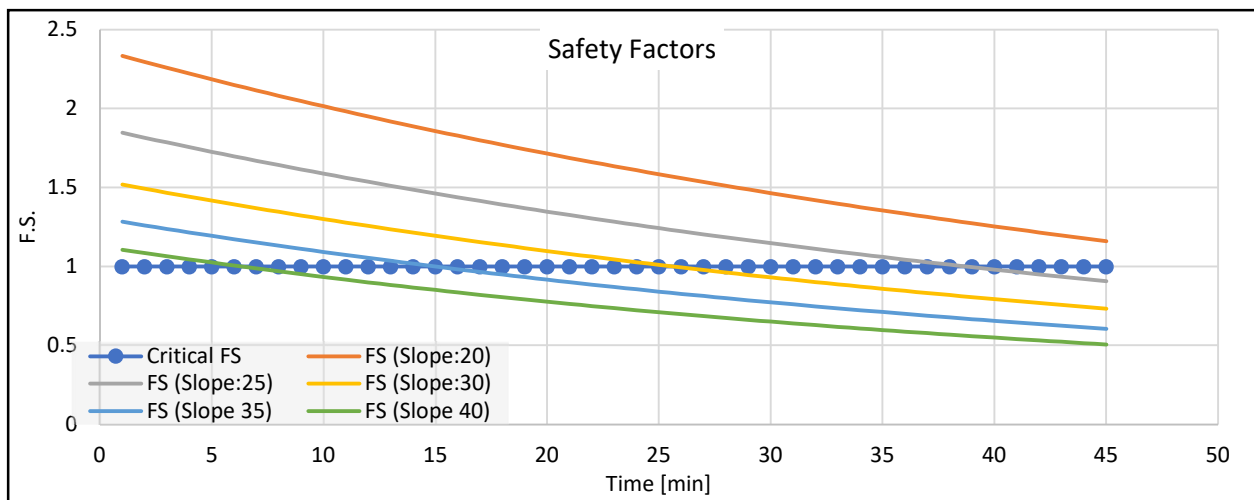## 4.4.3. Sensitivity of Model to Slope

Fig.38. Sensitivity of the SLIP model to Slope

Obviously, when we are talking about landslides, the most important factor is the slope. As the sensitivity analysis for Slope variation confirms, the SLIP model is also very sensitive to the slope variations *[Fig.24]*.

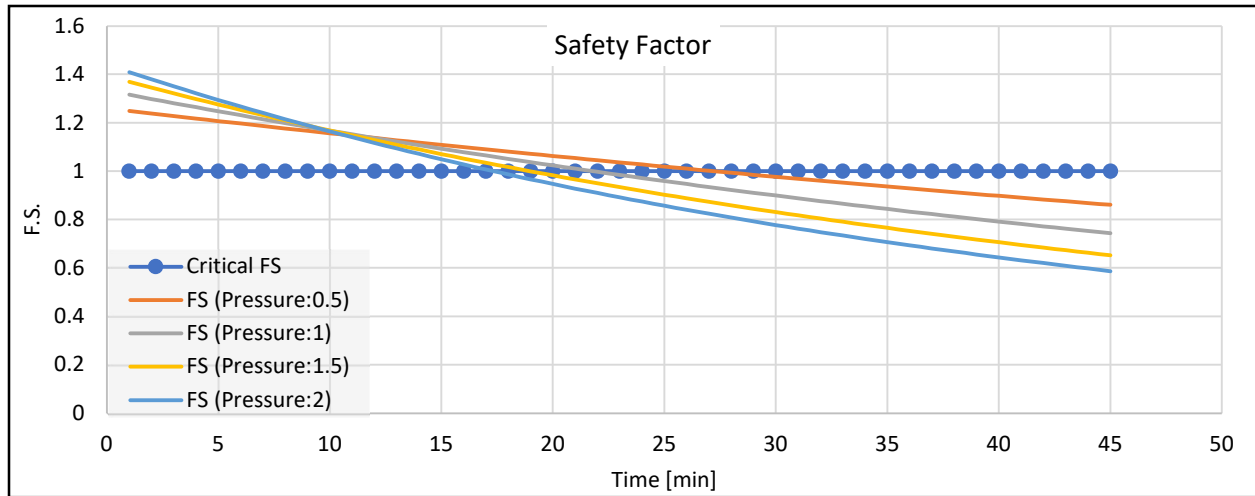## 4.4.4. Sensitivity of Model to Rainfall Intensity

Fig.39. Sensitivity of the SLIP model to Rainfall Intensity

Another important factor in rainfall-induced landslides is the intensity of the rainfall event. This is also considered in the SLIP model. As the figure above suggests, different intensities of the rainfall event affect the safety factor to some extent *[Fig.25]*.

4.5. Modification of the SLIP Model

As we discussed in the beginning of this section, according to the paper used to develop the spreadsheet for the SLIP model calculations, there are 2 limitations for SLIP model, which can be sources of inaccuracy. One of the limitations of the SLIP model is not considering the runoff water and considering the whole slope as a single layer characteristically. So in this part, we have tried to tackle these to limitations and develop a better SLIP model which can give us very accurate results, comparing with the previous, commonly-used SLIP model.

4.5.1. Tackling the Infiltration Problem

As said earlier, the SLIP model assumes 100% of the rainfall as infiltrated water. This means that in the SLIP model, the water saturation, which is a destabilizing factor, grows faster than what happens in reality. Because of that, the SLIP model gives us a crack time earlier than the real experiment performed in the laboratory. We have tried to consider different percentages of the rainfall as run-off, and check the results of the SLIP model, to see for what portion of the rainfall event, the SLIP model can give us a more precise value for the time of the first crack. According to our results, if we consider 25% of the rainfall event as the run-off water, and 75% of the rainfall as the infiltration, the time of the first crack in the laboratory experiment perfectly matches the time in which the Safety Factor gets equal to the critical safety factor. The validation of this assumption is also confirmed when we look at the values of the rainfall, run-off, and infiltration. According to the chart below, at the end of the experiment, the accumulated amount of rainfall was 64407 mL, and the accumulated amount of run-off water was measured as 16800 mL. By dividing the former by the latter, we would get a value of 0.26, which is very close to the proposed value of our model to use as the proportion of the run-off water (25%).

4.5.2. Tackling the Single Layer Problem

Another limitation of the SLIP model was the fact that it considers the full depth of the soil in the SLOP as if they had totally similar characteristics, in terms of Porosity, or other physical characteristics. Since in experiment 1, the physical characteristics of the soil was different in terms of compaction, which directly affect porosity, we have tried to take this into account, and develop the SLIP model formulas and the Equilibrium Equations in a way to enable us to give separate values of porosity for the two layers of the slope. According to the equations presented in the theoretical part of the SLIP model, there are two parameters directly affected by the porosity value, W' and N'. So, to enable to SLIP model to accept two different values for porosity we need to modify both stabilizing and destabilizing forces. The original formulas which have been used in the SLIP model are as below:

$$W' = cos\beta * H * \Delta s * \gamma_w [m(n-1) + cos(1-n) + nS_r(1-m)] \text{\small{Equation 6}}$$

$$N' = cos^2\beta * H * \Delta s * \gamma_w [m(n-1) + cos(1-n) + nS_r(1-m)] \qquad \text{\small{Equation 7}}$$

In these two equations, the parameter n represents the porosity of the soil, and H represents the depth of the whole soil layer. The modified formulas for W' and N' are as below:

$$W' = (cos\beta * 0.5 * H * \Delta s * \gamma_w [m(n-1) + cos(1-n) + nS_r(1-n)]) +$$
$$(cos\beta * 0.5 * H * \Delta s * \gamma_w [m(0.85*n-1) + cos(1-0.85*n) + 0.85*nS_r(1-m)]) \quad \text{\small{Equation 8}}$$

$$N` = (cos^2\beta * 0.5 * H * \Delta s * \gamma_w [m(n-1) + cos(1-n) + nS_r(1-n)]) +$$

$$(cos^2 * 0.5 * H * \Delta s * \gamma_w [m(0.85*n-1) + cos(1-0.85*n) + 0.85*nS_r(1-m)]) \quad \text{\small{Equation 9}}$$

By this modification, what we have done is explained in the following steps:

1. repeating all the parameters and multiplying the depth of both (H) in 0.5. So far, we have created two layers, but since none of their parameters have changed, we would get similar results.
2. In the top layer, we have used compacted soil, so the porosity of that would decrease to some extent. We have used different reduction factors for that and understood that if we decrease the porosity of the compacted layer by a value of 15%, the SLIP model will accurately give us the time of the first crack.

Below is presented the SLIP model results taking into account both modifications of runoff and porosity reduction in the top layer.
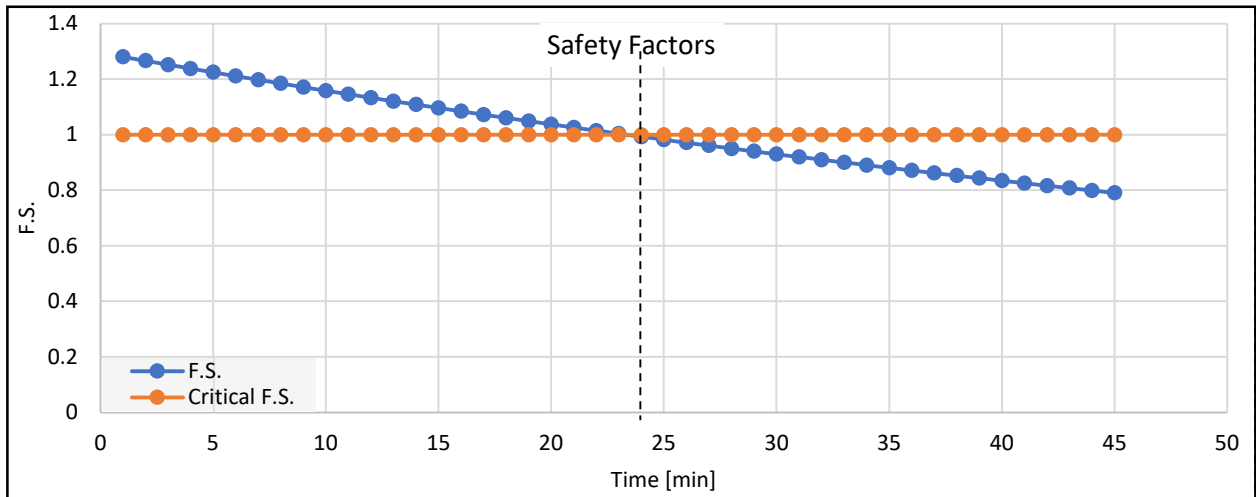

Fig.40. Sensitivity of SLIP Model to Friction Angle

5. Suggestions for Better Experiment

5.1. Boundary Condition Problems

Concerning the artificial rainfall, the placement of the sprinklers was in a way that a small portion of the produced rainfall was dropped on the plastic walls of the landslide simulator (highlighted in yellow), and those portions of rainfall would reach the landslide from two sides where soil was in touch with the plastic walls (the red line). So those parts of the soil in contact with the plastic walls would be washed away faster than other parts. So, this causes the failure of landslides almost always from one of the corners. This can be prevented by placing the sprinklers right in the middle, between the cameras. Another approach can be collecting the water spread on the walls before reaching the landslide surface, which is more complicated.

5.2. Run-off Water Measurement

Another problem which was common in our laboratory experiment, as well as experiments of other groups, is concerned with the run-off water collection. As we witnessed during the experiment, the procedure of the run-off water measurement was like the run-off water flowed into the wooden box, then from there through a channel it would flow into a measuring cup. However, during these steps, a good part of it was missed to collect and measure. Although the SLIP model itself doesn't take into account the run-off water, through some analysis as we did in the previous section, we can find a correlation between

Fig.41. Fume Experiment Frame

the run-off water, and the SLIP model crack time, therefore, it is important to have an accurate measurement of the run-off water.

6. Conclusion

According to the theoretical backgrounds and the general procedure of experiments, we mentioned that the SLIP model has some weaknesses such as considering the soil configuration as two layers, a fully saturated sub-layer, and a partially saturated top layer. However, this is not a general configuration of the laboratory experiment. What usually happens is that the characteristic of the soil is uniform in all depth in certain experiments, thus, this could be a point of weakness for experiments. Having said that, the soil configuration which can be a source of inaccuracy for general experiments, was totally in line with the soil configuration of experiment 1, so it worked in favor of experiment 1 results and increased its accuracy.

Another source of inaccuracy in the SLIP model was not taking into account the run-off water. So what happens when the SLIP model assumes all the rainfall infiltrates is that it takes a shorter period of time for the slopes sub-layer to get fully saturated, and in the equilibrium equations, the destabilizing forces equate the resisting forces sooner than the actual case happening in the laboratory experiment. To tackle this problem, we did a sensitivity analysis on different parameters of the SLIP model, and figured out the SLIP model is most sensitive to the slope, and the rainfall intensity (or discharge). So we did another analysis and reduced different percentages of the accumulated rainfall from the "h(t0i)m" and found for 25% rainfall reduced as the run-off water, the SLIP model accurately gives the time of the first crack.

This can be validated through the experiments that other groups have done/will do.

7. Photogrammetric Monitoring and Assessment

The advent in remote sensing technologies have greatly facilitated their creation and frequent updating for application in geomorphology, hydrology, geophysics, and natural hazards *[7]*. Photogrammetry has been considered a crucial aspect of the assessment and monitoring of different natural hazards *and,* in particular, landslides, given the small error they compute and the high level of details they can provide. During the landslide simulation experiments that were carried at Politecnico di Milano, Lecco, we have implemented some photogrammetric techniques-by the aid of advanced instruments- to increase the level of data acquisition and information about the landslide, thus, we would be able to understand the effect of the triggering factors and the phases of failure to further develop an Early Warning System.

7.1. Landslide Monitoring and Assessment using Photogrammetry

During the experiments, we used photogrammetry to evaluate the following: Surface point tracking using the 2D DIC technique; Developing 3D images of the landslide; Measurement of the volume change of the displaced material. The instruments that were used are: Three CMOS cameras, 2x FLIR BFS 31S, 1xFLIR BFS 50S -2x lateral cameras are used for constructing the 3D surface reconstruction of the landslide, and 1x camera is used for image sequencing for digital image correlation (DIC)-; Terrestrial Laser Scanner, long-range Rielg LMS 400Zi -Used for computing volume change-; Total Station-to geo-reference the computed points; Nikon Camera, to take timelapse images of the experiment. *[Fig.42 & Fig. 43].*
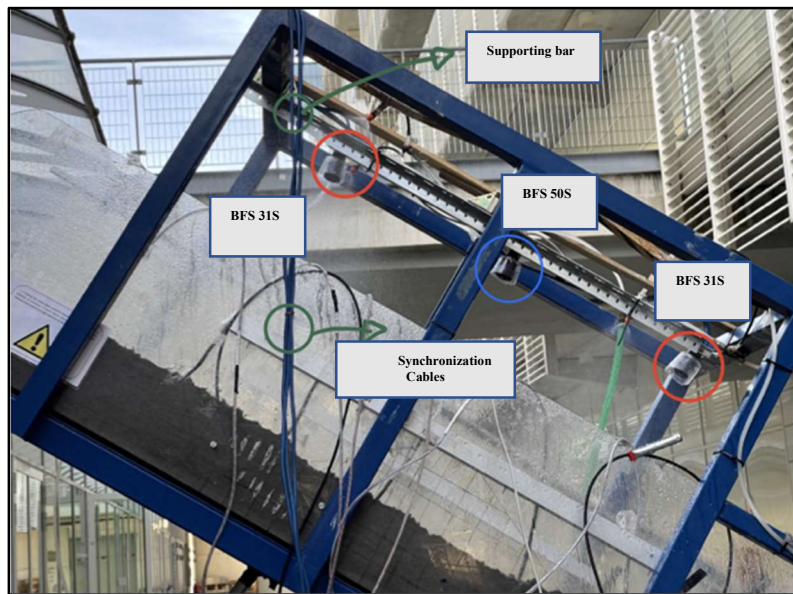

Fig.42. Three cameras for digital image correlation and 3D Surface construction Setup/   *Fig 43. Terrestrial Laser Scanner and Nikon*

Table 4. 3x Cameras Specifications

	Size	Pixel Size
BF 31S	(2048*1536pix)	3.45micron
BF 50S	(2448*2048)	3.45micron

7.2. 2D Digital Image Correlation Technique

Digital image correlation is a non-contact method for measuring motion, deformation, and strain in objects or materials subject to an applied load *[8]*. DIC depends on digital images processing, consequently, the main identification patterns that DIC follow depends on the pixels of the picture, moreover, DIC identifies a set of subset pixels that are pre-defined by the user to track the temporal displacement changes to selected subset. *[Fig.44]*

7.2.1. 2D DIC Procedures and Considerations

There are multiple solutions that optimize the Digital Image Correlation techniques (e.g., VIC 2D, VIC 3D, and MATLAB). In our experiment, we have used MATLAB's Digital Image Correlation and Tracking developed interface by Ebrel & Bundschuh *[3]*. The results obtained helped us to understand the behavior of the landslide in terms of displacement and velocity. Consequently, we could indicate the exact time of the start of a fracture, total failure, as well as the progression rate of these events that will be later compared with the results obtained from Experiment 0. First, a grid of points has been drawn over the first clear image that cover the whole slope- The grid is used to identify the points that will be tracked by the algorithm-, then an image sequence comparison will be performed by the MATLAB, comparing the different set of images. In our experiment we have more 259 captured images from the 3xCameras that enabled us to get lateral and central views of the whole area of the slope. And a fine grid of 506 points has been drawn to cover the whole area of the slope, to further analyze the points of interests.

Moreover, there have been some precautions to be applied before the start of the experiment to ensure a good quality of data and accurate results, e.g., making sure that the lenses of the camera are clean and set to the same focal length; considering errors as consequences of rainfall drops; sinkholes-which would give an initial displacement. Additionally, the results obtained from DIC are in *[pixels],* so we need to compute the GSD parameter to convert from *[pixels]* to *[mm]*.
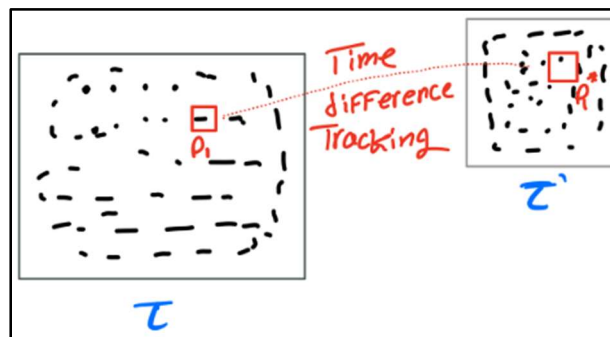

Fig.44. Image Surface tracking between Image 1 and 2

7.2.2. Ground Sampling Distance (GSD)

The GSD depends on three main parameters: Focal length [F]; Distance from the lens to the object [H]; Pixel size [px]. The focal length [F] has been fixed in both experiments (exp.1 & exp.0) by adjusting the three FLIR cameras before the beginning of the experiment. There are two main zoom values: 1.8mm, it has a wider view but smaller resolution; 3mm, which has a smaller field of view but higher resolution. The three cameras have been set on the 3mm focal length. Additionally, the distance between the lens and the surface of the landslide has been measured using a metric tap [H]. The GSD can be computed using the following equation *[Fig.45]*:

$$GSD = \frac{Distance\,from\,the\,lens\,to\,the\,object[H]}{Focal\,length[F]} * (Pixel\,Size[pix])$$

$$GSD \text{ (for experiment 0)} = \frac{550[mm]}{3[mm]} * (0.00345[pix]) = 0.6325\ [mm/pix]$$

$$GSD \text{ (for experiment 1)} = \frac{550[mm]}{3[mm]} * (0.00345[pix]) = 0.6325\ [mm/pix]$$

The GSD is a crucial parameter in Digital Image correlation as it decides the pixel size of the image. For example, having a GSD of 10cm means that each pixel corresponds to 10cm on the ground. The lower GSD we have the better resolution we get. The GSD is used to get the displacement and velocity values for each of the nodes that constitute the grid of points that cover the body of the landslide = *[GSD*pixel number]*.
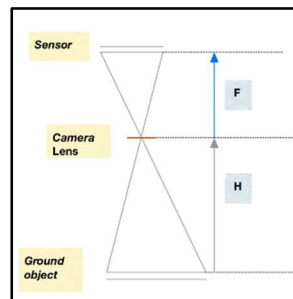
Fig.45. Ground Sampling Distance

7.2.3. Time Acquisition of the instruments

The Time Acquisition of the instruments depends on the user's preference in terms of the level of details that he/she would like to have out of the experiment. In our experiment, the time acquisition for the Laser Scanner is phase based, thus, when the phase of failure change during the experiment, a scan is taken to compare it with its predecessor, however, the time acquisition for the 3 FLIR Cameras was every 10 seconds.

7.2.4. 2D Digital Image Correlation Results and Analysis

After computing the GSD and setting the time acquisition, we started connecting the three cameras to a PC for further settings input using Multicamera System software. At the end of the experiment, we began processing the images taken by the three FLIR camera on MATLAB, following the steps mentioned below:

7.2.4.1. GRID selection

The grid was selected by using the rectangular shape on MATLAB and it was further enhanced by extra grid points in the downslope of the landslide-this area was characterized by an aggressive volume displacement during the experiment and having a finer grid around it would help us to better analyze these points. The grid has been divided into the following sections: downslope, first set of cracks-marked in dark red and red, and second set of cracks; upslope -using 50x50 pixel- *[Fig.46 & Fig.47]*

7.2.4.2. Displacement & Velocity graphs

The computation of the displacement and velocity is based on the multiplication of the (*pixel size* GSD* for the selected node in [mm]), and since the time of the data acquisition is known, the velocity can be computed in [mm/sec]. They have only considered the displacement and velocity in the X direction as the values in the Y direction is almost negligible. The choice has been made to a selected set of points; depending on the location of these points-the downslope area was prone to early cracks-; the results taken from Geology and Geophysics. We will be considering the downslope area, in which, most of the fractures occurred during the experiment-based on the frontal camera-. For experiment 0 and 1, visually, we identified 12 & 14 types of failures for both respectively, that occurred during the duration of the landslide.

7.2.4.3. Uncertainties in DIC Method & Nodes Selections

The choice of the nodes is sensitive to the location at which the failure has occurred, the nodes were chosen based on the displayed grid of the nodes on the image's number that corresponds to the beginning of the fracture. The DIC algorithm follows each node throughout a sequence of images, and whenever the algorithm loses the trace of a point, it shows two marks: green circle, which indicate the node location on the grid; Red x, which shows where the node tracing has stopped. Before picking the node for analysis, we must state the uncertainties that can be found in the DIC method: In our case of having a dynamic targets condition, uncertainties due to the motion effect (i.e., blurring) can be found *[9]*. In addition to that, rain drops from the sprinklers, lightning conditions and prior formation of holes can cause uncertainties in the results. In order to account for these prior-information we have differentiated between three different conditions that the surface point tracking does show: The nodes that have already reached its peak before the activation of the fracture in question; the nodes that have been lost early in due to, either been in a sinkhole or blurring condition; and finally the nodes that didn't reach its peak yet before the activation of the fracture in question and still being tracked by the image sequence. The latter has been filtered out and the choice of the nodes has been based on them. The node that was picked for each failure was the closest to the beginning of the presence of the crack, e.g., in *[Fig.47]* node 178 has been traced for *(Fracture 10)*. However, in some cases (i.e., failure 1) due the presence of some holes in that area, the results obtained were compromised, but will be later confirmed/adjusted by the Orthophotos obtained from Metashape. In the following sections, we have detected the fractures that have occurred in Exp0 & Exp1, computed the Displacement and Velocity values in the X-direction (the values of displacement are in negative sign as the X-axis [0,0] point is at the downslope),

thus, the dashed line(in section7.2.5 & 7.2.6) represents the failure time, beside which, you can find the location of each node (represented in XY coordinates) and the type of failure.
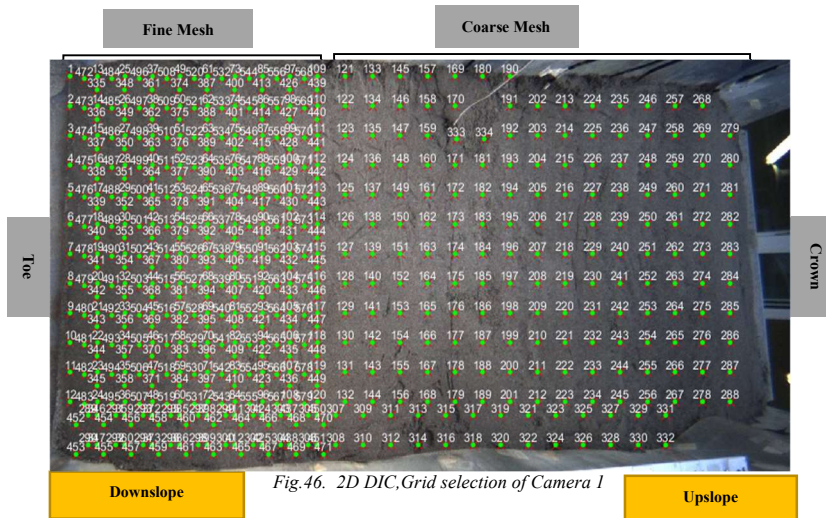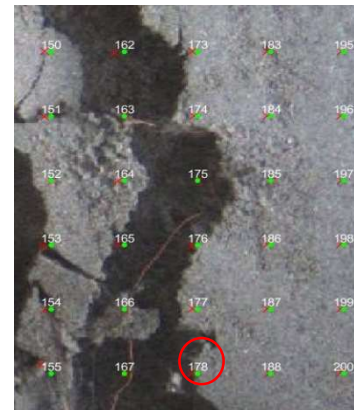

Fig.46. 2D DIC,Grid selection of Camera 1

Fig.47. Example of node selection for (Fracture 10)

7.2.4.4. Analysis Methodology

A methodology has been implemented to incorporate the geology, geophysics, and photogrammetry results and compare these with experiment 0.

1) *Quantify, visually, the fractures in the landslide body in both experiments, with the aid of the frontal and the three FLIR cameras. And point out the nodes on the generated MATLAB's grid to correspond to each different type of fracture [Fig.47]*

2) *Use 2D DIC to trace the displacement & velocity of the chosen nodes-to show the progression rate of fractures*

3) *Study the nodes' results in terms of location on the slope, failure time, displacement, and full strain change of the whole landslide body. Compare the results between experiment 1 and experiment 0 and interpret them with the help of the geological and geophysical information*

7.2.5 Experiment 1 results

Front Camera, Fracture 1   *Front Camera, Fracture 2*   *Front Camera, Fracture 3*   *Front Camera, Fracture 4,5,6*

Camera 1#103, Fracture 1   *Camera 1#148, Fracture 2*   *Camera 1#164, Fracture 3*   *Camera 1#173, Fracture 4,5,6*

Fracture 1

Coordinates of node 483(X=6.92, Y=9.84)

-Progressive Failure
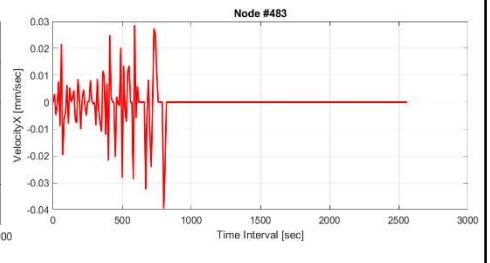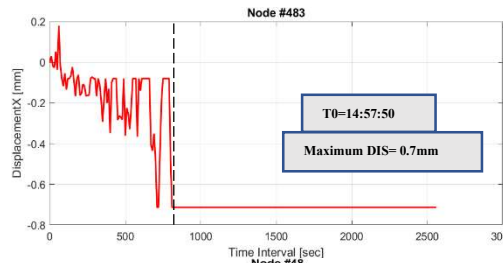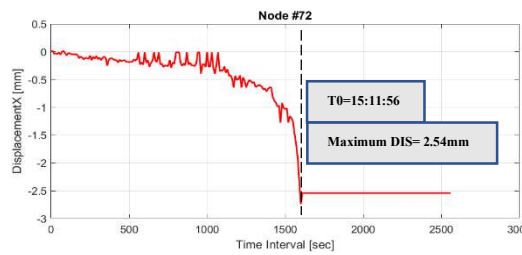

Fracture 2

Coordinates of node 48(X=8.16, Y=9.80)

-Gradually Increase in displacement
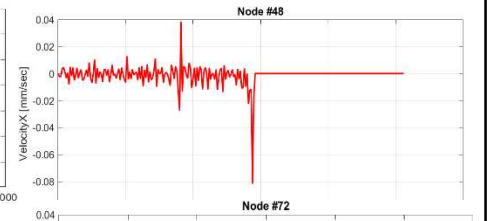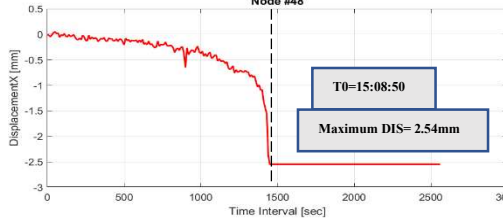
Fracture 3

Coordinates of node 72(X=9.16, Y=9.80)

-Progressive Failure
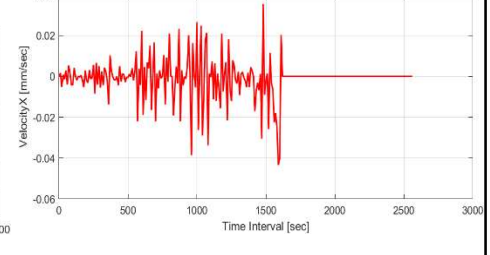
Fracture 4

Coordinates of node 422(X=1.01, Y=9.03)

-Gradually increase in the displacement
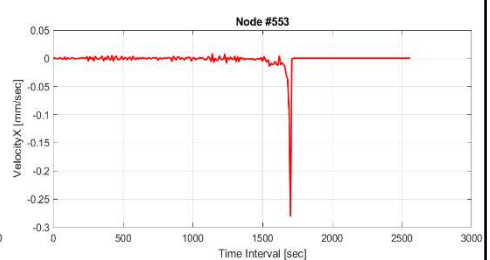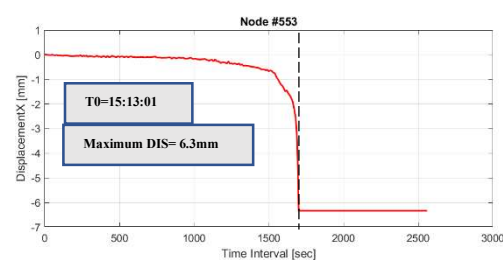
Fracture 5

Coordinates of node 305(X=1.09, Y=1.00)

-Phase Failure

Node #305 — DisplacementX [mm] vs Time Interval [sec]

T0=15:12:50

Maximum DIS= 2mm

Node #305 — VelocityX [mm/sec] vs Time Interval [sec]
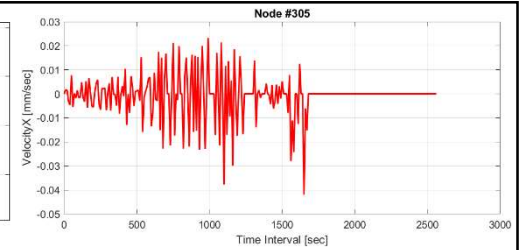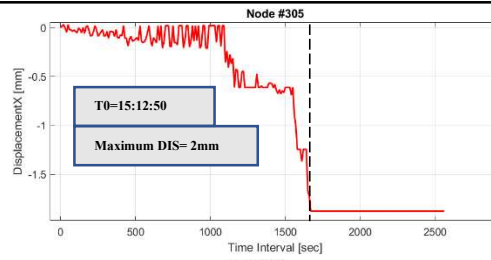
Fracture 6

Coordinates of node 408(X=9.65, Y=8.53)

-Progressive Failure

Node #408 — DisplacementX [mm] vs Time Interval [sec]

T0=15:13:20

Maximum DIS= 3.89mm

Node #408 — VelocityX [mm/sec] vs Time Interval [sec]
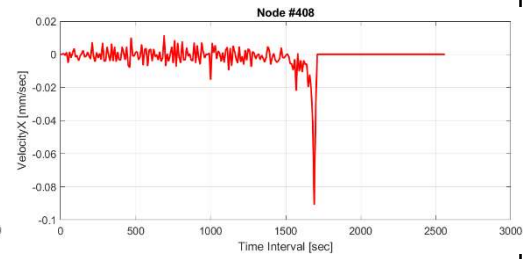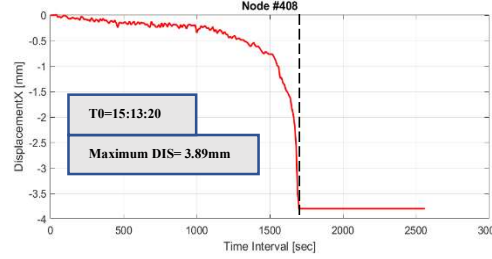
Front Camera, Fracture 7   *Front Camera, Fracture 8*   *Front Camera, Fracture 9*   *Front Camera, Fracture 10*   *Front Camera, Fracture 11*

Camera 1#186, Fracture 7   *Camera 1#198, Fracture 8*   *Camera 1#212, Fracture 9*   *Camera 1#222, Fracture 10*   *Camera 1#227, Fracture 11*
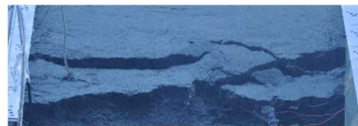
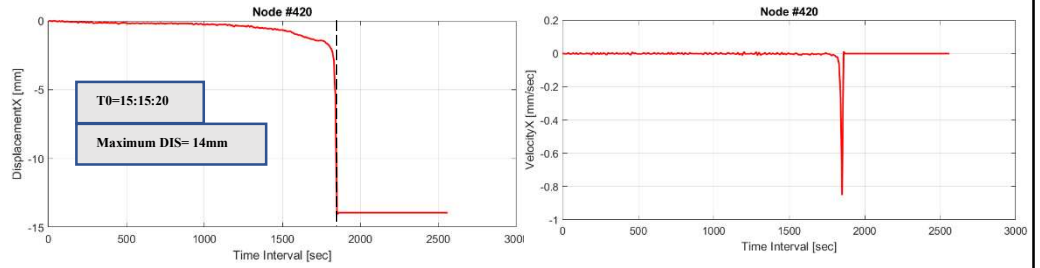*Frontal Camera, Fracture 12, 13, 14*

Camera 1#242, Fracture 12,13,14

46

Fracture 7
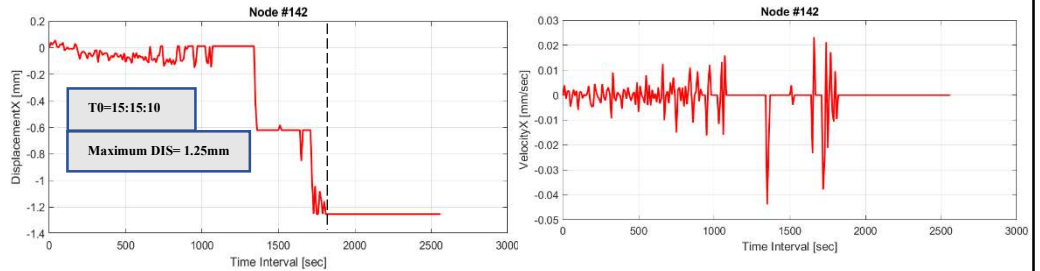
Coordinates of node 420(X=1.11, Y=9.30)

  -Gradual Increase in displacement

Fracture 8

Coordinates of node 142(X=1.21, Y=8.80)
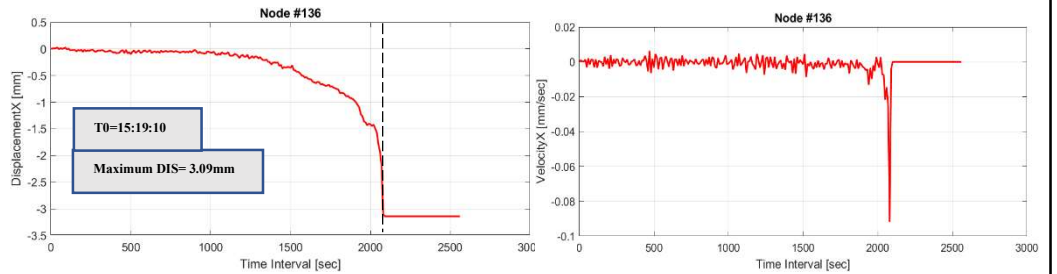
  -Phase Failure

Fracture 9

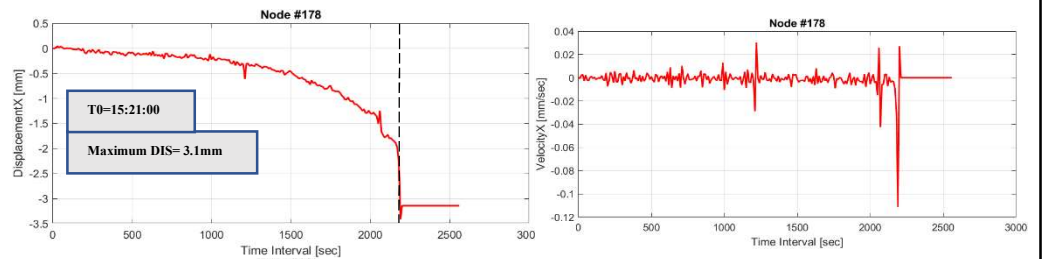Coordinates of node 136(X=1.21, Y=5.80)

  -Progressive Failure

Fracture 10
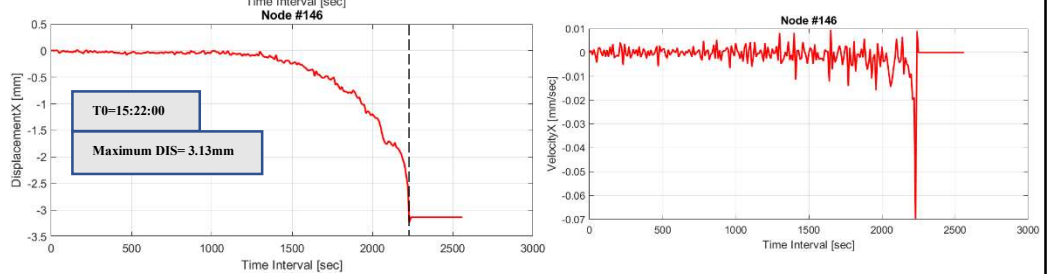
Coordinates of node 178(X=1.36, Y=9.30)

  -Progressive Failure

Fracture 11

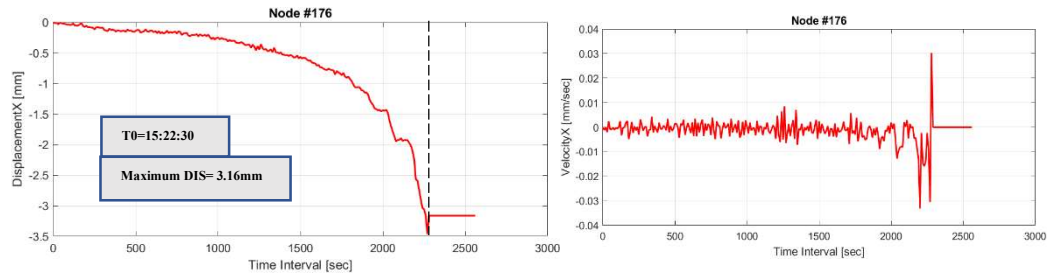Coordinates of node 146(X=1.26, Y=4.80)

  -Progressive Failure
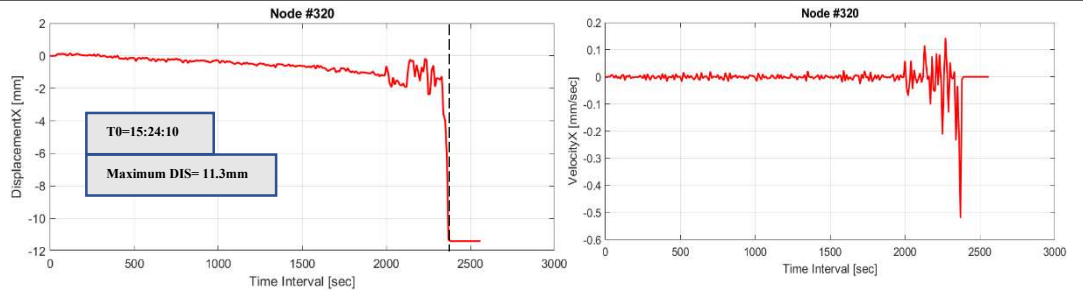
Fracture 12

Coordinates of node 176(X=1.36, Y=8.30)

-Progressive Failure

-

Fracture 13

Coordinates of node 320(X=1.44, Y=1.05)

-Phase Failure

Fracture 14

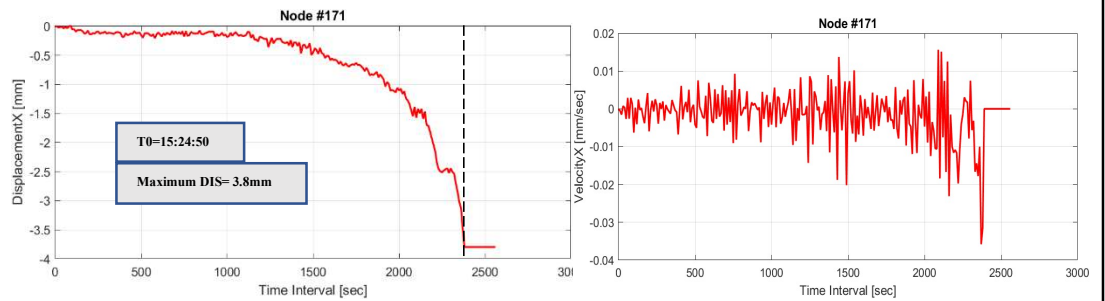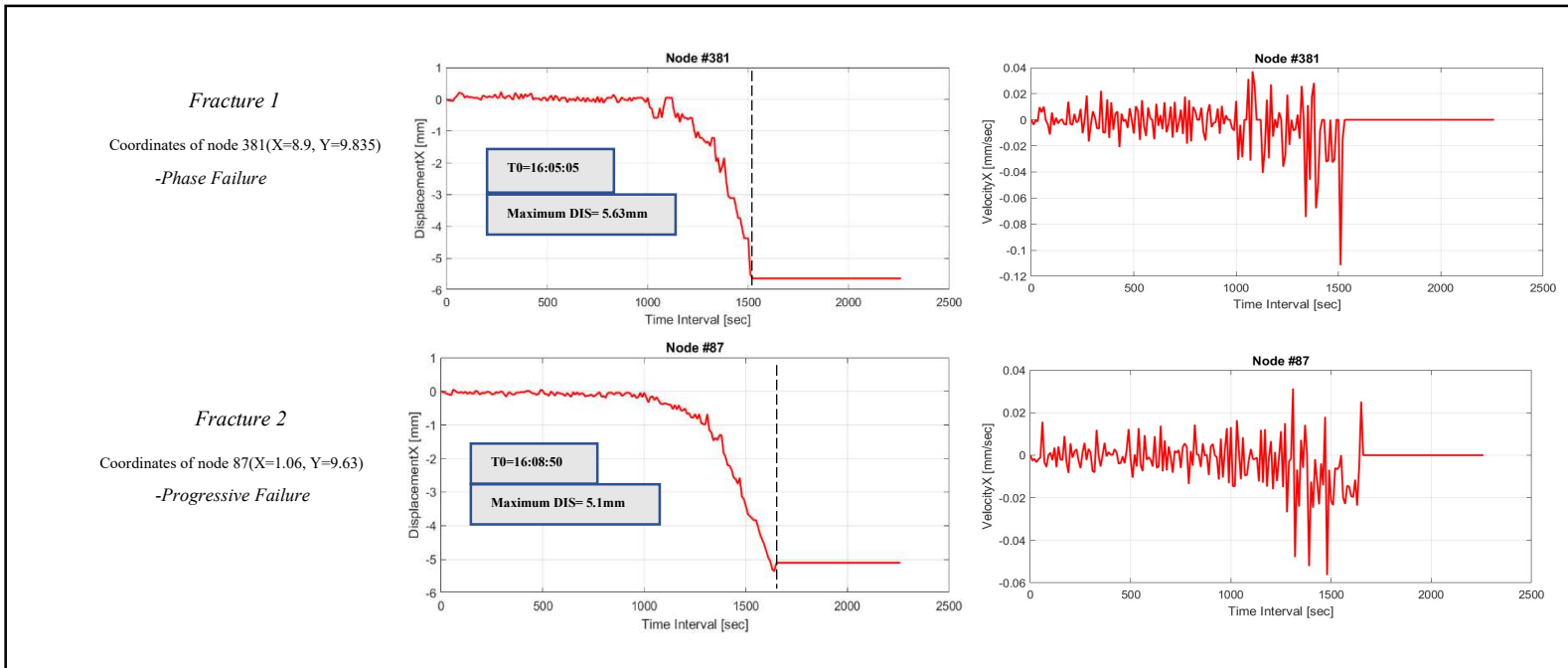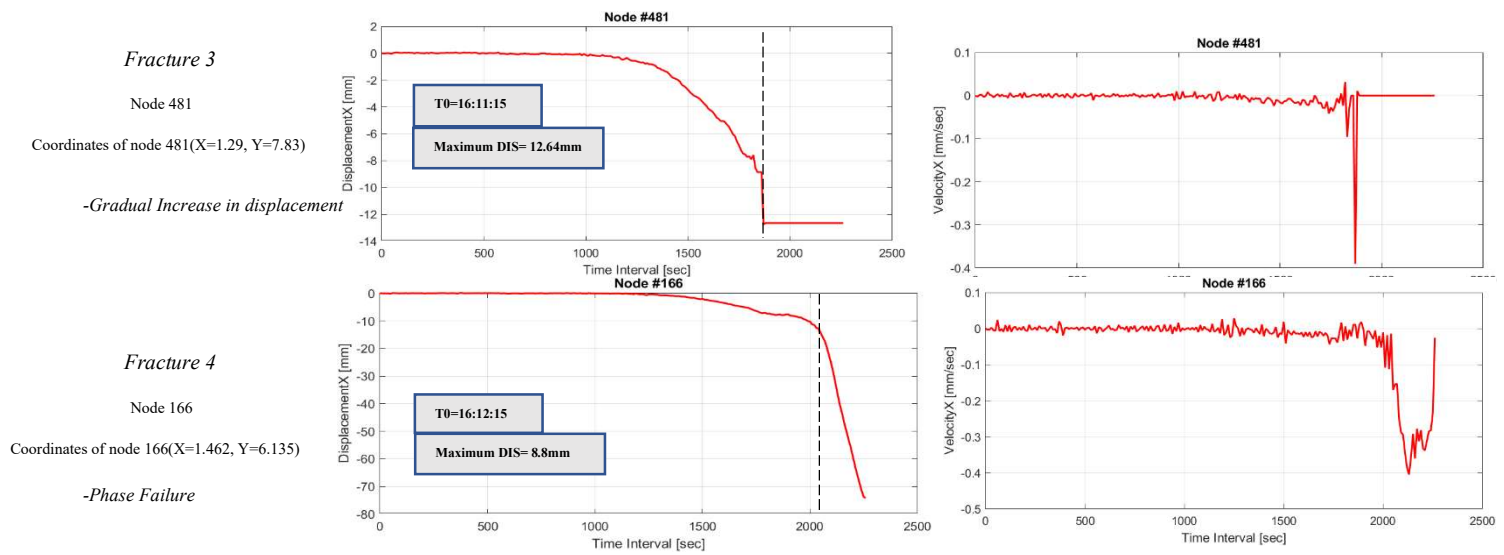Coordinates of node 171(X=1.36, Y=5.80)

-Progressive Failure

Fig.48. each colored circle represents the node chosen for its corresponding fracture, F.1, F.2, F.3, F.4, F.5, F.6, F.7, F.8, F.9, F.10, F.11, F.12, F.13, F.14

7.2.6 Experiment 0 results

In experiment 0, we focused on 4 types of fracture in which we computed the time of failure and the maximum displacement and velocity recorded during the landslide. The results obtained will be compared with experiment one's results to have a clear understanding of the time, displacement, and velocity differences, consequently, we would have a clearer idea of the mechanism of the landslide due to the different triggering factors.

Fracture 1

Coordinates of node 381(X=8.9, Y=9.835)

-Phase Failure

T0=16:05:05

Maximum DIS= 5.63mm

Fracture 2

Coordinates of node 87(X=1.06, Y=9.63)

-Progressive Failure

T0=16:08:50

Maximum DIS= 5.1mm

Fracture 3

Node 481

Coordinates of node 481(X=1.29, Y=7.83)

-*Gradual Increase in displacement*

Fracture 4

Node 166

Coordinates of node 166(X=1.462, Y=6.135)

-*Phase Failure*

7.2.7. Experiment 0 & 1 Analysis based on 2D Digital Image correlation

It's very clear, based on the computed relationships between displacement, velocity, and time, that experiment 0 landslide progression was more aggressive, in terms of the displacement's peaks; duration of between each two consecutive failures; the connectivity between failures. In fracture number 3, the displacement reached *1.2cm*, the time difference between two consecutive fractures was around *20seconds* from the activation of fracture 2. The time difference between the first fracture and the last was *10minutes,* which shows how aggressive and connected these fractures were to each other's.

For experiment 1, the fractures were less aggressive in terms of the recorded displacement and velocity, compared to experiment 0, however, in some cases the fractures were connected to each other which made one fracture would result into two other separate ones. The fractures were characterized by longer duration between each two consecutive fractures, and relatively smaller displacement and velocity. The peak recorded displacement due to a fracture is *1.13cm* and the time difference between the first and last fracture was *27minutes.* The True Strain vs Image in experiment 1 shows the phase failure of the landslide, lag time between each two fractures.
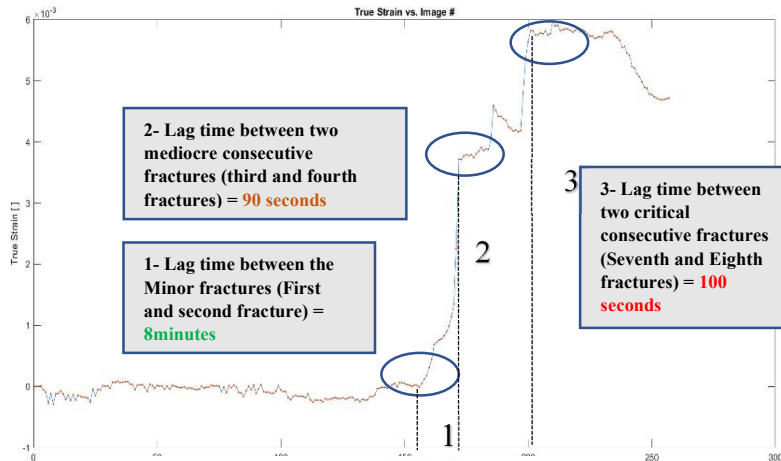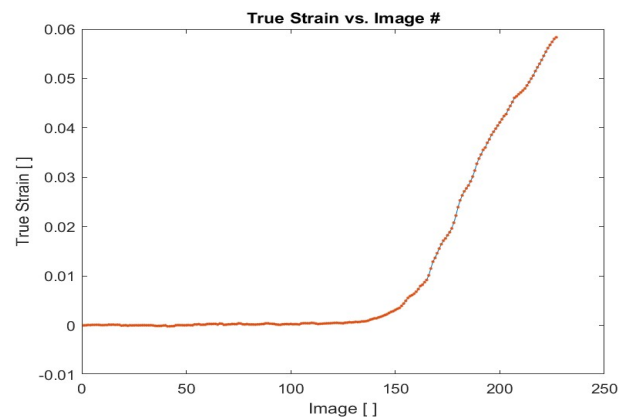

Fig.49. Exp1, True strain vs Image number

Fig.50. Exp0, True strain vs Image number

For experiment 0 the failure was shown as a gradual increase without obvious lag time between the fractures *[Fig.49 & Fig.50]* Additionally, to better visualize the phases of the landslide failures, we computed 3D images of the strain change with the help of DIC. However, in the plots below, the Y-axis is inverted, and the Z-axis values represent the changes happening in the X-axis. *[Fig.51 & Fig.56]*
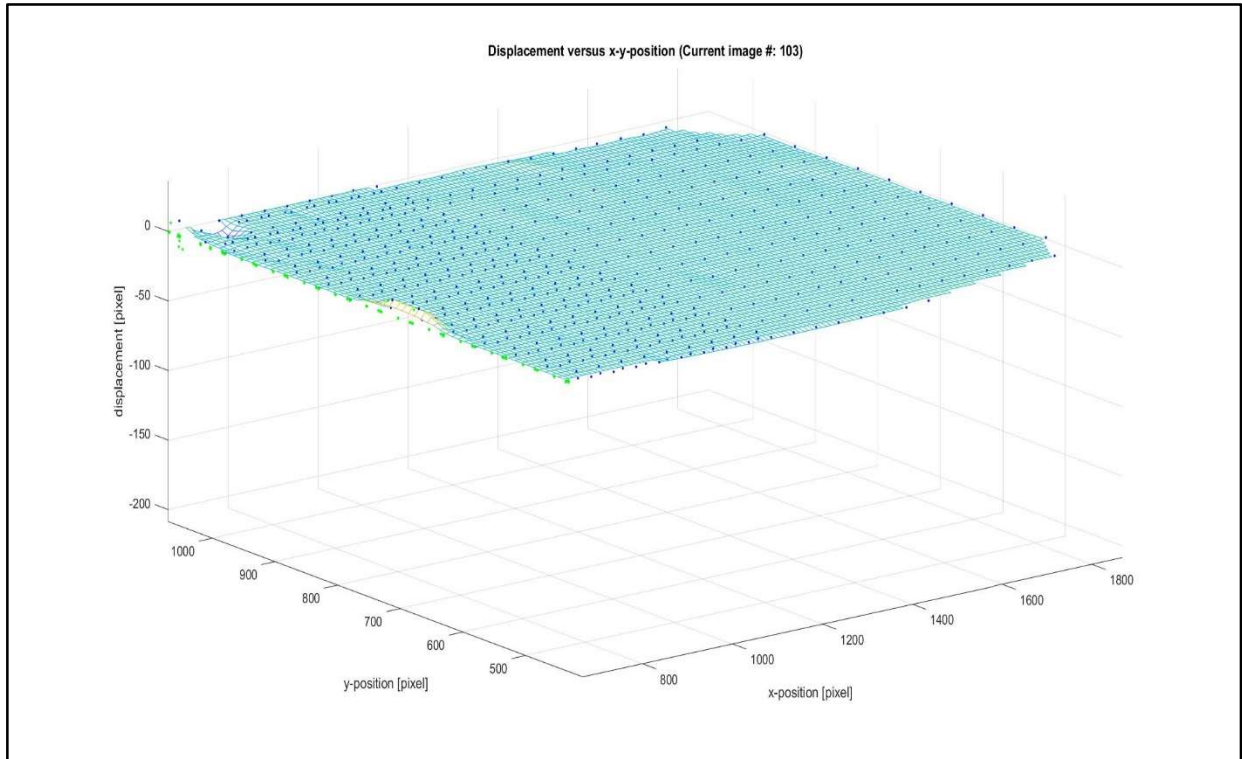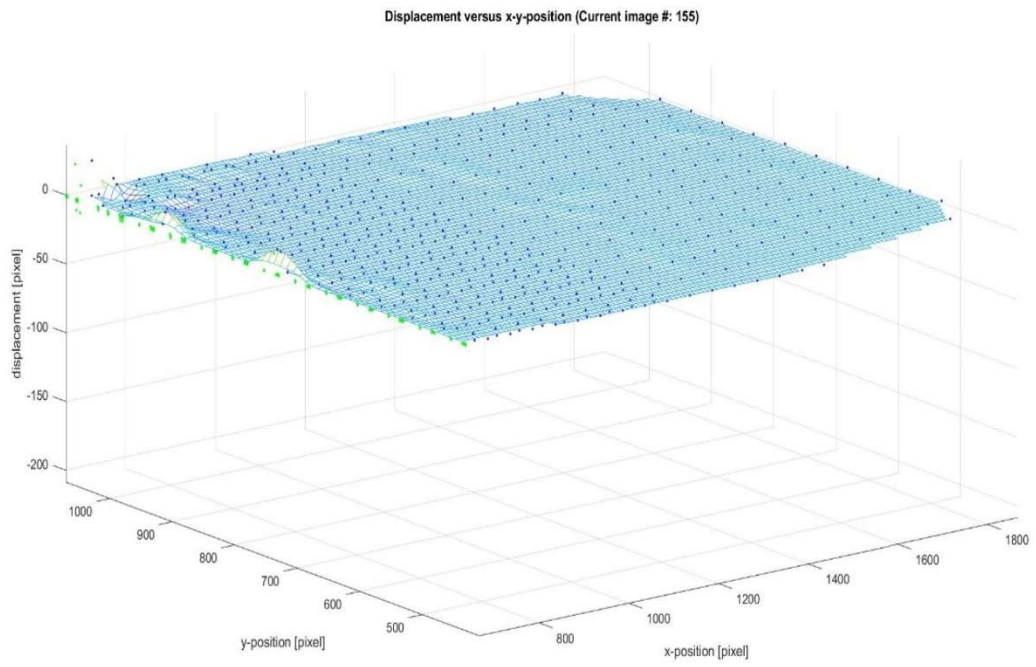

Fig.51. 3D presentation of fracture 1
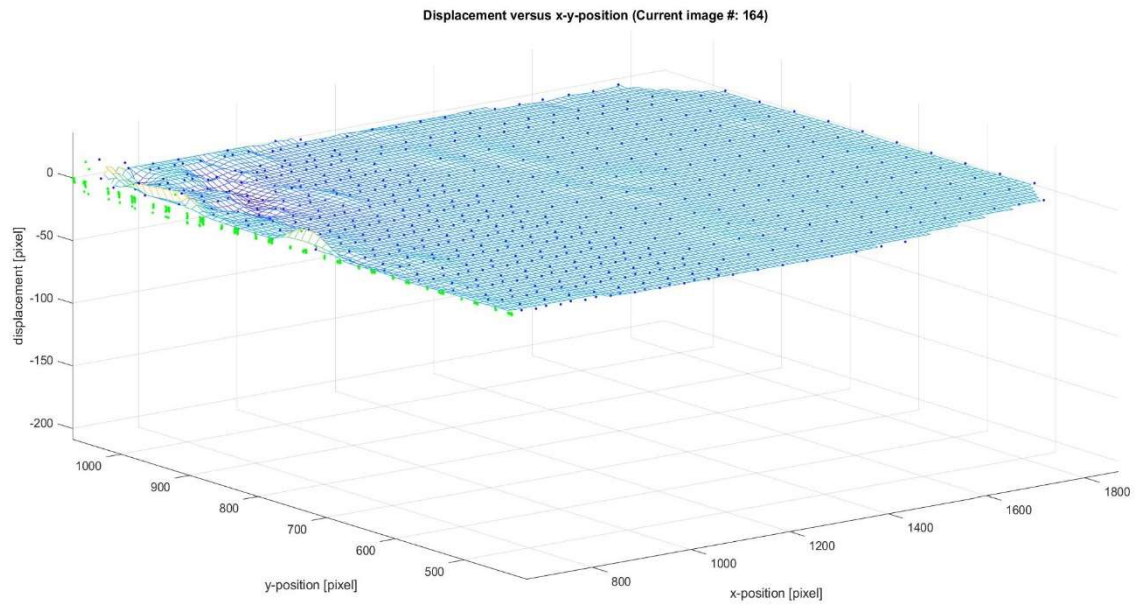
Fig.52.3D presentation of fracture 2

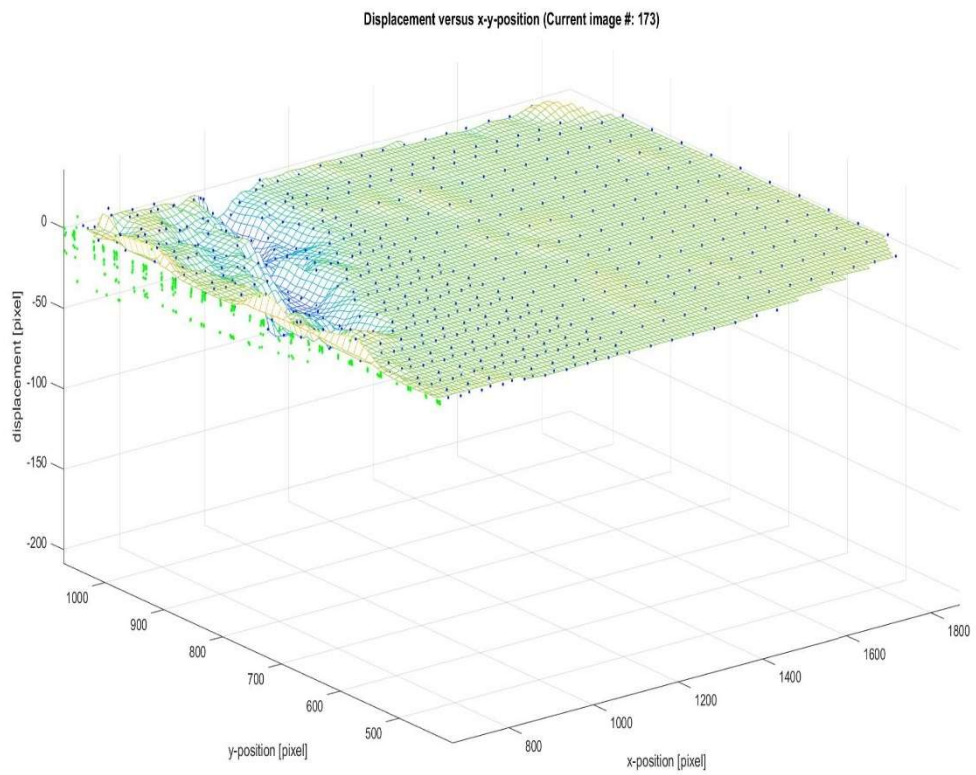*Fig.53. 3D presentation of fracture 3*

Fig.54. 3D presentation of fracture 4
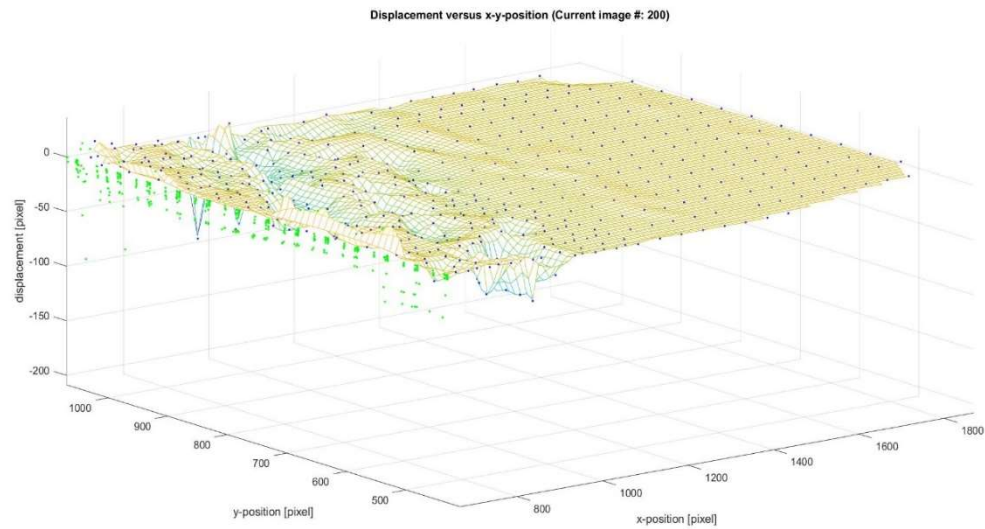
Fig.55. 3D presentation of fracture 8

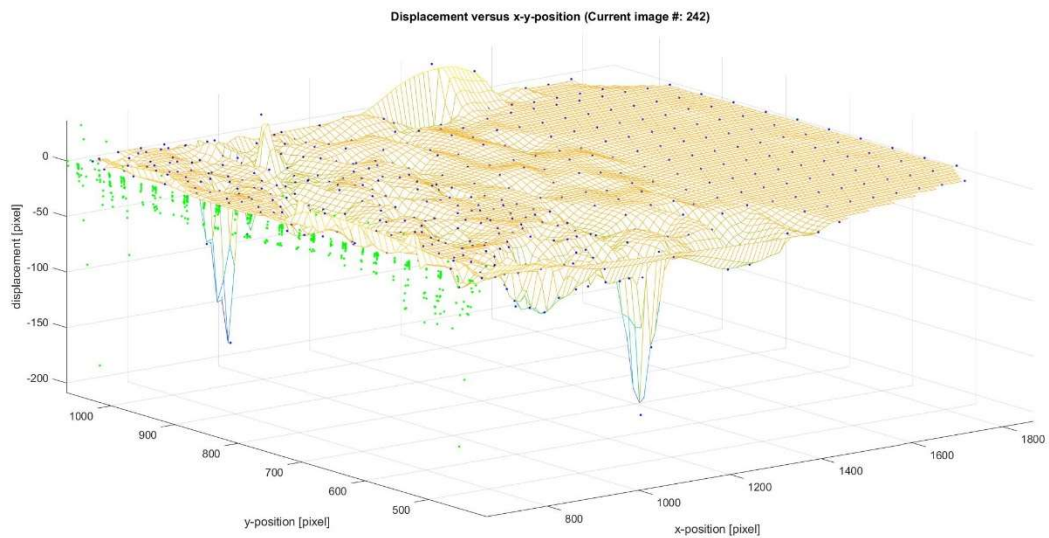*Fig.56. 3D presentation of fracture 12, 13, 14*

The time lag between each two consecutive fractures would give us a lead time that can be utilized into an early warning system that is designated to trigger alarms to warn the nearby stakeholders in the range of the landslides. This point is further discussed in the last section of the report by incorporating information about the geological triggering factors.

7.3. Photogrammetric Technique to Construct a 3D image of the landslide

7.3.1. Calibration of the Three Cameras

To generate a 3D-image of the three mounted FLIR cameras, a pre-data processing calibration must be carried out. This calibration is to consider the inclined surface of the landslide simulation experiment' slope. To illustrate, the three cameras have been un-mounted of the landslide frame and have been used to take multiple pictures of the 48 ground targets from different angles *[Fig.57 & Fig.58],* and then the taken pictures are uploaded on Agisoft Metashape, the software allow us to detect the targets coordinates taken from these images and then by aligning one image in common between the three different cameras we get the calibration parameters saved in each camera's file. There is another set of targets placed on the East and West boundaries of the fume test *[Fig.42],* these targets have been pre-previously surveyed using a total station. With the help of the Agisoft Metashape software, we were able to compare the coordinates taken from the sequence of images of the landslide and the coordinates surveyed. Then, the camera's positioning is calibrated by a set of parameters that consider the surveyed coordinates of these targets, these calibration parameters *[Fig.59 & Fig.60 & Fig.61],* are saved for each of the 3 FLIR cameras, and to be further exploited in the generation of the 3D image.

Fig.57. 48 Ground targets for the Three Cameras Calibration

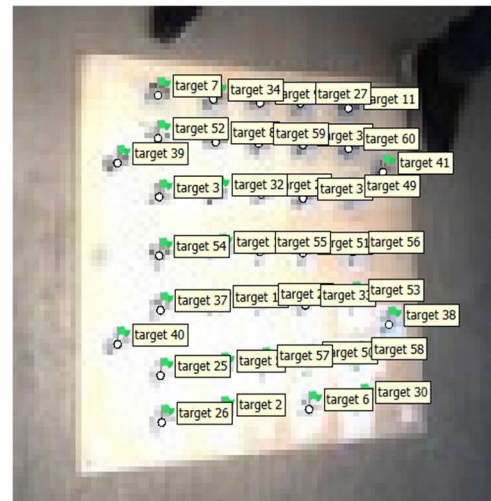*Fig.58. 48 Ground targets detected by Agisoft Metashape Software*

7.3.2. Generation of the 3D Image using Photogrammetry

Fracture 7 and 8, being represented in image 188 and image 200, respectively: from cameras 1, 2, 3, have been chosen to generate a 3D-image of the fracture that occurred. The three images-coming from three different cameras at the same time, representing each fracture- have been calibrated using the

calibration parameters that we have generated from the previous step (*check section 7.3.1*), moreover, with the help of the mounted targets that have been placed on the boundaries of the landslide, we could detect these markers on the image and comparing these coordinates with the ones generated from the Total Station(Agisoft Metashape could detect the targets on the boundaries, however, there could be a margin of error in the placement of these targets that can be adjusted manually by the user *[Fig.62]* which will help us in the following procedures;

 1- *Photos Alignment, each camera position at the time of the image capture is defined by the exterior and interior orientation parameters, alignment is done with the help of the collinearity equations.*

2-*Depth maps are then generated for each image using the interior and exterior image parameters and then filtered out (Dense Stereo Matching), furthermore, they are used to create simple Dense Points Cloud for each camera, which is then mixed with other clouds to have a final Dense Point Cloud [Fig.66].*

3-*a Mesh (Polygonal Mesh Model) is created using the previously generated Depth Maps [Fig.67 & Fig.68]): The size of the mesh can be adjusted, and we could have used the Dense Cloud to generate the Mesh, however, using the depth maps would allow us to full take advantage of the images taken and it's less resourcefully demanding. Lastly, a 3D model texture has been generated as a final stage of the generation of the 3D image of the fracture (During the experiment, we didn't face any critical lightning issues on the surface of the slope we didn't perform any coloring adjustment) [Fig.68].*

Fig.59. Calibration Parameters for Camera 1

Fig.60. Calibration Parameters for Camera 2

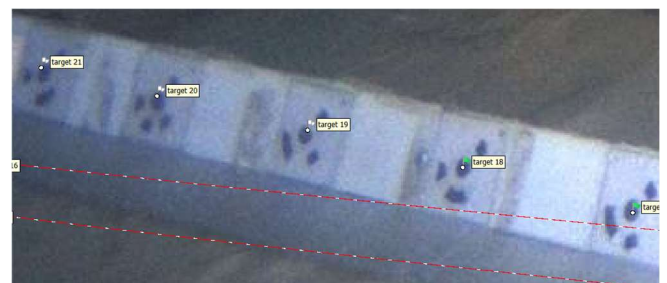*Fig.61. Calibration Parameters for Camera 3*

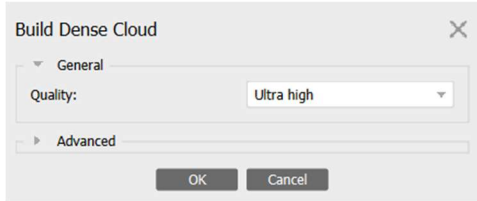*Fig.62. Targets Detection Adjustment for Targets*
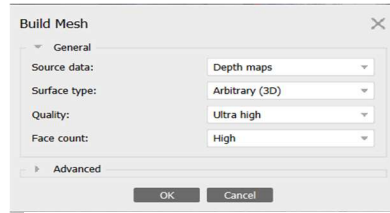
56

Fig.63. Dense Cloud's Quality

Fig.64. Build Mesh Parameters
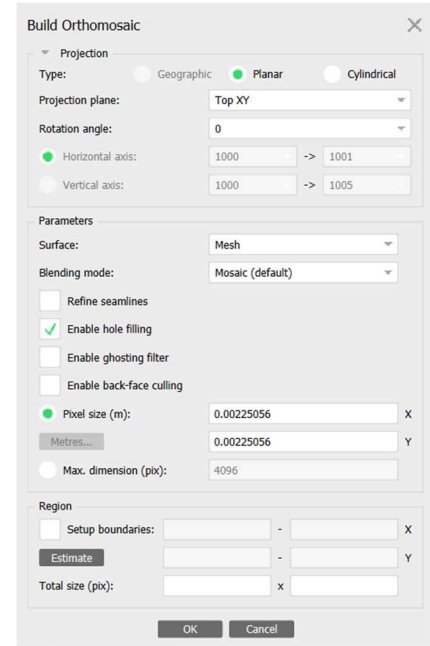
Fig.65. Orthomosaic Photo Parameters
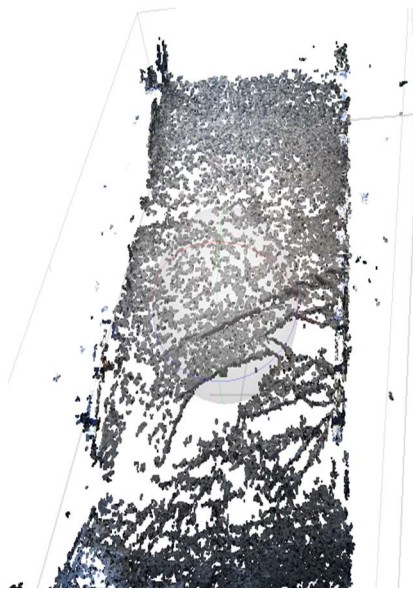
Fig.66. Dense Cloud Layer from Agisoft Metashape
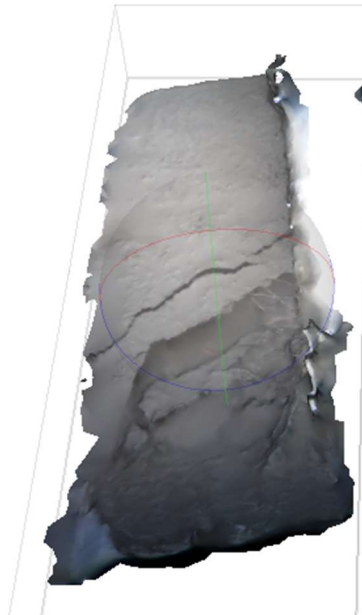
Fig.67. 3D-Image without Texture

Fig.68. 3D-Image of Fracture 8 with Texture

7.3.3. Generation of Orthophotos using Photogrammetry

To fully take advantage of the capabilities of Photogrammetry, we have generated orthophotos for both landslide slopes of the landslide slope surface to have displacement measurements that can be compared with the results obtained from 2D DIC. The orthophotos have been generated using the ("*Orthomosaic layer in Agisoft Metashape [Fig.71].*"). To better understand the scale of the distances in the orthophotos, we checked the distance of a previously known point on the landslide slope: *Distance of the placed TDR should*

57

*be = 86cm, measured from the TDR to the downslope, while the distance measured from the TDR to the downslope on the orthophoto is = 176cm.*Therefore, the distances measured from the orthophotos are *(2*displacement taken from the 2D DIC measurements*).

7.3.4. Displacement Comparison between Orthophotos and 2D-DIC

The comparison is carried out in Fracture 7 and 8, two 3D-images and two orthophotos have been created for each fracture respectively. To have an accurate displacement comparison with the results obtained from 2D-DIC, we must clarify that the traced displacement obtained by the DIC is a result of tracing sequence of images taken at different time, therefore, the displacement of the chosen node could have been already triggered by the predecessor fracture and has reached its peak with the successor one. Consequently, the displacement of the nodes chosen for both Fractures 7 & 8 has been traced by the plots obtained by the 2D-DIC and according to the image number, we have calculated the displacement triggered by the fracture in question.

The comparison showed a small difference in the measurement between the orthophoto and the 2D DIC. For Fracture 7 the error was *3mm [Fig.72 & Fig.73].*

Fracture 7

Fig.70. Zoomed 3D-Image of fracture 7

Fig.71. 90 degrees inclined Orthophoto of

Fig.69. Fracture 7 3D-Image Texture

Fig.72. Displacement as measured for fracture 7 from the orthophoto
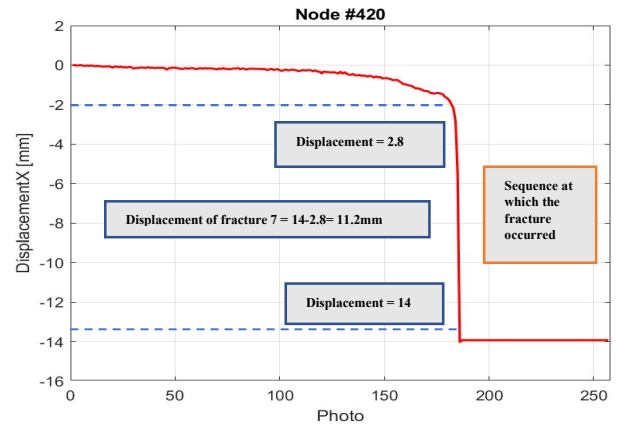

Fig.73. Displacement as measured for fracture 7 from 2D DIC

Fracture 8

Fig.74. Zoomed 3D-Image of fracture 7

Fig.75. Zoomed 3D-Image of fracture 7

Fig.76. Zoomed 3D-Image of fracture 7

59

7.4 Volume Computation Using Terrestrial Laser Scanner Data

To compute the volume of the landslide, we have taken advantage of the Laser Scanner's scans that were carried out during the experiment- 3 Scans have been taken for *experiment 1, the first was very distorted and was dismissed from the analysis*-. These scans have been taken at different times, to fully cover the volumetric changes that occurred during the landslide. The main objective of the Laser Scanner data processing is to find the volume change and better visualize other geometrical changes by comparing the two scans.

The Laser Scanner that was used is *Long-Range LS [Fig.43]*, which allowed higher resolution scans. Cloud Compare Software has been used for the data processing.

7.4.1. Cloud Compare Data Filtration & Co-Registration

The scans data format was obtained i, which contains three main parameters: Coordinate (x), (y) and (z). The scans were taken at the very beginning of the landslide and the end of it, at t=0 and t=42, respectively. Moreover, the scans needed some filtration of the surrounding environment to study the area of interest *[Fig.77]*, the filtration was carried out by the "*Segment function in CC*"- both of Scans were aligned thanks to the embedded GNSS option in the laser scanner-. To register the obtained data, 5 targets were placed on the frame of the flume frame *[Fig.78]* and were surveyed by an external Total Station: The main objective of this step is to Geo-reference the points taken from the Laser Scanner to GNSS. The targets coordinates taken from the total station are then exported to CC and then two scanned frames are aligned to the exported targets using the "*Align two clouds function in CC*" that computes the transformation matrix *[Fig.77 & Fig.78 & Fig.79]*.
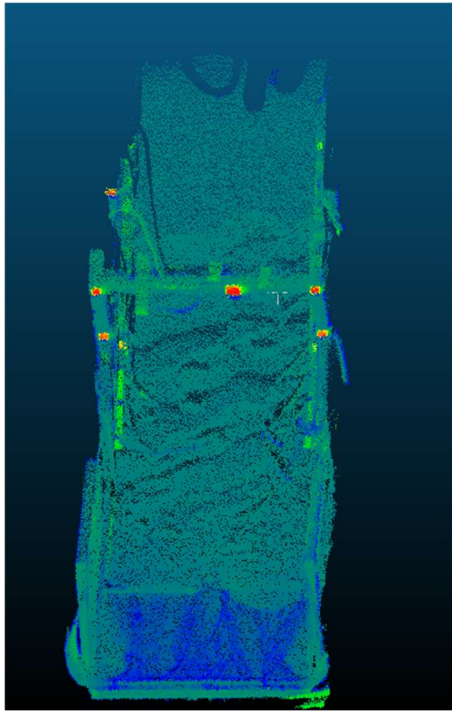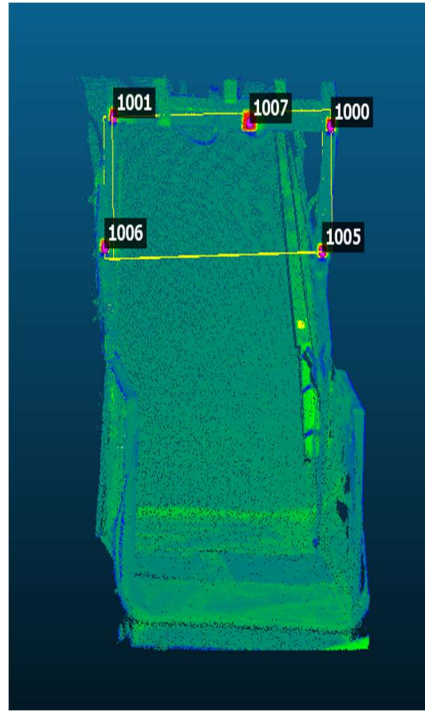
Fig.79. Transformation Matrix of the
Alignment between the scans and the targets

Fig.77. Scan cut from the surrounding
noise in CC

Fig.78. Co-Registration of Scan 1 and Scan 2
using total stationed targets

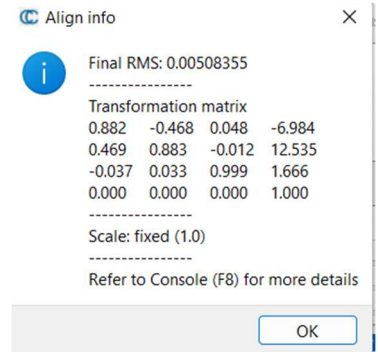## 7.4.2. Cloud Compare Normal Vectors & Volume Computation

To prepare the scanned clouds, the main body of the landslide that contains most of the displaced materials has been segmented from the two aligned scans. In addition to that, we computed the Normal Vectors which show the orthogonal directions on the surface of the body of the landslide using "*Normal Computation function in CC*" *[Fig.80 & 81]*. Furthermore, the volume change between Scan01 and Scan02 was computed using "*Compute 2.5D Volume in CC*" by having Scan01 as the reference scan and Scan02 as the scan of comparison. The volume calculation is done by the multiplication of each cell's X, Y, and the height difference between the two obtained scans, the height difference between Scan01 and Scan02 can be better shown in *[Fig.82]*. As a result, we got the following volume change results *[Fig.83]*: Added volume=+*0.026*; Removed volume=*0.021[Fig.84]*. The Added volume can be considered the accumulated volume of the soil, and the removed volume is the eroded soil. The difference between the two volumes could be a reason for accumulated soil that was collected by the baskets.
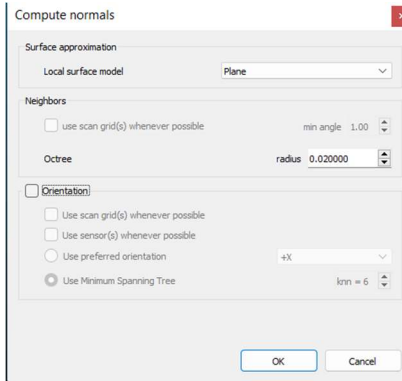
Fig.82. Side View of the Scan 2 and Scan 3 on

Fig.80. Normal Vector Parameters

Fig.81. Normal Vector Computation on the landslide
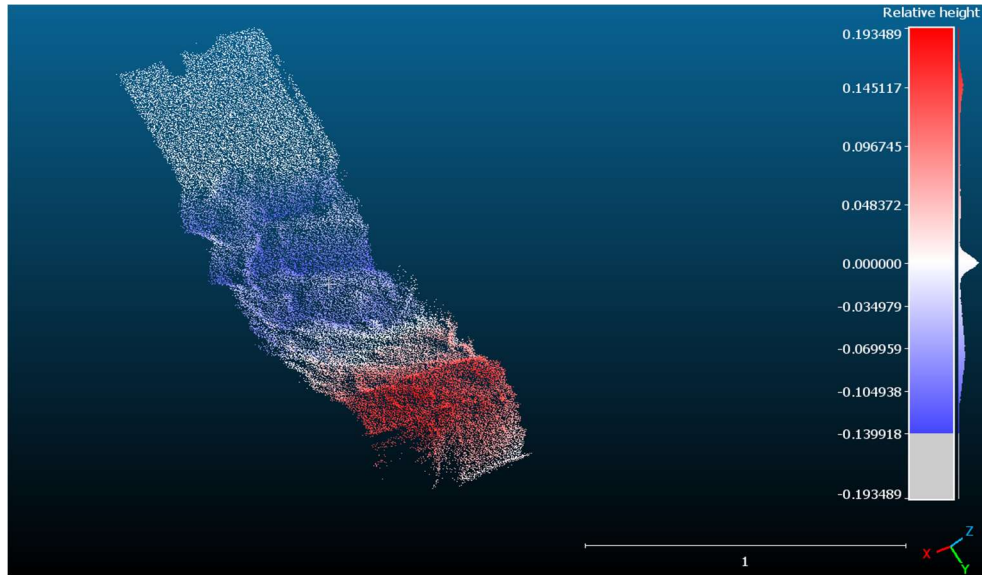
Fig.83. Volume Change Computation
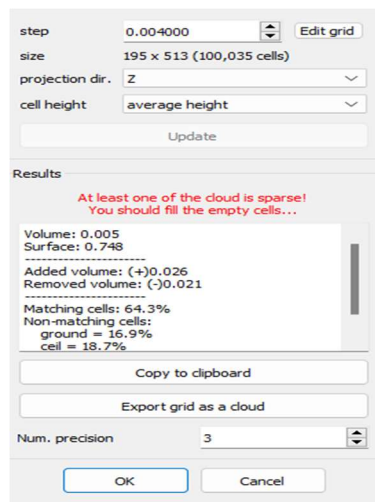
Fig.84. Values of Added Volume & Removed Volume

7.4.3. Distance Computation and Cloud2Cloud Distance&Cloud2Mesh& M3C2 Comparison

For better visualization of the results of the two scans in terms of height difference, we computed the distance difference in the Z direction between the two segmented portion of the landslide's body obtained from scan 1 and scan 2, thus, we could identify the shallow landslide's body sections: Crown; Toe; Depletion zone; Accumulation zone *[Fig.89]*.

We have used Different methods for computing the height difference in the Z direction that will be further compared to get the most precise results of the CloudCompare: "*Cloud/Cloud Distance function in CC" [Fig.86]* which depends on measuring the distance based on the "nearest neighbor distance" for each point. For the local model, we have used the Least Square Plane. Other signed methods used to calculate the distance difference in the Z-direction is; "*Cloud/Mesh Distance in CC*" *[Fig.87]*, which is used in case

of having global model scan, and based on the comparison between the point cloud of the scan and a mesh that is made of a predecessor scan (scan1); "*M3C2 (Model to Cloud) Plugin in CC*" *[Fig.85 & Fig.88]*, it's based on point cloud to point cloud comparison, there is main parameter that need to

be calculated: normal scale, is the diameter of the spherical neighborhood extracted around each core point to compute a local normal. This normal is used to orient a cylinder inside which equivalent points in the other cloud will be searched for.
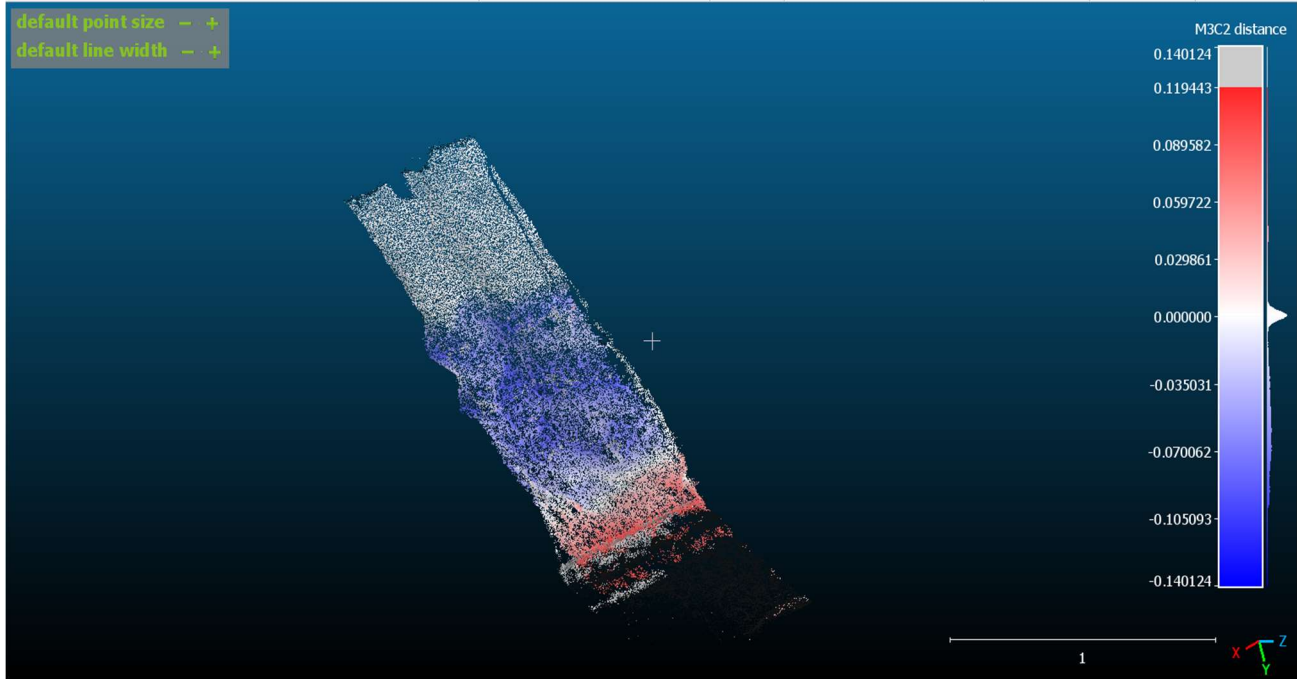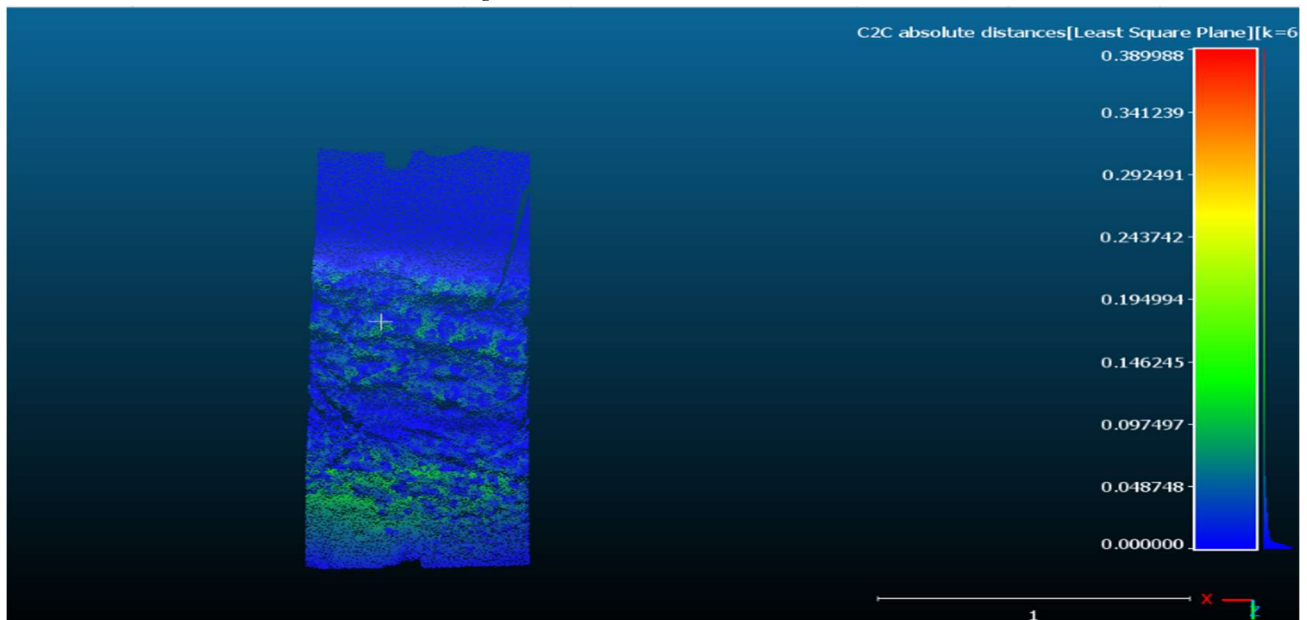

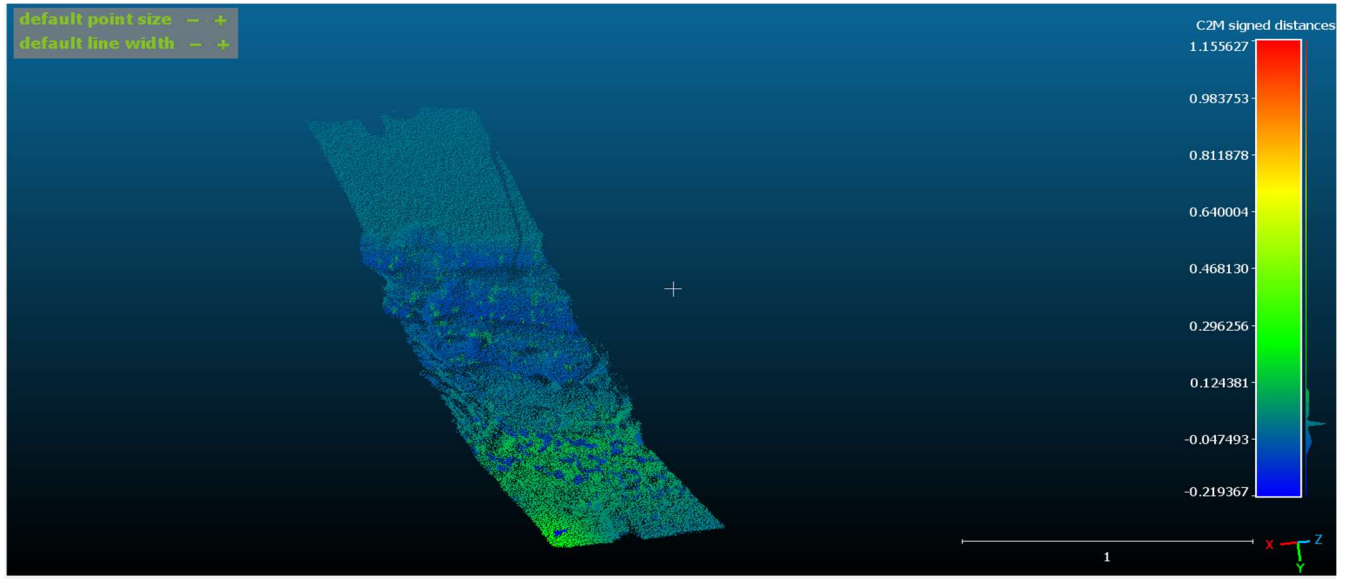*Fig.85. M3C2 distance calculation*

Fig.86. C2C distance calculation

Fig.87. C2M distance calculation
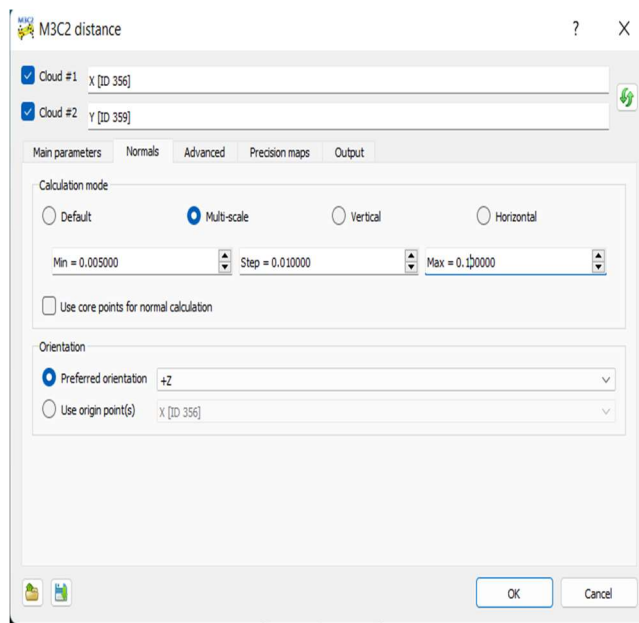
Fig.88. M3C2 inputs values
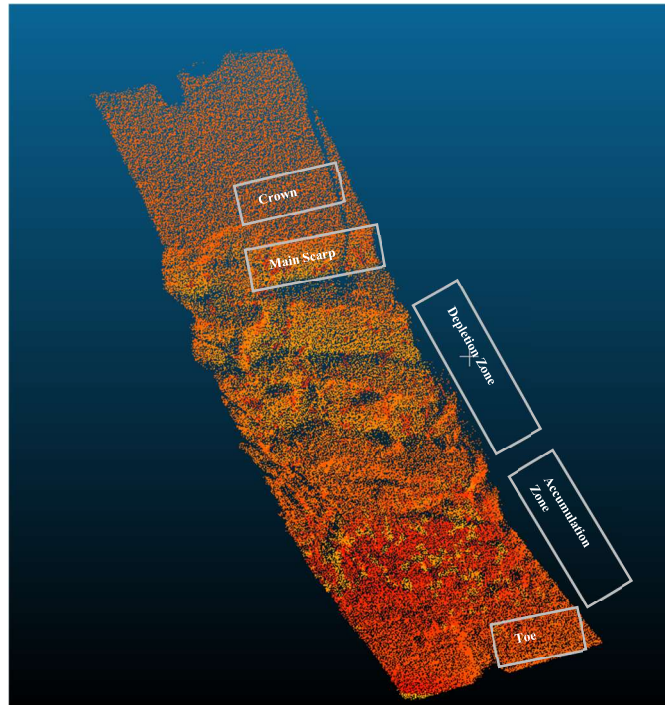
Fig.89. C2C distance calculation

7.4.4. Comparison between Cloud2Cloud, Cloud2Mesh and M3C2

The distance calculation in the three methods has been done by taking Scan01 as the reference layer. The C2C method gave a reasonable result compared to the actual experiment. On the other side, C2M did gave more accurate signed results, however, based on literature *[10],* these method poses problems when the two points cloud don't overlap, which can be proven at the toe area of the landslide. M3C2 gave the most accurate results of the three methods, it has provided a reasonable result in terms of the distance change that happened during the landslide.

7.5. Conclusion

To conclude, the photogrammetric techniques have proven to be a great addition in the monitoring and assessment of the landslides. The results obtained from the 2D DIC analysis have helped us to understand the aggressiveness rate of the failures and interpret the results obtained from the geological instruments. It also enabled us to have a concrete understanding of the temporal change of the failures that occurred, which would help in developing an early warning system. However, the results obtained from photogrammetry do hold some inaccuracies as explained in the previous section that has to be considered. We have tried to limit these inaccuracies by removing the outliers' nodes from the 2D-DIC and confirming its results in terms of the displacement with the orthophotos obtained from Agisoft Metashape.

8. Geophysical Monitoring and Assessment

Geophysical techniques try to provide a characterization of the subsurface material based on different parameters. DC resistivity method is used for extracting the apparent resistivity values for the artificial slope. In laboratory 0 and 1, we use the method of Electrical Resistivity Tomography (ERT) with Wenner array which is relatively sensitive to vertical changes (and less sensitive to horizontal changes) in the subsurface resistivity below the center of the array. The exact step and results will be described in the following analysis.

8.1. Equipment

Aside from the landslide simulator with sprinklers and sensors, already described in the geological assessment, the main equipment used consisted in adapting the cables and electrodes to the scale of the slope. The landslide simulator is as shown in the pictures below *[Fig.90]*.

Fig.90. landsides simulator

Mini electrodes and cables: 48 stainless steel electrodes with 2 cm long and 2 mm diameter. The cables were connected to the IRIS Syscal Pro instrument *[Fig.91]*

Fig.91. Electrode spacing

IRIS Syscal Pro instrument: It is an all-in-one multinode resistivity and induce polarization sounding and profiling system used for geophysical studies. It's compact, easy-to-use and field proof. The Syscal Pro measures resistivity and is connected by cables which are stainless steel electrodes 2cm long, 2mm diameter. Before starting the simulation at T0, IRIS Syscal Pro performs resistance check (RS check) between each 2 adjacent electrodes. The instrument sends the current, measure the potential and calculate the resistence (starting from the first 2 electrodes, then 2 after that…). The value of resistance ranging from 10-40kOhm. *[Fig.92]*

Fig.92. IRIS Syscal Pro

The measurement of soil resistivity was performed using the Wenner array with a=3cm along the longitudinal direction of the slope, centered. Electrode 1 at the toe of the slope (x=0) and electrode 48 at the crown (x=1.41). Data measured with 47 electrodes because electrodes 39 had contact problems and it was removed from measurements. *[Fig.93]*
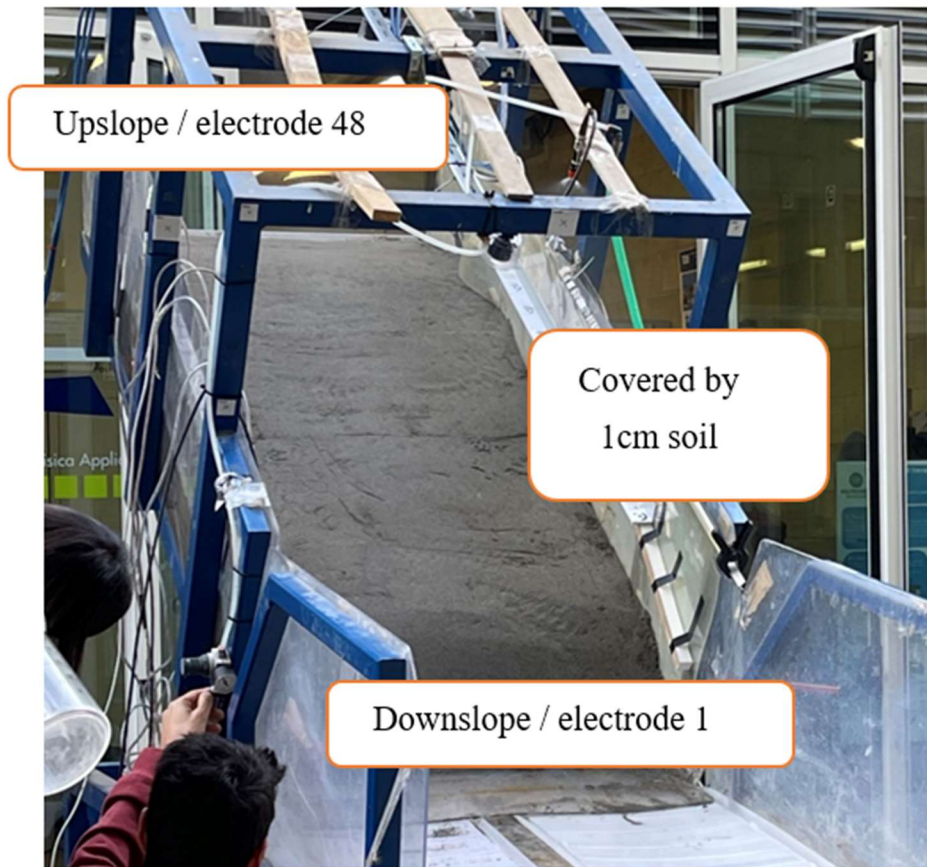
Fig.93. Electrodes configuration on the landslide

8.2. Experiment 1

In the Experiment 1 we consider a 7.5cm layer of well compact sand (with the average 15% initial volumetric water content), followed by 7.5cm of natural sand on the top of it on a 35° slope. TDR sensor located horizontally, 5cm left of the ERT line in the center of the landside body (pointing towards to ERT line) at the depth of about 7.5cm. It is 80cm from electrode 48. During the real experiment, Electrode 39 was disconnected, and it's removed from measurements. When employing them, there are 313 data that can be used in experiment 1. The cables were connected through the IRIS Syscal Pro instrument which will show the resistivity data on it. The RS check at T0 is 13-50kOhm.During the landslide simulation 11 experiment measurements were performed: T0-T10, and from T7, the collapse begins to happen. Only 66 data can be used in that case.

8.2.1. Resistivity model in Res2Dinv and discussion

While developing the resistivity model by using software, we set the initial conditions as:

1. *Measurements are in apparent resistivity.*

2. *The initial resistivity was considered as 500 Ωm.*

3. *The presence of the geotextile was considered through sharp boundaries with resistivity value of 100000 Ωm.*

4. *The initial damping factor value was selected as 0.15, and the minimum damping factor value selected as 0.02.*

5. *For very large resistivity variations near the ground surface, model cells with widths of half unit spacing are used (0.015m)*

6. *No extended models of topography were used.*

7. *Usually, resistivity models apply 6 iterations and the RMS errors is smaller than 6%.*

8. *For type of Contour intervals, we use logarithmic contour intervals.*

Eleven measurements were performed at the following time points to measure the apparent resistivity:

1. *T0 measured as background measurement (0min)*
2. *Continuous rainfall started at 14:45*
3. *T1 measured at 14:46 (1min)*
4. *T2 measured at 14:51 (6min)*
5. *T3 measured at 14:56 (11min)*
6. *T4 measured at 15:02 (17min)*
7. *T5 measured at 15:07 (22min)*
8. *T6 measured at 15:12 (27min)*
9. *Then increment in collapse happened and some electrodes stopped working.*
10. *T7 measured at 15:18 with electrodes 25-48 (33min)*
11. *T8 measured at 15:20 with electrodes 25-48 (35min)*
12. *T9 measured at 15:22 with electrodes 25-48 (37min)*
13. *T10 measured at 15:24 with electrodes 25-48 (39min)*

So, eleven times measurements were done; each time resistivity demonstrates the fluctuations in the resistivity of the soil layer shows in the following figure: *[Fig.94]*

T0 at 0 min

T1 at 1 min
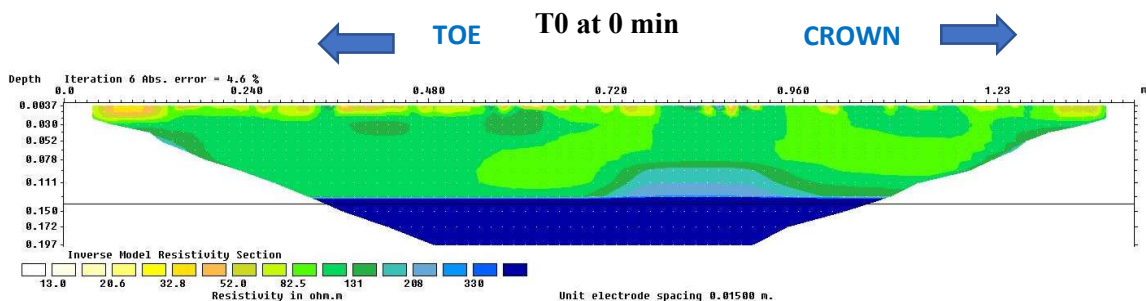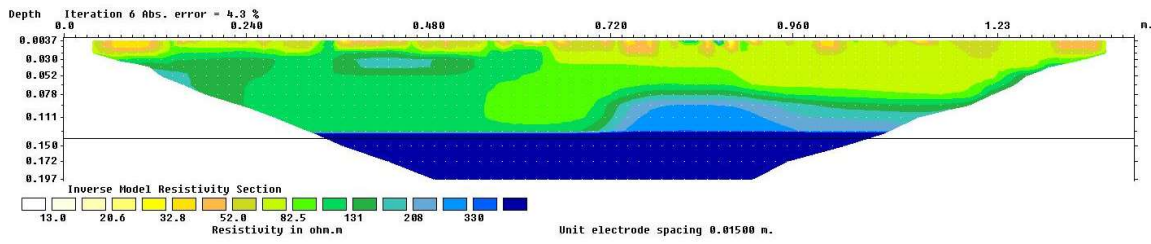
T2 at 6 min
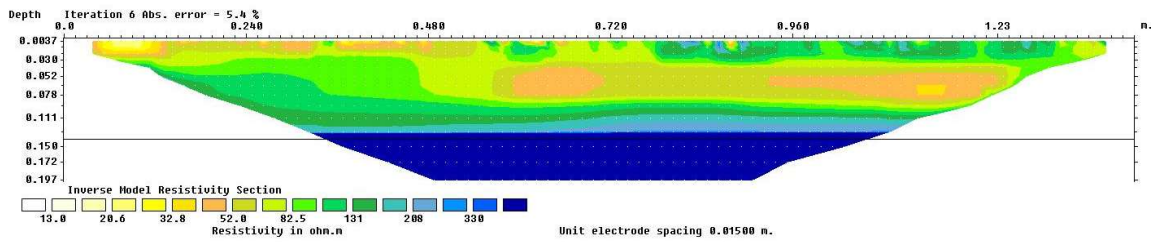
T3 at 11 min

T4 at 17 min

T5 at 22 min

T6 at 27 min
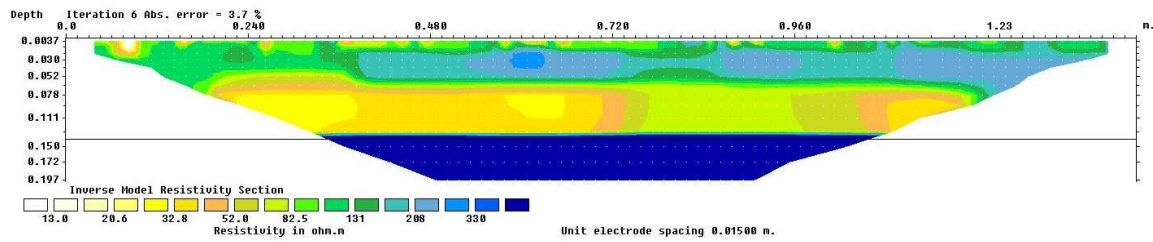
T7 at 33 min
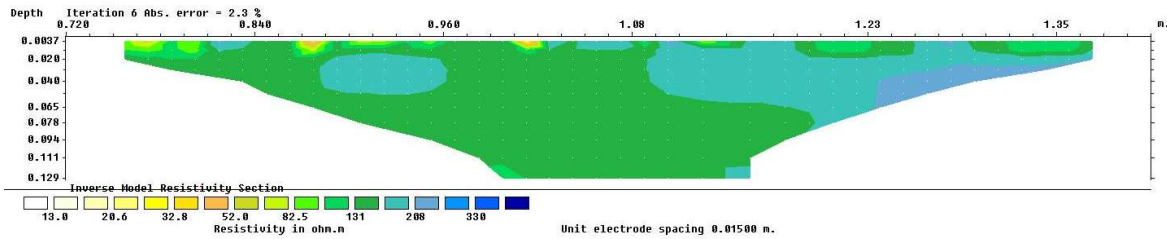
T8 at 35 min
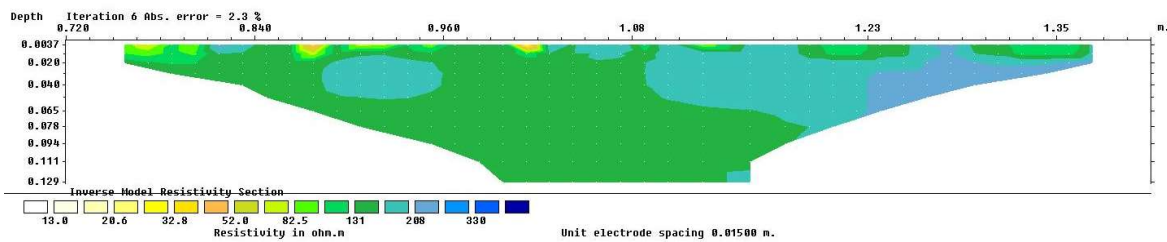
T9 at 37 min

T10 at 39 min
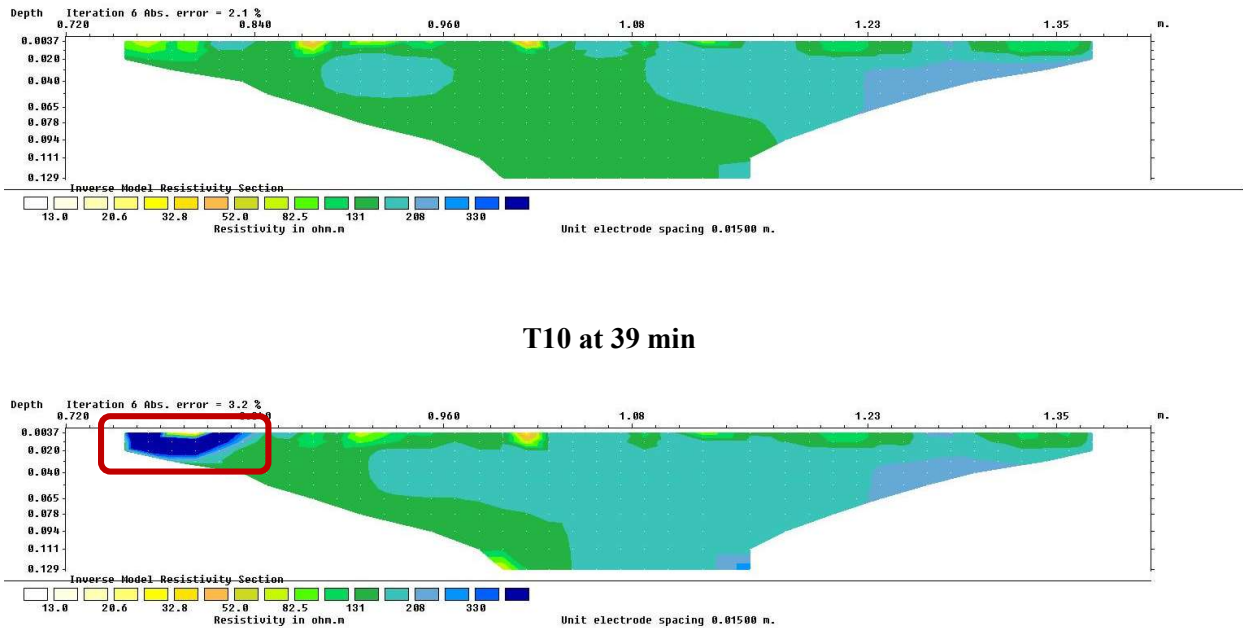
Fig.94. Inverse Model Resistivity at different time

8.2.2. Inverse Model Resistivity at different time

From the 11 different graphs, we can do some analysis: From graph T0-T3 we can easily observe that the whole slope resistivity of soil is decreasing through the slope which caused by rainfall, especially the toe of the slope for gravity of drops influence. But during the Time-lapse and sharp boundary in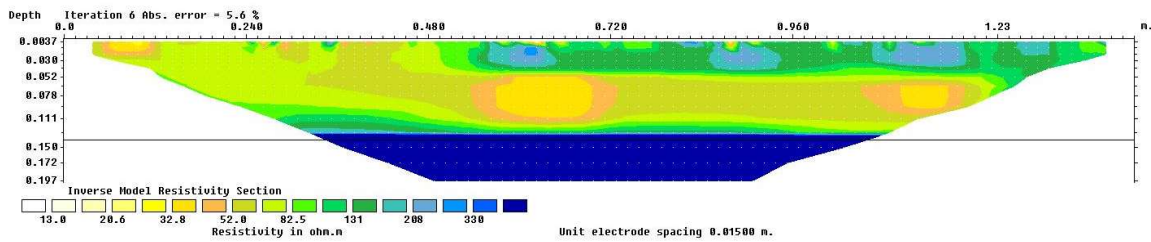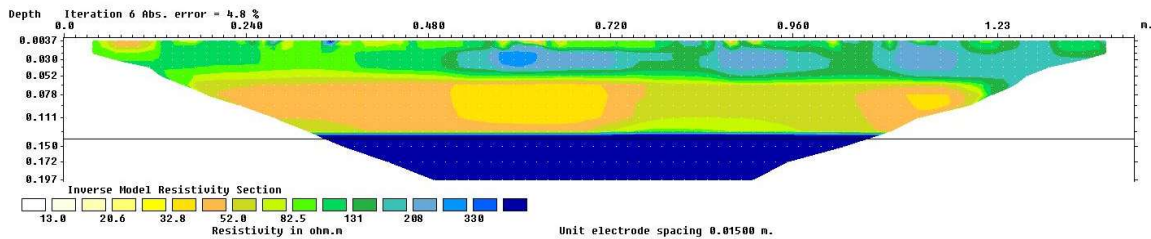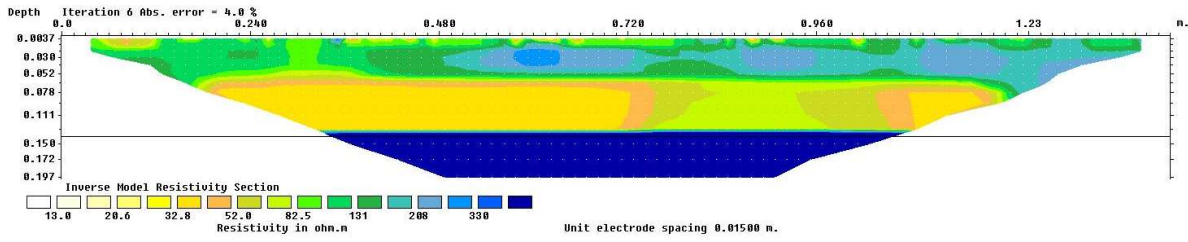 landslide simulation, the decrease in soil resistivity wasn't in a smooth trend. In the case, we considered that the soil didn't compact in an exact uniform way.so the water infiltration paths in the soil slope were not homogenous. Additionally, the rainfall coming from the 4 sprinklers was also not uniform in the whole slope. From graph T4-T6, the soil resistivity began to increase in the crown part meanwhile the toe part kept decreasing. However, in the increasing part, the resistivity is still smaller than 200Ωm, we cannot consider it as the real crack but only the zones of different saturation.

Considering the gravity effect, we think that the water in the soil is flowing downward, which also explains why the resistivity at the foot of the slope is so low, even reaching 30Ωm. From graph T7-T10, accompanying the collapse of the slope, some of the electrodes stopped working. The whole slope was in a high resistivity condition. We can see the toe of the slope in graph T10, much higher resistivity occurs which represents the whole collapse of the slope.

We can compare this part with the photogrammetry data to have a more observable result *[Fig.95]*

Crown Toe T0= 0 min	T1= 1 min	T2= 6 min
T3= 11 min	Shallow landslide T4= 17 min	Big crack occurs T5= 22 min
T6= 27 min	Some electrodes began to fail T7= 33 min	T8= 35 min

| T9= 37 min | T10= 39 min |
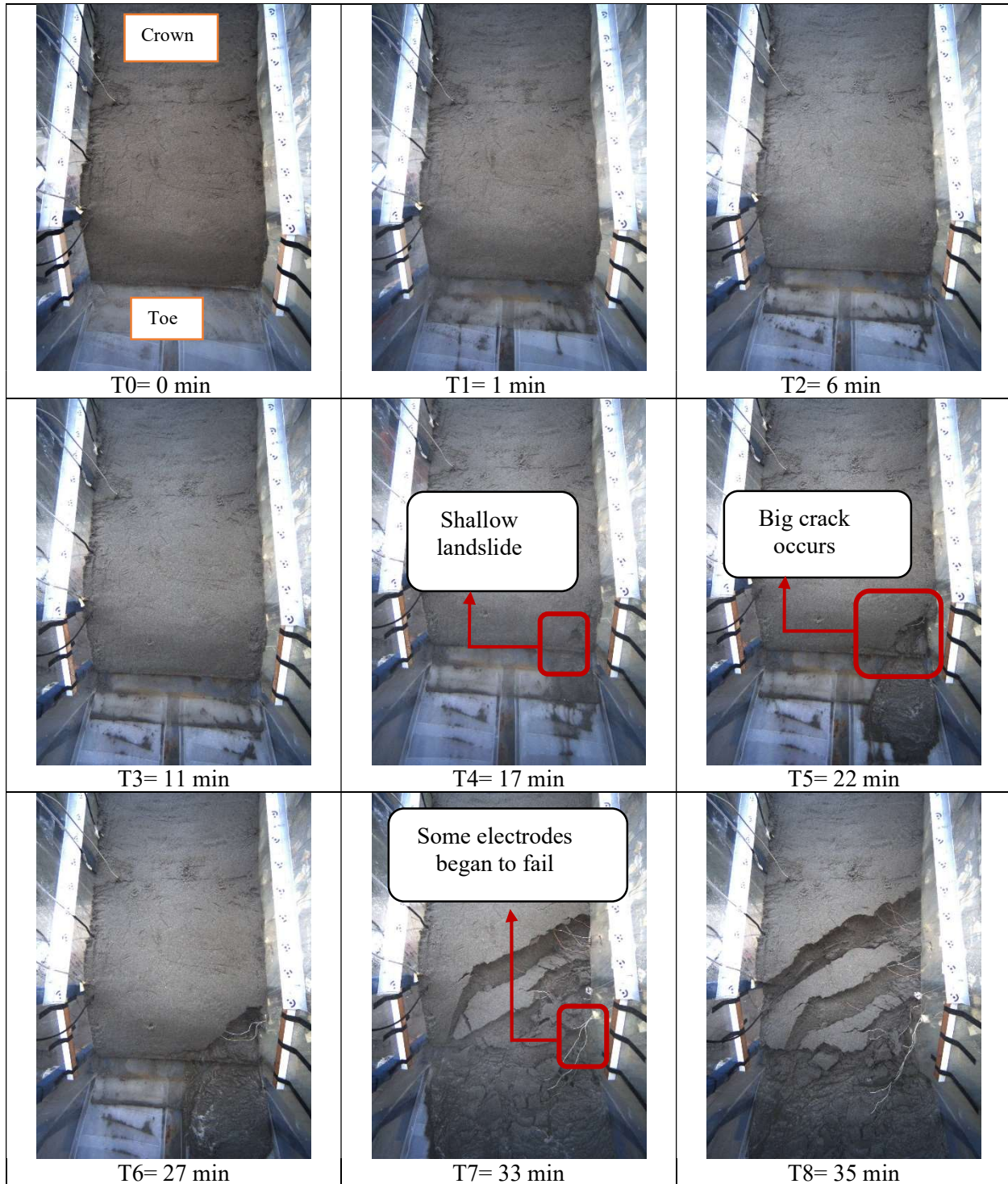
Fig.95. Water Saturation values from resistivity calibration

From the images of above figure, we can see more clearly about the situation of the slope. Comparing to the ERT models we analysis before. At beginning in T0-T3 no noticeable changes were observed. And then in T4 a shallow landslide is observed in the landslide simulator's left side. Continuing this landslide, in T5, a toe failure in the left part of the landslide simulator. And the crack kep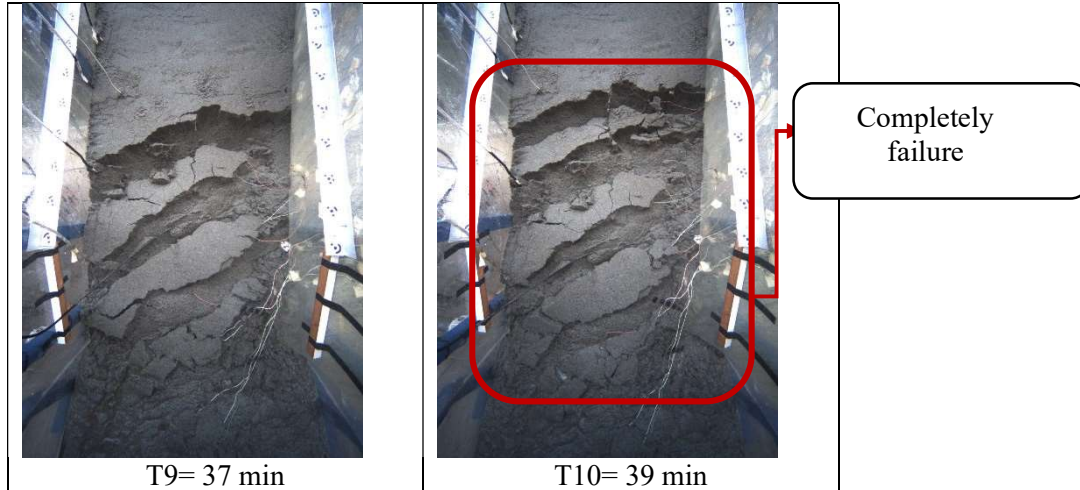t expanding in T6 , when time reached 33min, T7-T10 some electrodes were fail and until the slope reached total failure.

But in ERT images ,about T4-T6 ,we don't observe any cracks in the toe part, the resistivity keeps decrease there.We think it's because the electrodes was located in the in the center of the longitudinal line in the flat surface. However , the crack occurs from the part inclined at the bottom.The distance between them is too far to record any crack data.Also due to the gravity of water influence, we will find the resistivity kept decrease in toe. Until T10 the complete failure happening, electrodes began to aware this situation ,so we can find that in T10 ERT image, there is obviously a large resistivity part in the toe part.

8.2.3. Mathematical resistivity model

After the assessment, we have already known the volumetric water content which was measured by TDR, the porosity and so on. Furthermore Archie's law relates the in-situ resistivity of soil sample to its porosity and fluid saturation of the pores. Regarding the previous results and parameters, a calibration analysis is going to be implemented.

-Archie's Law

$$\rho = F\, S_w^{-n} \rho_w$$

-Formation resistivity factor

$$F = a\, \varphi^{-m}$$

Where:

ρ: resistivity of the material,F: formation resistivity factor ,S_w: water saturation ,ρ_w: resistivity of water in pores ,n: saturation exponent varying in the range $1.2 \leq n \leq 2.2$,a: parameter varying in the range $0.5 \leq a \leq 2.5$,m: parameter varying in the range $1.3 \leq m \leq 2.8$,φ: porosity

From the analysis of geological: the porosity value is extracted which is 0.55, then the resistivity of water in pores is considered as 27Ωm. And for the following parameters:

-Volumetric water content

$$\theta = \frac{V_w}{V_t}$$

where: V_w: volumes of water, V_t: volumes of the total material.

We have already known that θ is the same as volumetric water content that is also drawn from the TDR measurements at the point where TDR sensor is located.

-Water saturation

$$S_w = \frac{V_w}{V_{pore}} = \frac{\theta}{\varphi}$$

where:

V_w: volumes of water , V_{pore}: volumes of pores.

The TDR was located 1.1m from the crown position and about 10cm left side of the ERT profile (looking upslope). Therefore, Resistivity values for this point of TDR 6.5cm below the electrodes are considered at times where there is an overlap between the time of TDR measurement and electrodes' measurement for calibration purposes, We compared the calculated resistivity values at each time with the inverted resistivity values at the location of TDR at the same time in order to find the agreement. Finally, we can get the calibrated values for a, m, n:

Table 7. Calibrated Archie's Law parameters

a	m	n
0.5	1.3	1.2

A comparison is provided between the results from the experimental data and acquired Archie's Law, in the table below.

Table 8. Calibration between Archie's Law and Experimental

Case	Time	Elapsed time	θ	φ	SW	ρw	F	ρ Archie's Law	Experimental	Relative variation
T0	14:45	0	0.19	0.55	0.35	27	1.09	103.54	90.55	12.55%
T1	14:46	1	0.22	0.55	0.39	27	1.09	90.10	92.24	2.37%
T2	14:51	6	0.24	0.55	0.44	27	1.09	79.28	57.92	26.94%
T3	14:56	11	0.26	0.55	0.46	27	1.09	73.80	38.35	48.03%
T4	15:02	17	0.28	0.55	0.50	27	1.09	66.97	31.42	53.09%

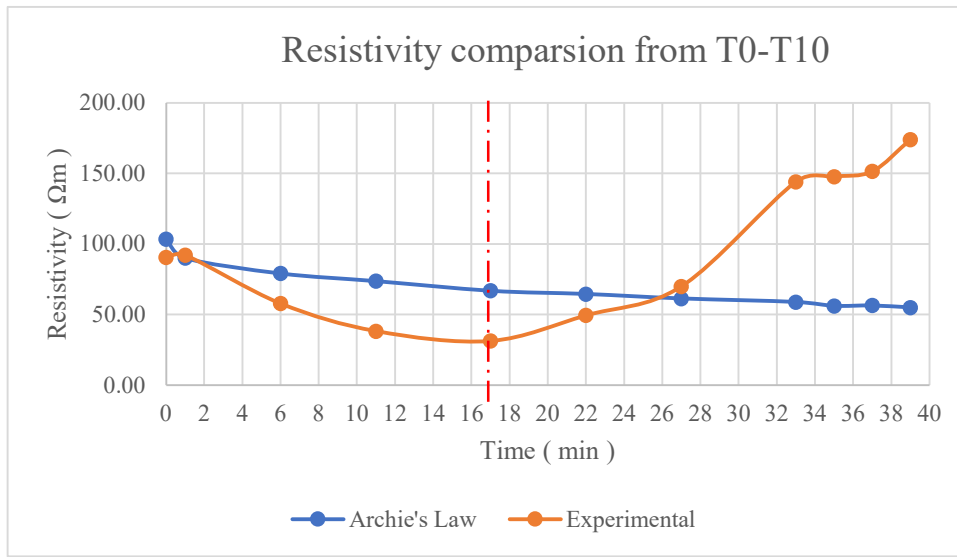|										
T5	15:07	22	0.29	0.55	0.52	27	1.09	64.61	49.55	23.30%
T6	15:12	27	0.30	0.55	0.54	27	1.09	61.49	70.02	13.87%
T7	15:18	33	0.31	0.55	0.56	27	1.09	58.96	144.26	144.68%
T8	15:20	35	0.32	0.55	0.58	27	1.09	56.23	147.84	162.92%
T9	15:22	37	0.32	0.55	0.58	27	1.09	56.57	151.56	167.92%
T10	15:24	39	0.33	0.55	0.59	27	1.09	55.11	174.19	216.06%

Fig.96. Resistivity comparison from T0-T10

From the results [Figure 96] , we can know that the relative difference is quite high, it's obviously that from Archie's Law the resistivity will keep decreasing accompanying for water content increasing. However, the experimental resistivity didn't behave like the same trend. As we analyzed earlier, there are several possible reasons for this situation. From the 17min the shallow landslides happens, so the resistivity began to increase. Also not uniformly compacted soil will affect this trend. Moreover ,another reason for the flaws that happened in this experiment is that the position differences. Furthermore, we need to inform that during the experiment, the time when we tested the resistivity from the electrodes is not completely accurate compared with the time measuring porosity and volumetric water content for geology parts. Because the parts is operated by different people. It can also affect the value coming from Archie's Law.

From previous calculation, we got:

F = 1.09

$\rho = 1.09 \times S_w^{-1.2} \times 27 = 29.43 \times S_w^{-1.2}$

As a result, we developed the following equation to obtain the water saturation of the landslide body from inverted resistivity data:

$S_w = (\frac{29.43}{\rho})^{0.83}$

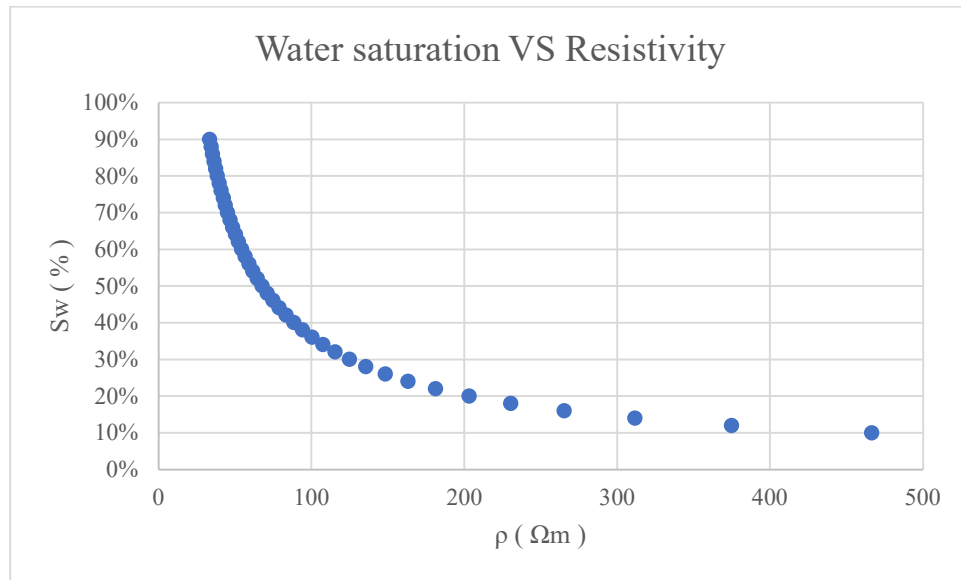The following graph represents this equation:[Figure 97]

Fig.97. Soil water saturation versus resistivity values based on equation

From the graph we can easily observe that resistivity is always decrease while the water saturation increasing, but the relationship between the two isn't linear.

From the almost dry sand to the water saturation of about 30%-40%, the resistivity values decrease from 500Ωm to 100Ωm approximately due to the water flows in the soil. When it goes further increase in water saturation beyond about 40%, the resistivity keeps decreasing, but more softly and gently. Until the soil is almost full of water, the resistivity is getting closer to zero.

8.3. Experiment 0

In the experiment we use 15cm of fine sand with an average initial volumetric water content of 15%, with the slope of 35^0 (3 layers of 5cm each). TDR sensor located horizontally in the center of the landside body (pointing upslope) at the depth of 7.5cm.

ERT profile was located 14cm from the base and covered by 1cm sand. Stainless steel electrodes 2cm long, 2mm diameter.

During the landslide simulation experiment measurements were collected, putting in 9 ERT files:

T0: After covering the electrodes and before starting the rainfall.

Continuous rainfall started at 15:41

T1 measured at 15:41

T2 measured at 15:48

T3 measured at 15:53

T4 measured at 15:59

T5 measured at 16:04

T6 measured at 16:09

T7 measured at 16:14 with only 23 electrodes (25-48)

T8 measured at 16:17 with only 23 electrodes (25-48)

8.3.1. Resistivity model in Res2Dinv and discussion

To invert ERT data, we use software Res2Dinv with following parameters:

- The initial resistivity is 300Ωm (Since the electrodes were buried into the humid sand layer so we take a low resistivity)
- Resistivity value of geotextile, considered by using sharp boundaries: 100000 Ωm
- For the inversion, 'No extended models' of topography were considered
- For type of Contour intervals, we use logarithmic contour intervals.

Showing in following figures *[Fig.98]*

T0 at 0 min
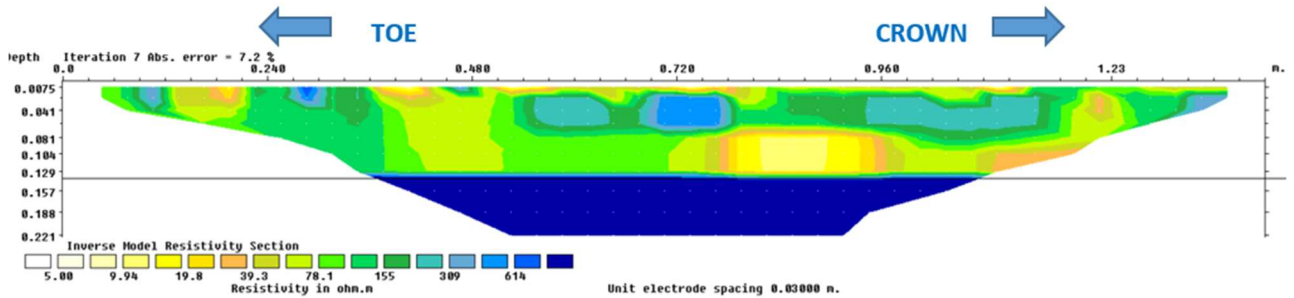
T1 at 5 min
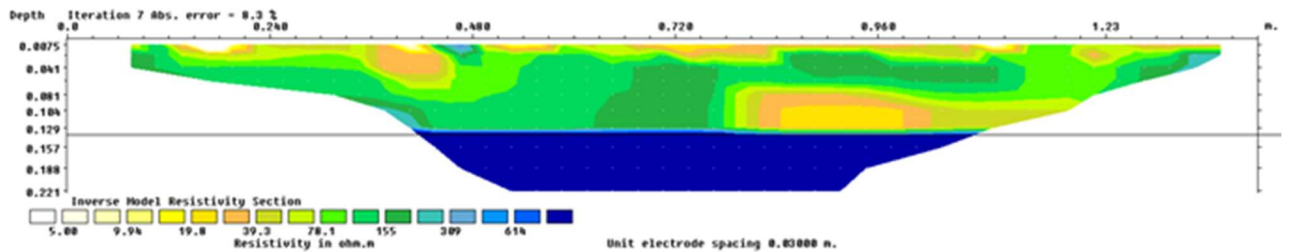
T2 at 12 min
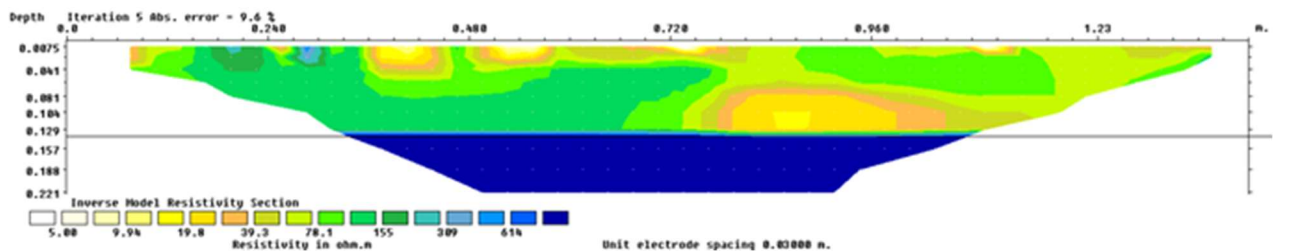
T3 at 17 min
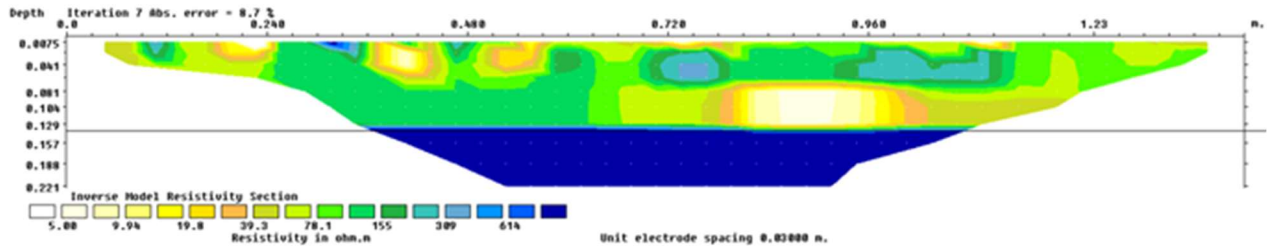
T4 at 23 min
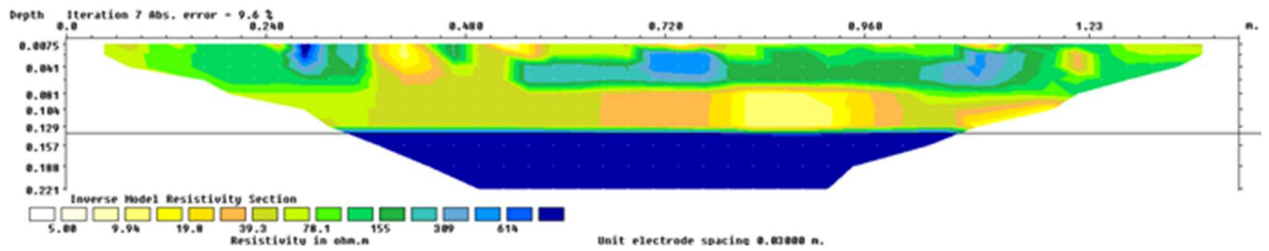
T5 at 28 min
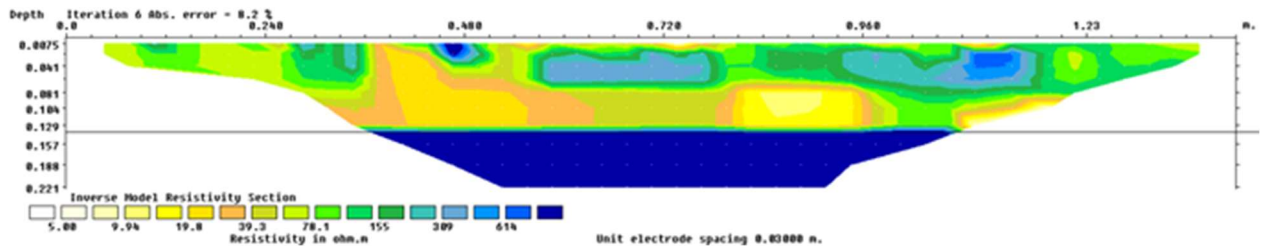
T6 at 33 min
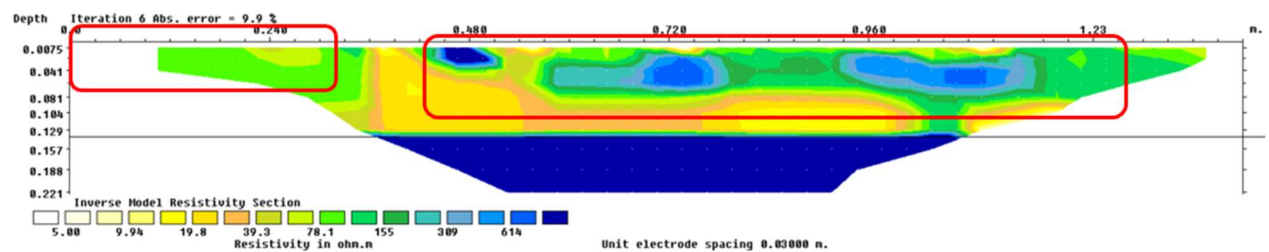
T7 at 38 min
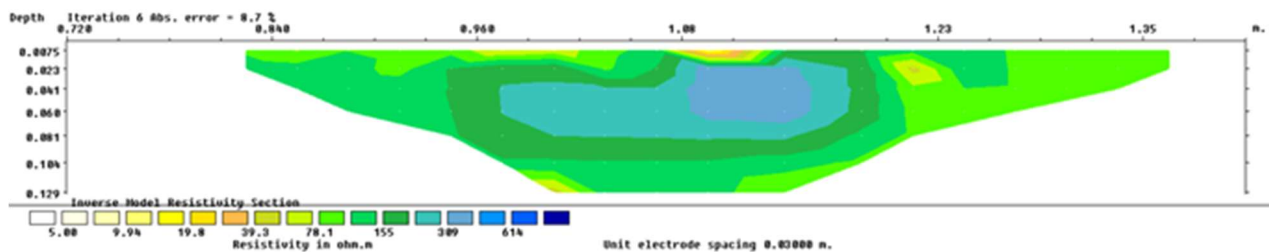
T8 at 41 min
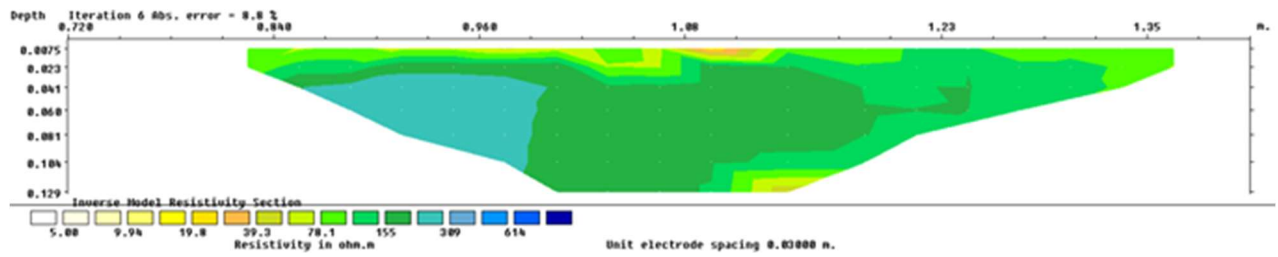
Fig.98. Inclination Angle of the fume test

To make comparison, during the rainfall, photos of landslide body were taken by the cameras set up above *[Fig.99]*
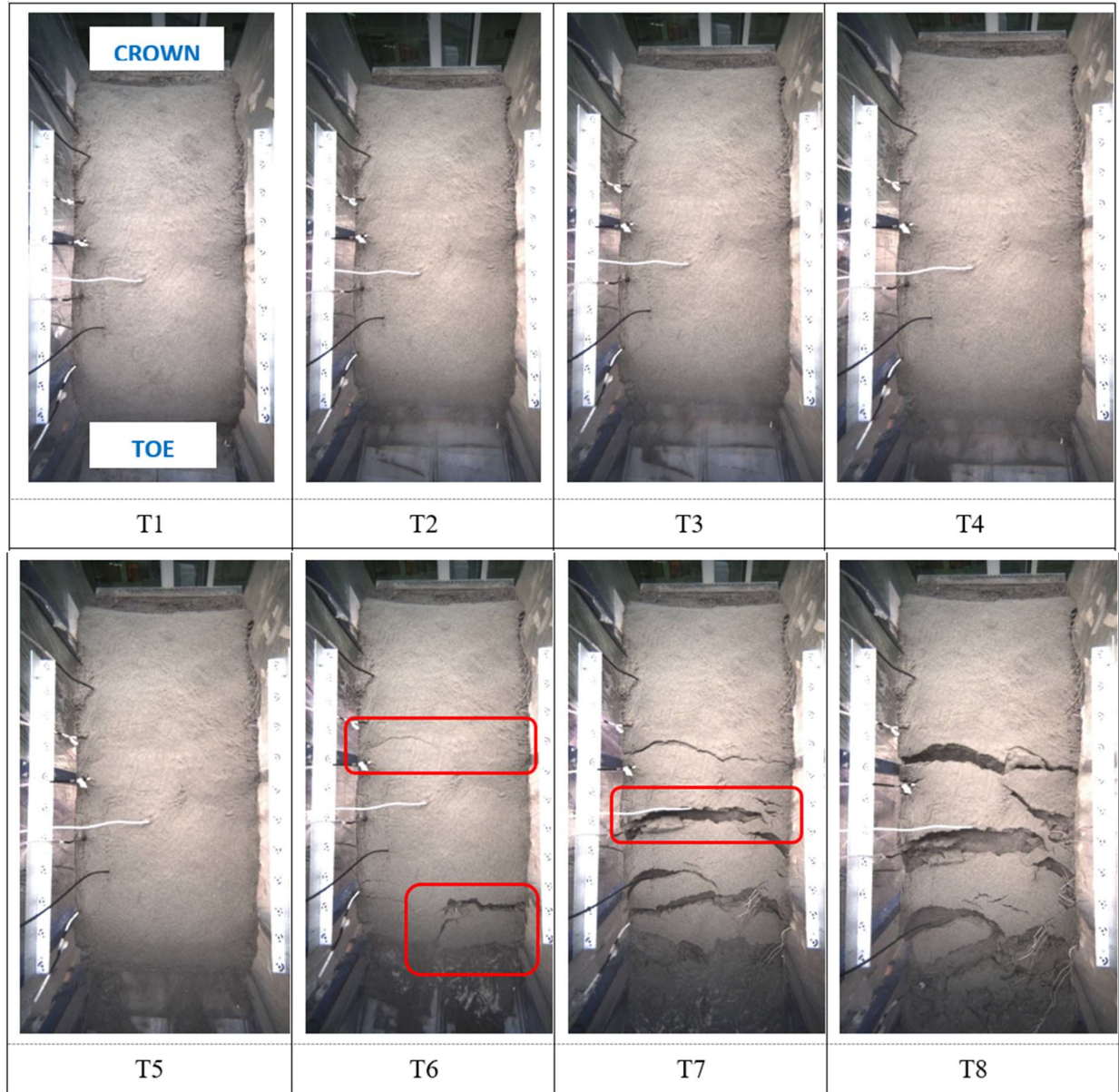
Fig.99.

Remarks:

1. *For experiment 0, the results collected at the start were disorganized due to the conditions of the experiment, therefore, higher error occurs (around 22%). We can improve this error by improving our input, using the tool "Exterminate bad data points".*

2. *The resistivity change can be divided into 2 parts: the first part from x=0 to x=0.6m. This part has a steady decreasing of resistivity that conforms to the increasing of water content. Then second part x=0.6 to the upslope, on the other hand, has decreasing trend from time T0-T2, and increasing trend in time T3-T6.*

3. *From T0 to T2, the pseudosections show reduction of resistivity as the moisture content increases. Since our landslide simulator is inclined toward electrode 1, the area here tends to get saturated faster due to gravity (we can see low resistivity here in all of the pseudosections) and lanslide could occur*

around this area first. In the pseudosection at T6, some electrodes downslopes are lost due to a small landslide.

4. From T3 to T6, resistivity increases in 2/3 part of the upslope body. Especially at x=0.5m, x=0.7m, x=0.9m. High resistivity in these regions indicates the cracks later occur in the body. In the upslope part we also see an increase in resistivity due to formation of cracks.

5. This result matches with what we observe in photogrammetry images at time T6: there is a slide region at the toe, and a small crack at the middle (x=0.7m), then later a bigger crack downslope (x=0.4m). At time T7, T8, from x=0.75m to x=1.35m there is no region with exceptionally high resistivity in the graph, and we see no cracks in those areas.

8.3.2.   Mathematical resistivity model

From the inversion result, we can use inverted resistivity values together with TDR data to calibrate the relation between resistivity and water saturation, using Archie's law, which is a formula that relates the resistivity of the whole sample to the resistivity of the water that is present in the pore space. Since we use sand in landslide experiments, Archie's Law formula is appropriate because it is valid for clay-free formations with highly resistive mineral grains [1].

$$\rho = FS_w^{-n}\rho_w$$

where

- ρ : the resistivity of the material,
- ρ_w : the resistivity of water used in the rainfall sprinklers, about 28 Ωm
- F : the formation resistivity factor,
- S_w : is the water saturation, and is the resistivity of the water in pores.
- n : is the saturation exponent varying in the range $1.2 \leqslant n \leqslant 2.2$, determined empirically.

The formula for resistivity factor: $F = a\varphi^{-m}$

where

- $0.5 \leqslant a \leqslant 2.5$ and $1.3 \leqslant m \leqslant 2.8$.
- φ : porosity
- θ : volumetric water content measured by TDR data monitor, with
- V_w, V_{pore}, V_t: volume of water, pore, and total material

We only consider the data from T0-T6, as after this time the landslide body fractured and would not give appropriate result for our calibration. Since we use volumetric water content measured by TDR, the values of inverted resistivity are also taken at the position of TDR which is 7.5cm depth in the sand. TDR is placed in the middle along of the landslide body, so we take values at electrode 24 (x=0.69m). [Figure100]

Table 5. Parameters of calibration

a	m	n
0.5	1.40	1.26

Table 6. Calculation of resistivity

Interval	Time	φ	F	Sw-TDR (%)	θ (%)	ρw (Ωm)	Calculated ρ (Ωm)	Experimental ρ (Ωm)	Relative variation (%)
T0	-	0.47	2.13	31.9%	15.0%	28	203.2	148.5	14.4%
T1	15:41	0.47	2.13	33.8%	15.9%	28	186.8	166.3	5.1%
T2	15:48	0.47	2.13	47.2%	22.2%	28	115.1	115.0	9.9%
T3	15:53	0.47	2.13	57.0%	26.8%	28	87.6	78.9	3.6%
T4	15:59	0.47	2.13	60.6%	28.5%	28	80.1	126.6	40.2%
T5	16:04	0.47	2.13	64.7%	30.4%	28	73.0	177.9	60.8%
T6	16:09	0.47	2.13	68.5%	32.2%	28	67.1	210.3	69.1%

The following equation is calibrated using the inverted resistivity, to calculate the water saturation:

$$S_w = \left(\frac{40.3}{\rho}\right)^{0.79}$$
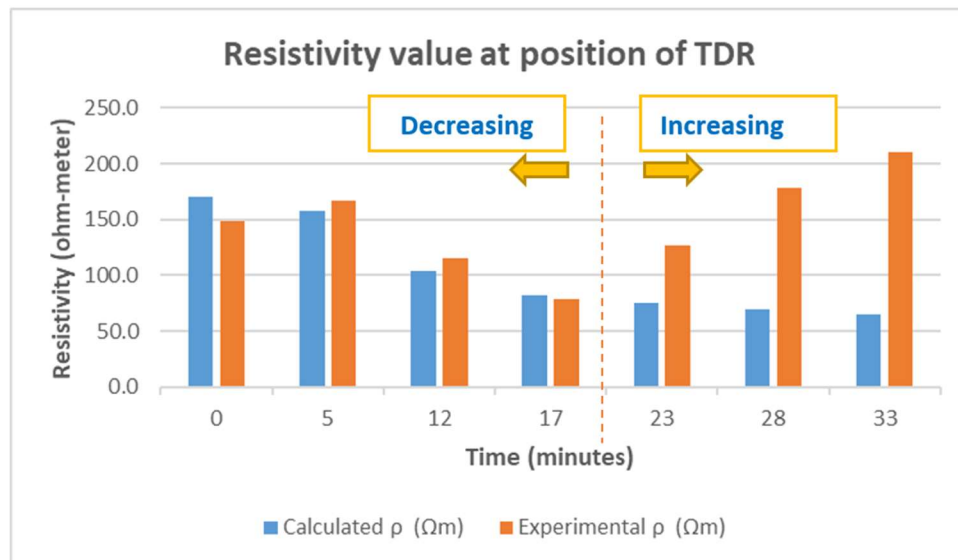
Fig.100. Resistivity from inverted result and from Archie's law

We can see, for electrode 24, an increase in the experimental resistivity value, despite volumetric water content also increases. This trend also happens for neighboring electrodes (near x=0.69m) up until the crown, while the electrodes at the toe side decrease in resistivity. If we look back at the pseudosections, from T3 (17min) to T4 (23min) there is a region with high resistivity around this area. So it is possible that some cracks occur here, although not yet visible in the photogrammetry images, we can still see a small crack at time T6. This could also be the reason for the discrepancy between Archie's law and experimental data: We can see resistivity values from Archie's law equation decreases with the increase of volumetric water content, that matches with the behavior of resistivity downslope but does not match well at the position of TDR. [Figure101]

Fig.101. Water Saturation values from resistivity calibration

8.4. Geophysical Conclusion
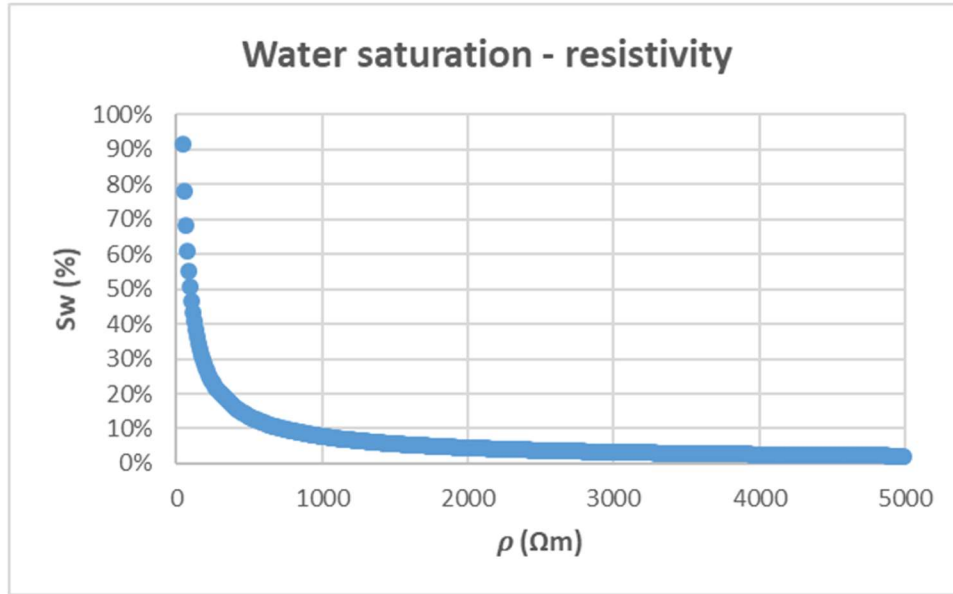
From both experiment1 and experiment0, we set the electrodes in the 14cm in the sand layer, however they covered by different thickness of soil. In lab1 we use 7.5cm layer of well compact sand followed by 7.5cm of uncompacted natural sand, as well as in lab0 we use we use 15cm of fine sand.

For the analysis of calibration of Archie's law, the same value of porosity is considered for both experiments and the TDR was also located as the same depth for both experiments. For two experiments, we did optimization of parameters a, m and n of Archie's law which laboratory 1 (a=0.5, m=1.3, n=1.2) and laboratory 0 (a=0.5, m=1.35, n=1.45). Furthermore ,in experiment1, the reason that the crack happened on the toe of the slope where really far away from the electrodes caused the bad recording about data ,we can just see the resistivity decreased by water saturation increasing ,no crack sign. It can also explain why a, m, n chosen in experiment1 are not really perfect optimization of parameters which makes our variation even over 100%. In experiment0 , the situation was much better, cracks occurred in the middle of the slope and we can confirm this information from the resistivity increasing according to electrodes. We can see smaller variation from experiment0 which are much more acceptable.

9. Conclusion

To conclude, it's obvious that the results obtained from geology, photogrammetry and geophysics were supplementary to each other; and from which we could understand the failure triggering factors and the failure mechanism: It was obvious that from the geology part that the main contributing factor to the shallow landslide was the rainfall and the increasing volumetric water content of the soil, by comparing the results with the SLIP model, we found a big difference in terms of the timing of the value of the factor of safety, in particular, the SLIP model over-estimated the stability of the soil which gave us almost 3 minutes time difference between the actual experiment, however, by calibrating the SLIP model: adding the contribution of the run-off water and changing the limit equilibrium equation to take into account the different porosity values of the two layers(compacted and uncompacted) we have succeeded in calibrating the SLIP model to give the actual result of the landslide, and now can be used for different experiment and soil conditions.

Additionally, with the aid of photogrammetry, we could understand the timing of each fracture, the actual displacement, and the actual distance of the fracture from a datum line (Toe), furthermore, we could identify the different elements of the landslide body. The information obtained from Photogrammetry did help us in corelating the geological and the geophysical results to obtain the different values of the volumetric water content of the soil for the fractures that occurred during the experiment. The geophysical results were used to confirm the values of the VWC at different locations of the soil and to detect the cracks that occurred it covers a larger area of the landslide body.

10.   Early Warning System

Finally, we developed an Early Warning system, which could help in monitoring an active area of landslide and send warnings (alarms) to the affiliated organization to act upon. From the geological part we could understand that the two main complementary triggering factors are: Rainfall intensity, and the rate of rainfall infiltration into the soil, these factors contributed to the failures that have occurred during the experiment. From the photogrammetric part, we could confirm the time and displacement and failure mechanism that resulted from these triggering factors. We have compared the values from geology and geophysics *[Table.5]*, for instance, anomaly 1, which represents (fracture 2) happened after *24 minutes* of the start of the experiment and its displacement was *0.7mm* with a volumetric water content of 0.36 & 0.2975, from geophysics and geology instruments respectively – The difference in the volumetric content between the geophysics and geology is due to the different location of the measurement of the VMC, in the geology calculation, the measurement was based on the TDR which was placed away from the fracture's location upwards, that's why the value is a bit under-estimated, as the VWC in the down-slope is supposed to be higher. Based on this information, we can identify the thresholds that trigger the landslide. For instance, having a TDR(or Piezometer) which would give us a live measurement of the volumetric water content, and whenever the value reaches 0.15(if placed upslope), or 0.18(if placed downslope), a warning alarm is to be sent to the relevant organization to be able to respond to it: either by evacuation or for further monitoring, that would give around *5 minutes* of lead time before the occurrence of the fracture(phase 1), *and 4 minutes* before the occurrence of a more critical fractures(phase 2). Having ERT instruments that cover the whole landslide could be an expensive alternative but would increase the

level of precision. *[Table.9]*

Table 9. VWC calculations from geophysics and Geology

Fracture Number	Electrode Number	VWC (Geophysics)	VWC (Geology)
Fracture 2	1	0.36	0.2975
Fracture 3	3	0.45	0.3201
Fracture 4	24	0.31	0.3284

11.   Bibliography

[1] C. Dictionary, "landslide," English meaning - Cambridge Dictionary. https://dictionary.cambridge.org/dictionary/english/landslide.

[2] "Landslides," Springer. https://www.springer.com/journal/10346.

[3] R. L. Schuster and L. M. Highland, "Socioeconomic and environmental impacts of landslides in the Western Hemisphere," Open-File Report, 2001.

[4] U. Haque et al., "Fatal landslides in Europe," Landslides, vol. 13, no. 6, pp. 1545–1554, May 2016

[5] O. Hungr, S. Leroueil, and L. Picarelli, "The Varnes classification of landslide types, an update," Landslides, vol. 11, no. 2, pp. 167–194, Nov. 2013

[6] corporate body. J. R. Centre, "Science for disaster risk management 2017: knowing better and losing less.," Publications Office of the EU, Jul. 22, 2019 https://op.europa.eu/publication/manifestation_identifier/PUB_LBNA28034ENC

[7] Stumpf, A. et al. 2015. Ground-based multi-view photogrammetry for the monitoring of landslide deformation and erosion. *Geomorphology*. 231, (Feb. 2015), 130–145.

[8] Introduction to Digital Image Correlation - Guest lecture at Oregon State University April 22, 2021: 2021. *https://www.youtube.com/watch?v=GtZjxx55Pis*. Accessed: 2023-01-07.

[9] Zappa, E. et al. 2014. Uncertainty assessment of digital image correlation method in dynamic applications. *Optics and Lasers in Engineering*. 56, (May 2014), 140–151.

[10] CloudCompareWiki: *http://www.cloudcompare.org/doc/wiki/index.php/Main_Page*.

[11] Geotomo Software - Home: *https://www.geotomosoft.com/*.